January 2010

An Examination of Oxysterol Effects on Membrane Bilayers Using Molecular Dynamics Simulations

Brett Olsen
Washington University in St. Louis

Washington University in Saint Louis

Division of Biology and Biological Sciences

Program in Molecular and Cellular Biology

Dissertation Examination Committee:

Nathan Baker, Chair

Douglas Covey

Katherine Henzler-Wildman

Garland Marshall

Daniel Ory

Paul Schlesinger

An Examination of Oxysterol Effects on Membrane Bilayers Using Molecular Dynamics Simulations

by

Brett Neil Olsen

A dissertation presented to the Graduate School of Arts and Sciences of Washington University in partial fulfillment of the requirements for the degree of Doctor of Philosophy

August 2010

Saint Louis, Missouri

Acknowledgments

I would like to thank my doctoral adviser Nathan Baker, whose guidance and advice has been essential to my development as an independent researcher, and whose confidence in my abilities has often surpassed my own.

Thanks to my experimental collaborators at Washington University: Paul Schlesinger, Daniel Ory, and Doug Covey, without whom this work never would have been begun.

Many thanks to the past and present members of my thesis committee: Nathan Baker, Paul Schlesinger, Daniel Ory, David Sept, Lev Gelb, Doug Covey, Garland Marshall, and Katherine Henzler-Wildman, for their direction and criticism.

Thanks to the multitude of other scientific colleagues who have offered contributions to and criticisms of this work in private discussions: Michael Bradley, Rachel Rice, Sunjoo Lee, Albert Mao, Marc Sherman, Peter Jones, Diana Wong, and others too numerous to mention.

Thanks to the Texas Advanced Computing Center, which generously provided supercomputer time on which most of these simulations were run and to Malcolm Tobias, who has been instrumental in keeping the computational resources needed for this work up and running.

Thanks to Leslie Lamport and Donald Knuth for LaTeX and TeX, without which I would have had much less fun formatting my thesis.

Thanks to my friends and family who kept me sane through the course of my doctoral work: my parents Reed and Lorraine Olsen, my brother Cullam and my sister Janel, and my friends Robin and Salomon Trujillo, Jon and Andrea Hunt, Daniel and Lena Koslover, Joe and Tina Wasem, Mike and Erin Connor, Tom and Sarah Pierce, Rebecca Craig-Shapiro, Albert Mao, Adam Greenbaum, Peter and Sarah Freddolino, and Robert Kern.

This work is dedicated to my wife Clare. You have been in my life for nine years, and you have brought nothing but joy, happiness, and love into it. You have borne with my eccentricities with a smile and a kiss, you have been with me to laugh in happy times and comfort in sad. I picked up and started a new life to be with you, and every day I am grateful that I made the right decision. Thank you.

Contents

List of Figures

Chapter 1

Background and Introduction

1.1 Biomembranes

1.1.1 Phospholipid Bilayers

The fundamental structure of biological membranes is provided by amphipathic phospholipids. While membrane phospholipids have a variety of structures, their basic shape and polarity remains the same: a polar or charged headgroup connected to one or more long hydrophobic tails. The combination of polar and nonpolar regions gives lipids an amphiphilic character that causes them to self-assemble into an ordered structure when in an aqueous environment. Lipids such as glycophospholipids or sphingomyelin spontaneously form liposomes or bilayers in aqueous solution, aggregates composed of two stacked layers of lipids. Each layer orients so that the hydrophobic tails of that layer interact with those of the other layer, while the hydrophilic headgroups of each layer interact with the aqueous environment. Phospholipid bilayers serve to separate the inside of the cell from its environment, as well as segregate different organelles within the cell.

The most common lipid components of biological membranes are glycerophospholipids. Glycerophospholipid structure is based on a glycerol core. Two of the glycerol hydroxyl groups form esters with long chain fatty acids, while the third is attached to a hydrophilic headgroup through a phosphate linker (Figure 1.2). Variation in structure among different glycerophospholipids comes from different fatty acids and headgroups. Fatty acids range from 12 to 20 carbons and can be either fully saturated or contain multiple *cis* double bonds. Most biologically-relevant phospholipids contain one saturated and one unsaturated fatty acid [96, 128]. The most common phospholipid headgroup in biological membranes is choline, but other headgroups such as ethanolamine, serine, and inositol may be present in varying amounts as well [128].

While most membrane lipids are glycerophospholipids, sphingomyelin is also an important component

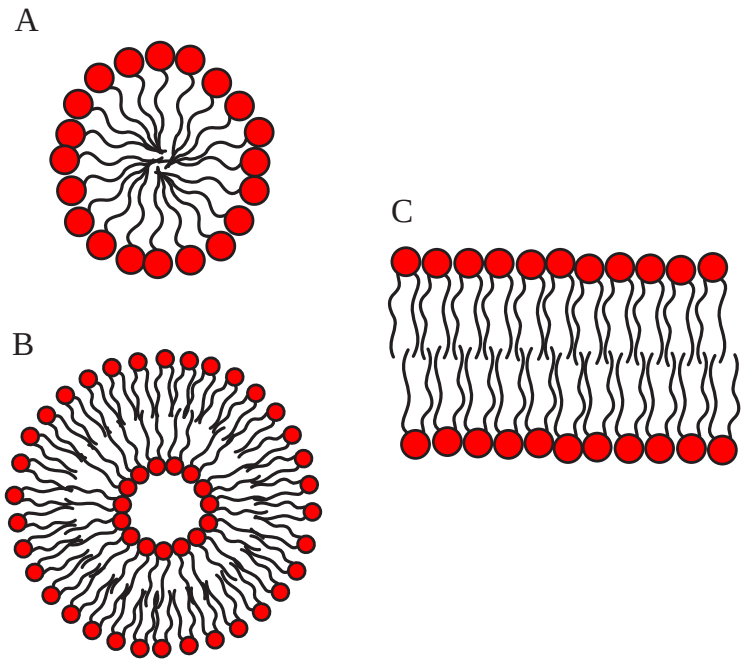

Figure 1.1: Three possible self-assemblies of amphiphilic lipids. Lipids with smaller tails form micelles (A), while those with larger tails form liposomes (B) or bilayers (C).

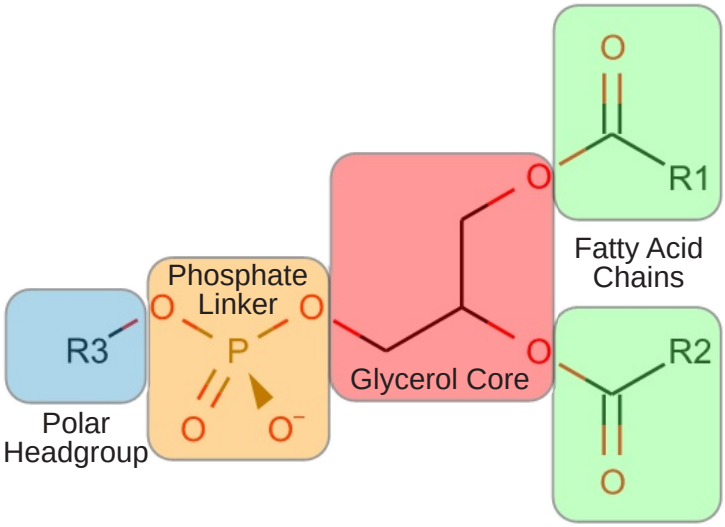

Figure 1.2: A breakdown of the functional groups of glycerophospholipids. The glycerol core is attached to two variable fatty acid chains and, through a phosphate linker, to a variable polar headgroup.

of membranes [35, 96]. Unlike glycerophospholipids which are based around a glycerol core, sphingomyelin is based around a sphingosine core attached to a saturated fatty acid and phosphocholine headgroup. This gives it a more polar interfacial region containing both an amide and an alcohol, unlike the esters seen in phosphatidylcholine. These functional groups allow sphingomyelin to donate as well as accept hydrogen bonds, increasing its ability to form lipid-lipid interactions [96].

Lipid bilayers can exist in several different phases. These phases are distinguished by the behavior of the component lipids. In the solid or gel phase (s_o), lipids have low lateral diffusion rates and are highly ordered, with extended acyl chains [30, 128]. This phase is characterized by strong interactions between neighboring lipids that restrict lipid movement and constrain acyl chains to ordered conformations [30, 128]. In the liquid crystalline or liquid disordered phase (l_d), lipids diffuse rapidly and are less ordered [30, 128]. The liquid ordered phase (l_o) is an intermediate phase with highly ordered lipids but fast lateral diffusion [30, 128]. Non-lamellar phases such as cubic or hexagonal phases may also be important in transient events such as bilayer fusion, budding, and pore formation [30, 128].

Bilayer phase is dependent on temperature and lipid composition of the membrane. Lower temperatures promote solid phases. Each individual type of bilayer-forming lipid has a characteristic melting temperature (T_m), denoting the transition temperature between the s_o and l_d phases [12, 128]. Melting temperatures are higher for lipids with saturated fatty acid chains due to improved packing between the flexible saturated chains [12, 128]. The position of the double bond in unsaturated chains also affects the T_m, with double bond positions near the center of the chain causing the largest decrease in T_m [82]. This is due to packing defects caused by the kinks of the *cis* double bonds. l_o phases are not seen in bilayers composed of only phospholipids. Rather, they are produced through the addition of the steroid lipid cholesterol to phospholipid membranes. This orders the acyl chains while retaining high levels of lateral lipid diffusion.

1.1.2 Membrane Composition and Regulation

The lipid composition of mammalian membranes varies drastically between different cellular membranes and even between different leaflets of the same membrane. Endoplasmic reticulum (ER) membranes contain mostly phosphatidylcholine and phosphatidylethanolamine, with low levels of phosphatidylinositol, phosphatidylserine and cholesterol [128]. Plasma membranes contain higher levels of phosphatidylserine, significant amounts of sphingomyelin, and may be up to 50% cholesterol [128]. Plasma membranes are also known to be asymmetric, with most sphingomyelin found in the outer leaflet and phosphatidylserine exclusively found in the cytosolic leaflet [28,96]. Golgi membranes tend to have compositions intermediate between those of the ER and plasma membranes [128]. Some compartments may have specifically high levels of other lipids such

as cardiolipins, exclusively found in the inner mitochondrial membrane, and bis(monoacylglycero)phosphate, mostly found in endosomal compartments [128]. These compositions are tightly regulated and are essential for proper cellular behavior.

Membranes play important roles as regulatory organelles of the cell. The most obvious way in which membranes regulate cellular behavior is through segregation of separate cellular compartments. Selective permeability of membranes allows different organelles to contain separately regulated enzymatic activities and is essential to eukaryotic cell viability. Disruption of this compartmental segregation between the mitochondria and the cytosol through membrane permeabilization appears to trigger apoptotic cell death [16].

The regulatory behavior of membranes is generally due to regulation of integral and peripheral membrane proteins. Many membrane-associated proteins have important enzymatic behavior that is regulated through the structure and composition of membranes with which they are associated [74]. For example, the activity of adenylate cyclase is regulated by the fluidity and cholesterol composition of its membrane environment [53], membrane structure regulates G-protein activity [132], and phospholipid chain length alters the behavior of diacylglycerol kinase through hydrophobic matching of the membrane to the protein [74]. Membrane structure also regulates protein sorting and association. Reversible protein association with membranes to form enzymatically active complexes is controlled in part through the composition and structure of membranes [89]. Integral membrane protein distribution within cell is regulated by hydrophobic matching of the protein to membranes of different thicknesses within the cell [79].

Membrane lipids themselves can also play a role as signaling molecules. The best understood lipid signaling pathways are those involving the phosphatidylinositols PIP2 and PIP3 [19]. These are rare lipids but function as messengers in a number of signaling pathways. PIP2 can be cleaved to form two different signaling molecules, diacylglycerol and inositol(1,4,5)P3 [19]. PIP3 regulates large-scale membrane behaviors such as endocytosis, exocytosis, and membrane-cytoskeletal interactions [19]. Sphingolipids are also known to act as signaling molecules, involved in the control of apoptosis, the cell cycle, and differentiation [35, 43]. The movement of common lipids can also serve as a signal: transfer of phosphatidylserine to the outer leaflet of the plasma membrane appears to mark apoptotic cells [28] and depletion of cellular cholesterol alters protein localization and trafficking [57, 112].

1.2 Sterols

While phospholipids and sphingolipids are responsible for forming the basic structure of biological membranes, sterols are essential for the proper functioning of membranes. While a wide array of different phos-

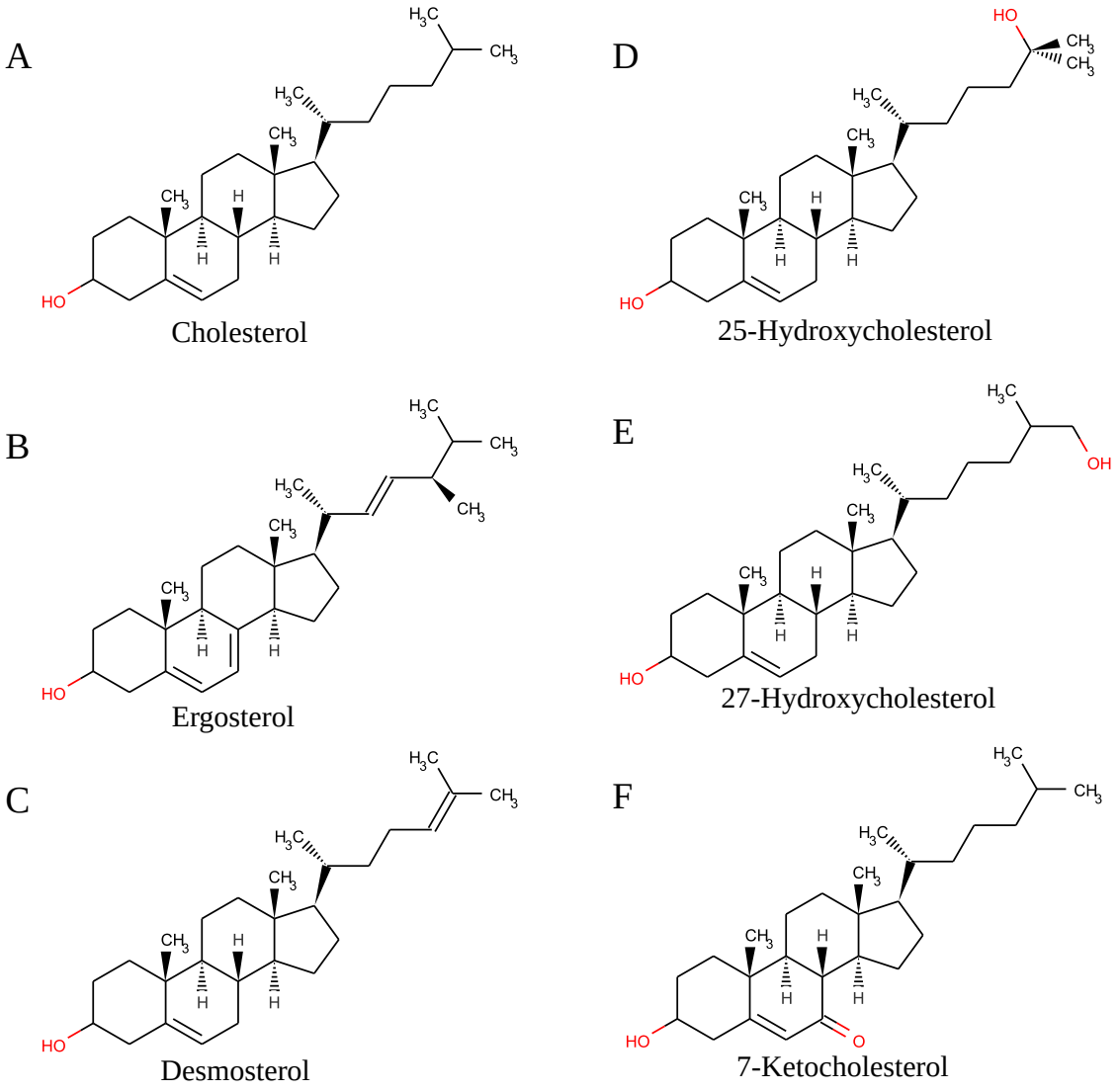

Figure 1.3: Chemical structures of some common sterols.

pholipids have been identified in biological membranes, most contain only one dominant sterol. Cholesterol (Figure 1.3) is the primary sterol found in mammalian cells, while its role is taken by other sterols in fungi and plants [128]. Cholesterol is required for mammalian cell function and viability.

1.2.1 Sterol Structure

All sterols have a structure based around four rings fused in a *trans* configuration. These fused rings give sterols a rigid, planar, and hydrophobic structure. Different sterols decorate this base steroid ring structure with different functional groups, such as methyl, hydroxyl, iso-octyl, keto, and other groups. Cholesterol contains a flexible iso-octyl tail attached to one end of the steroid rings, a hydroxyl group attached at the

other end, and two methyl groups attached to one face of the steroid rings. While most of the cholesterol structure is highly hydrophobic, the hydroxyl headgroup gives it an amphiphilic character. Because the hydroxyl group is so small, cholesterol cannot form bilayers by itself but instead incorporates into existing phospholipid bilayers, modulating their structure and behavior.

1.2.2 Cholesterol

When incorporated into phospholipid bilayers, cholesterol aligns so that its polar hydroxyl group is near the interface with the aqueous environment while its hydrophobic body is buried in the bilayer [96, 97]. This alignment places the rigid steroid ring in close proximity to the acyl chains of nearby phospholipids. Because the acyl chains are flexible, they tend to align themselves along the surface of the steroid ring, ordering and extending them [57, 118]. Cholesterol interactions with phospholipids change membrane structure. The alignment and ordering of nearby phospholipid tails causes a condensation of membranes, decreasing the area of the membrane and increasing the thickness [96]. Cholesterol also broadens the liquid-to-solid phase transition, inducing an intermediate liquid-ordered phase that retains lateral mobility while gaining increased lipid order [30, 118, 128]. These changes result a mechanically stronger membrane with decreased permeability due to tighter packing among lipids [57, 118]. The effects of cholesterol on membranes are dependent on the composition of the membrane. The condensation effect on proximal phospholipids is strongest on lipids with saturated acyl chains [57, 118]. This is because the kinks in unsaturated tails interfere with packing between the tails and the rigid steroid ring [57,118]. Because of this, in cell membranes, cholesterol segregates into separate domains with the saturated sphingomyelin lipids away from the mostly unsaturated glycerophospholipids [57, 118].

Cholesterol is asymmetrically distributed between different membranes in the cell [128]. Most cellular cholesterol is found in the plasma membrane, with much lower concentrations in the ER, Golgi, and endosomal compartments [128]. However, this is not a static distribution; there is constant trafficking of cholesterol back and forth between the ER and the plasma membrane [57, 96]. This trafficking allows changes in the concentration of cholesterol at the plasma membrane to cause much larger changes in ER cholesterol levels [57]. When cholesterol is added to the plasma membrane past physiological levels, the excess is quickly trafficked to the ER where it is processed for storage as cholesterol esters [71,73]. Similarly, when cholesterol is partially depleted from the plasma membrane, ER cholesterol drops even further, triggering mechanisms intended to restore cholesterol levels [57, 73].

1.2.3 Oxysterols

While cholesterol is the dominant sterol present in mammalian cells, oxygenated derivatives of cholesterol, called oxysterols, are present at low concentrations as well. Oxysterols are produced by either the uncontrolled reaction of reactive oxygen species with cholesterol or by controlled enzymatic reactions. The enzymatic production of oxysterols indicates that they are not simply unwanted side products but rather serve a useful purpose within the cell. Two major roles of oxysterols in the cell have been identified.

First, oxysterols are involved in important cholesterol excretion pathways. The addition of polar oxygen-containing groups to cholesterol increases its ability to pass through membranes and is used to transform excess cholesterol into a more easily removed form [7]. For example, excess cholesterol in cholesterol-loaded macrophages is converted into 27-hydroxycholesterol and cholestenoic acid for excretion, while excess cholesterol in the brain is converted to 24S-hydroxycholesterol in order to pass through the blood-brain barrier [7]. Oxysterols are also intermediates in the bile acid synthesis pathway for excretion into the digestive system, with the liver enzyme cholesterol 7α-hydroxylase being the rate limiting step. Secondly, oxysterols have strong effects on the regulation of cholesterol homeostasis, in multiple different pathways. They are activators of the liver X receptor family of transcription factors, upregulating the expression of enzymes involved in cholesterol efflux [7,60,61]. Oxysterols have also been found to be potent suppressors of cholesterol synthesis, with some oxysterols having inhibitory activities orders of magnitude stronger than cholesterol itself [6].

Oxysterols can be broadly divided into two classes: those oxygenated on the steroid ring structure, usually at the 7-position, such as 7-ketocholesterol, 7α-hydroxycholesterol, and 7β-hydroxycholesterol, and those oxygenated on the iso-octyl tail, such as 25-hydroxycholesterol, 27-hydroxycholesterol, and 24S-hydroxycholesterol [10]. Generally the side-chain oxysterols are produced enzymatically while the ring oxysterols are produced non-enzymatically, although both 25-hydroxycholesterol and 7α-hydroxycholesterol can be produced by both methods [10]. The different side-chain oxysterols are produced by different enzymes: sterol 27-hydroxylase is a mitochondrial enzyme highly expressed in liver and macrophage cells where it catalyzes bile acid synthesis [10], cholesterol 24-hydroxylase is found in the ER, mainly expressed in brain cells [10], and cholesterol 25-hydroxylase is is a structurally dissimilar enzyme found in the ER and Golgi [10].

Oxysterols also have significant effects on the physical structure of model membranes. Ring-oxygenated oxysterols have generally similar but weaker effects as cholesterol, inducing membrane condensation and increasing phospholipid order [36, 125]. Side-chain oxysterols have quite different effects, expanding rather than condensing membranes [36, 125], and increasing the permeability of membranes to ions and polar molecules [49, 125]. The mechanisms for these effects have not yet been eludicated.

1.2.4 Cholesterol Regulation

Because cholesterol is such an essential part of mammalian membranes, cells expend significant amounts of energy to regulating their cholesterol levels. Cholesterol levels are controlled through multiple different processes, including *de novo* synthesis within the cell, transfer of cellular cholesterol to and from circulating lipoproteins, storage of cholesterol within the cell as cholesterol esters, and excretion of cholesterol as bile acids [52,98]. The rate-limiting step of cellular cholesterol synthesis is performed by the enzyme 3-hydroxy-3-methylglutaryl CoA reductase (HMGCoAR) [39]. Cholesterol synthesis is tightly regulated by ER cholesterol levels through transcriptional and non-transcriptional regulation of HMGCoAR activity [39].

The HMGCoAR gene contains a promoter known as the sterol regulatory element (SRE) [39]. Transcription factors known as sterol regulatory element binding proteins (SREBPs) bind to SREs and activate transcription from genes containing SRE promoters [11, 52]. SREBPs are transmembrane proteins that are produced in the ER [11, 52]. When initially synthesized, they are inactive and must mature in order to become active transcription factors [11, 52]. This activation occurs through transport of the transmembrane SREBP from the ER to the Golgi complex where Golgi-resident proteases cleave the transmembrane domain, producing an active fragment [11, 52]. This fragment can then enter the nucleus and induce transcription from cholesterol synthesis and uptake genes including HMGCoAR [11, 52]. Transport of SREBPs from the ER to the Golgi is done with the aid of the SREBP cleavage-activating protein (Scap) [11,52]. Scap binds to the regulatory domain of SREBPs, thus forming SREBP-Scap complexes [11,52]. Scap also contains a sterol sensing domain (SSD), which causes conformational changes in Scap in the presence of cholesterol [11, 52]. When ER cholesterol levels are low, Scap binds to vesicular packaging proteins, initiating the transfer of the complex to the Golgi [11,52]. Under cholesterol-rich conditions, Scap instead binds to the ER resident Insig proteins, blocking vesicular transport and SREBP maturation [133]. This pathway provides transcriptional feedback to help control cholesterol levels. When ER cholesterol is low, SREBP is activated and initiates production of HMGCoAR and thus cholesterol synthesis. When ER cholesterol is high, SREBP is not activated and no cholesterol synthesis is initiated.

While transcriptional regulation of cholesterol synthesis is essential, it occurs on a slow timescale of several hours. This is not fast enough to quickly shut off cholesterol synthesis when large amounts of new cholesterol are introduced, either through uptake from lipoproteins or synthesis. For faster response times, non-transcriptional regulation is required. HMGCoAR is an ER resident transmembrane protein [39]. Like Scap, HMGCoAR contains a SSD that induces conformational changes in the presence of cholesterol [39, 68]. These conformational changes expose ubiquitination sites on HMGCoAR [37, 68]. Once ubiquitinated, HMGCoAR is targeted to the proteasome where it is degraded [37, 68]. This sterol-dependent proteolysis

of HMGCoAR prevents cellular energy from being expended to produce unnecessary cholesterol by shutting down cholesterol synthesis as soon as enough is present in the ER to bind and activate SSDs.

While cholesterol itself can regulate HMGCoAR synthesis and degradation, side-chain oxysterols have also been shown to play a role. Side-chain oxysterols are more potent suppressors of SREBP activation than cholesterol itself when added to cells [40,55]. Oxysterols have been shown to interact with Insig, retaining the Insig/Scap/SREBP complex in the ER and blocking SREBP maturation [109]. Studies with enantiomeric 25-hydroxycholesterol have shown that oxysterol suppression of SREBP activation is not enantiospecific, suggesting that its effects are not due to direct protein interactions but instead may be mediated through membranes [36]. 27-hydroxycholesterol is a potent activator of HMGCoAR degradation [7]. Cells which lack cholesterol 27-hydroxylase have normal sterol content and respond properly to cholesterol depletion, but do not suppress HMGCoAR activity upon cholesterol enrichment [7,70]. This suggests that the feedback effects of cholesterol on these pathways are mediated through cholesterol conversion into oxysterols.

Oxysterols also play a role in the regulation of cholesterol efflux through the liver X receptor family of transcription proteins. Side-chain oxysterols bind to and activate LXRs at physiological concentrations [7,60, 61]. LXRs in turn activate the expression of a number of genes involved in export of excess cholesterol from the cell, including bile acid synthesis proteins such as Cyp7A1 [7], the ABCA1 transporter which transfers excess cholesterol to circulating apolipoproteins [124], and apolipoproteins themselves [124]. Experiments with enantiomeric 25-hydroxycholesterol demonstrate that LXR activation by oxysterols is enantiospecific, confirming direct binding between LXR and 25-hydroxycholesterol [36].

Chapter 2

Examination of Oxysterol Membrane Effects

Abstract

Cholesterol is essential for proper function and regulation of eukaryotic membranes, and significant amounts of metabolic energy are dedicated to controlling cellular cholesterol levels. Oxidation products of cholesterol, the oxysterols, are enzymatically produced molecules that play a major role in mediating cholesterol homeostasis through mechanisms which have not yet been fully elucidated. Certain oxysterols are known to have direct effects on membrane permeability and structure; effects that are strikingly different from that of cholesterol. We use molecular dynamics simulations of these oxysterols in 1-palmitoyl 2-oleoyl phosphatidylcholine (POPC) bilayers to explain the structural origins for the differing effects of cholesterol and 25-hydroxycholesterol on bilayer properties. In particular, we demonstrate that the source for these differing perturbations is the much wider range of molecular orientations accessible to 25-hydroxycholesterol when compared to cholesterol. This study shows that direct membrane perturbation by side-chain oxysterols is significant, and suggests that these membrane perturbations may play a role in the oxysterol regulation of cholesterol homeostasis.

2.1 Introduction

While the major components of cellular membranes are phospholipids, sterols are essential for membrane function [96]. Cholesterol is the most prevalent sterol in mammalian cells, where it is distributed unevenly among mammalian membranes with the plasma membrane containing significantly more cholesterol than the mitochondrial or ER membranes [78, 96]. Cholesterol is required by all mammalian cells, and can either

be produced endogenously or taken up from plasma lipoproteins [78, 96]. Its functions in the cell include binding to sterol-sensing domains to regulate protein function [27,68], participating in the formation of lipid rafts [23, 59], and serving as a precursor for steroid hormone and bile acid synthesis [15]. Homeostasis of cholesterol levels is maintained through regulation of *de novo* synthesis, cholesterol uptake, and cholesterol efflux [52, 98]. Cholesterol influences cellular behavior both directly and indirectly. Conserved sterol-sensing domains (SSDs) are found in many different membrane proteins and respond to concentrated levels of sterols in the local membrane by changing their binding affinities and enzymatic activities, allowing sterols to signal in a number of pathways through these proteins [68]. In particular, both the cholesterol synthesis and intracellular cholesterol transport pathways contain proteins with SSDs, indicating a role for the SSD in sterol homeostasis [68]. Cholesterol also alters membrane structure, increasing membrane thickness, bending modulus, and lipid order while decreasing membrane fluidity [26, 56, 86, 94, 108, 129]. These physical changes can affect membrane proteins as demonstrated in membrane protein sorting [79], cellular signaling [23], and changes in ion channel properties [90].

Oxysterols are also known to exhibit a variety of biological activities. Of particular interest is their effect on cholesterol synthesis through feedback inhibition [40]. Transcriptional regulation of cholesterol synthesis is mediated by sterol regulatory-element binding proteins (SREBPs), a family of membrane-bound transcription factors [40, 52]. SREBPs form a complex with the SREBP cleavage-activating protein (SCAP). When this complex moves to the Golgi apparatus, SREBP is cleaved by Golgi-resident proteases, and the transcription factor domain of SREBP is released to activate transcription of cholesterol biosynthetic enzymes [40,52]. High levels of membrane sterols also induce binding of SCAP to ER-resident Insig proteins, retaining the SREBP-SCAP complex in the ER and blocking upregulation of cholesterol synthesis [40, 52]. While cholesterol alone is sufficient to induce this feedback inhibition, it has been known for many years that oxysterols, including 25-hydroxycholesterol, are greater than 50 times more effective at suppressing the expression of sterol synthetic enzymes such as HMGCoA reductase [40, 55]. In conjunction with the discovery of oxysterol-synthesizing proteins and oxysterol-binding proteins, this has led to speculation that cholesterol's feedback inhibition may be partially mediated through oxysterols [38]. Like cholesterol, the 25-hydroxycholesterol oxysterol can act through both specific ligand-protein interactions [38, 109] and by altering the structural properties of membranes. Specifically, 25-hydroxycholesterol has been shown to increase membrane permeability and monolayer per-lipid area [49, 63, 125].

The molecular structure of cholesterol (Fig. 2.1A) is based around four fused rings in a *trans* configuration, making the ring structure planar and rigid. This rigid ring structure contains two methyl groups protruding out of one face of the planar ring and is connected to a flexible iso-octyl hydrocarbon chain at carbon 17.

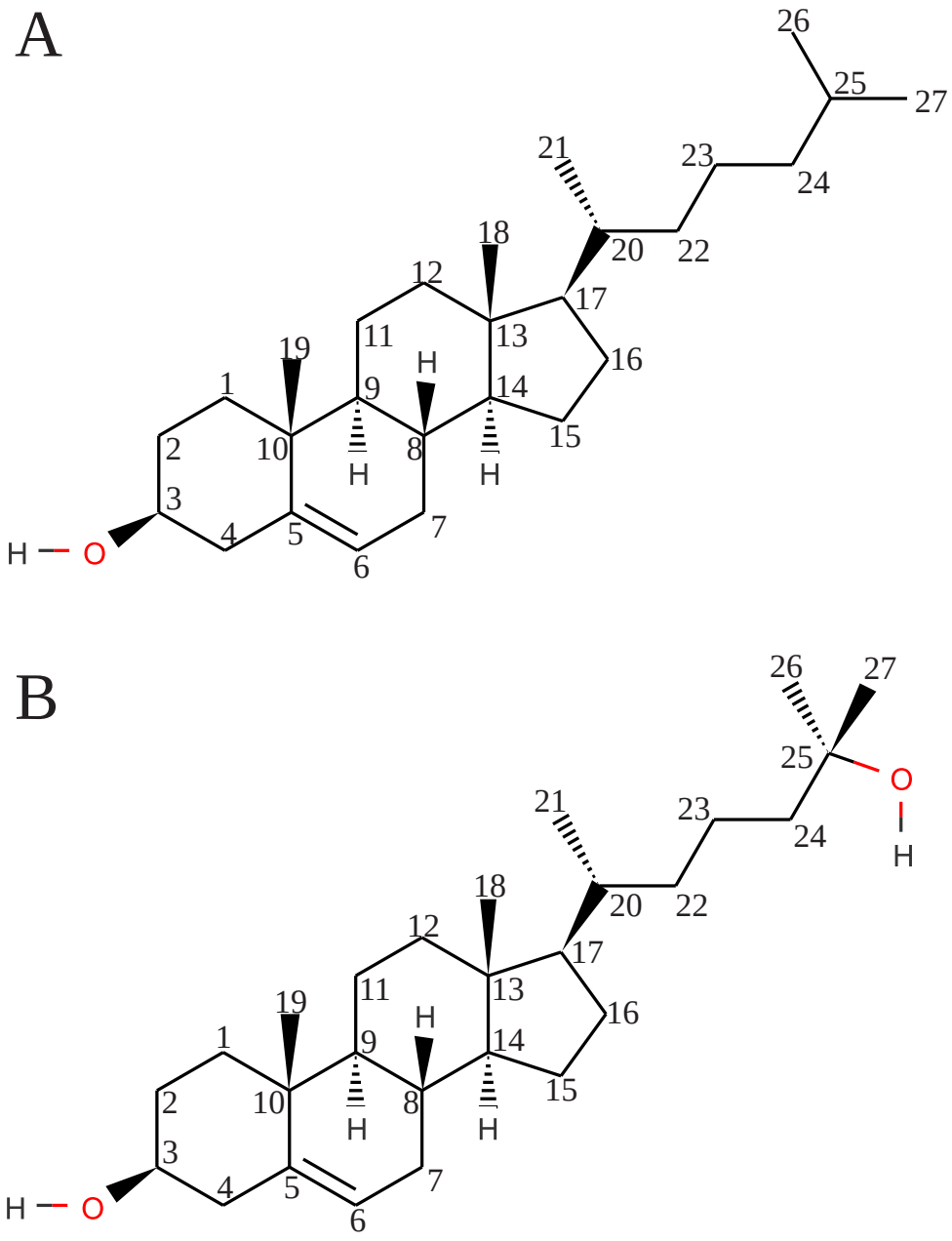

Figure 2.1: Cholesterol (A) and 25-Hydroxycholesterol (B), with standard carbon numbering schemes.

Due to the hydroxyl group located at carbon 3, cholesterol is an amphiphile. In the membrane, this tends to orient cholesterol with the hydroxyl group facing water and the polar regions of nearby phospholipids to maximize hydrogen-bonding interactions [96]. Another important aspect of cholesterol is that the 3-hydroxyl group, the iso-octyl hydrocarbon chain, and the two methyl groups are all attached to the same face of the planar ring, giving it "smooth" and "rough" faces that influence its interactions with other molecules [96]. While cholesterol is the dominant sterol within mammalian cells, oxidation products of cholesterol are formed at low levels by both reactive oxygen species and enzymatic action on cholesterol [115, 119]. The oxysterol 25-hydroxycholesterol (Figure 2.1B) is one such oxidation product which contains an additional hydroxyl group at the end of the iso-octyl tail, on the other side of the molecule from the 3-hydroxyl group. Addition of this 25-hydroxyl group to a non-polar region of the cholesterol structure significantly alters the amphiphilic characteristics of this molecule.

The molecular-level interactions of cholesterol and 25-hydroxycholesterol with phospholipid membranes are essential to understanding their dramatically different effects on mammalian cells. Both of these sterols can perturb the bulk properties of membranes [49,96,125]with significant effects on the behavior of membrane-bound proteins [23,79,90]. In this study, we use molecular dynamics simulations of mixed sterol/phospholipid membranes to examine the influence of chemical differences in sterol structure on membrane interactions. This technique, while limited to very fine details of interactions and simple membrane structures, allows us to gather atomic-level information about how these small molecules interact with membranes and the mechanisms by which they can perturb membrane behavior.

2.2 Methods

2.2.1 Parameters and Structures

The initial united atom structure and GROMACS topology for cholesterol modeling were taken from Höltje *et al.* [50]. An additional hydroxyl group was added to both the structure and topology to produce 25-hydroxycholesterol (Fig. 2.1B).

Atomic charges for both cholesterol and 25-hydroxycholesterol molecules were calculated using quantum mechanical/molecular mechanical (QM/MM) methods. Our starting structures for these calculations were taken from short MD simulations of a single sterol (cholesterol or 25-hydroxycholesterol) solvated in SPC water with imprecise atom charges, taken from the original Höltje topology [50]. QM/MM minimization was performed with the QSite program [58]. The QM/MM methodology has been described elsewhere [92, 106]. A solvation sphere of 15 Å around the sterol was retained, and the outer 3 Å of waters were constrained in

place. Water molecules were modeled using MM methods, using the OPLS-AA force field [62]. The sterol molecule was converted to an all-atom structure and modeled using density functional QM methods with the B3LYP functional [2,122] in combination with the LACVP* basis set [34,45].

Sterol atom charges were obtained from the minimized QM/MM systems by fitting the molecular electrostatic potential (ESP) surface to atomic point charges [9,17,130]. Charges for non-hydroxyl hydrogen atoms were added onto their attached heavy atom's charge to prepare united atom charges. These charges were then adjusted slightly to create net-neutral charge groups for MD simulation and are shown in the Appendix (Table 6.1).

1-palmitoyl-2-oleoyl-phosphatidylcholine (POPC) lipids were simulated using the united atom parameters of Berger and Lindahl [5], along with SPC water [3] and Straatsma-Berendsen potassium and chloride ion parameters [123]. Sterol bonded and non-bonded parameters were taken from the GROMOS force-field native to GROMACS [77]. This combination of force-field parameters has been successfully used in a number of previous studies [5,8,126,127] and yields good agreement with experimental observables such as area per lipid headgroup and tail order parameters. While good results have also been obtained using all-atom models for POPC [31,54], united atom models allow us to use longer timesteps and simulate larger systems while still retaining a useful level of molecular detail. An initial bilayer structure of 128 POPC molecules was obtained from Tieleman and coworkers [127]. This structure was replicated in the bilayer plane and trimmed to produce a larger, 256 lipid bilayer, with approximate dimensions of 10 nm $\times$ 10 nm in the bilayer plane.

To prepare low-concentration mixed sterol/POPC bilayers, the 256 POPC bilayer was solvated with 14260 SPC water molecules along with 30 K^+ and Cl^- ions for a nominal KCl concentration of 110 mM. A single molecule of cholesterol or 25-hydroxycholesterol was placed 1-2 nm from the surface of each monolayer at the start of the low-concentration simulation. This system was then simulated for 40 ns to allow the sterols to associate with the POPC bilayer. Both cholesterol and 25-hydroxycholesterol inserted themselves into the bilayer within 10 ns. High-concentration sterol/POPC structures were prepared from the converged portions of these low-concentration simulations as follows. 7 sterol and 16 POPC molecules were extracted from the converged low-concentration simulation and arranged in a 5 $\times$ 5 array to form an oriented monolayer. This monolayer was then stacked on an inverted copy of itself to produce a 14 sterol, 32 POPC bilayer. These very small bilayers were simulated for 10 to 15 ns to allow them to relax. The relaxed structure was then copied 3 $\times$ 3 in the plane of the bilayer and 16 POPC and 7 sterols removed from each monolayer of the resulting structure. This process produced final structures consisting of 256 POPC and 112 sterols, or bilayers of about 30 mole percent of sterols. These structures were solvated with 17541 (cholesterol) or 17325 (oxysterol) SPC water molecules and 36 K^+ and Cl^- ions for an approximate molar concentration of 110mM KCl.

2.2.2 Simulations

All molecular dynamics (MD) simulations were performed using GROMACS version 3.3.1 [4, 77]. All simulations followed the same molecular dynamics protocol. Conjugate gradient energy minimization was first performed on the initial structures to relax any unfavorable contacts between molecules. The system was then gradually warmed with a series of 30 ps constant temperature, constant pressure MD simulations from 0 to 300 K in 15 K increments, with 2 fs time steps. Production simulations were then run for 207 (cholesterol) or 208 (25-hydroxycholesterol) ns. Anisotropic pressure coupling was applied at 1 atm using the Parrinello-Rahman method with a time constant of 1 ps [103]. Temperature coupling was applied independently to lipids and solvent using the Nosé-Hoover algorithm with a time constant of 0.2 ps [51]. Electrostatic interactions were calculated using the particle-mesh Ewald method (PME), with both the direct space PME cutoff and the Lennard-Jones cutoffs set to 1 nm [20]. Constraints were applied to all bonds [29, 102] using the LINCS algorithm incorporated in GROMACS to allow 2 fs timesteps [47].

2.2.3 Analytical Methods

Bootstrap Errors

Some time-independent observables, such as bulk membrane properties or hydrogen bonding probability distributions, are calculated as cumulative properties of an entire stationary trajectory. For such observables, errors can be estimated using a bootstrap method [24, 107]. In the following description, we assume we are analyzing a trajectory containing N frames of data $f_1, f_2, \ldots, f_N$ and are interested in calculating an observable property $P(f_1, f_2, \ldots, f_N)$ which depends on multiple frames of this trajectory. Furthermore, we use the statistical inefficiency method described in the Appendix (Section 6.1.1) to estimate the number N' of trajectory frames that are statistically independent. The main step in the bootstrap method is the generation of a synthetic trajectory dataset with N' frames of data $\{f_{1'}, f_{2'}, \ldots, f_{N'}\}$. Generation of this synthetic dataset proceeds by drawing N' frames randomly with replacement from the real trajectory. The observable of interest is then calculated from this synthetic trajectory as $P(\{f_{1'}, f_{2'}, \ldots, f_{N'}\})$. A distribution of observable values is produced by repeating this main resampling step over many randomly-generated synthetic trajectories. The distribution of these synthetic observable values can then be used to estimate errors in the calculated value by measuring the standard deviation (or other error metrics) from the bootstrapped distribution of observable values.

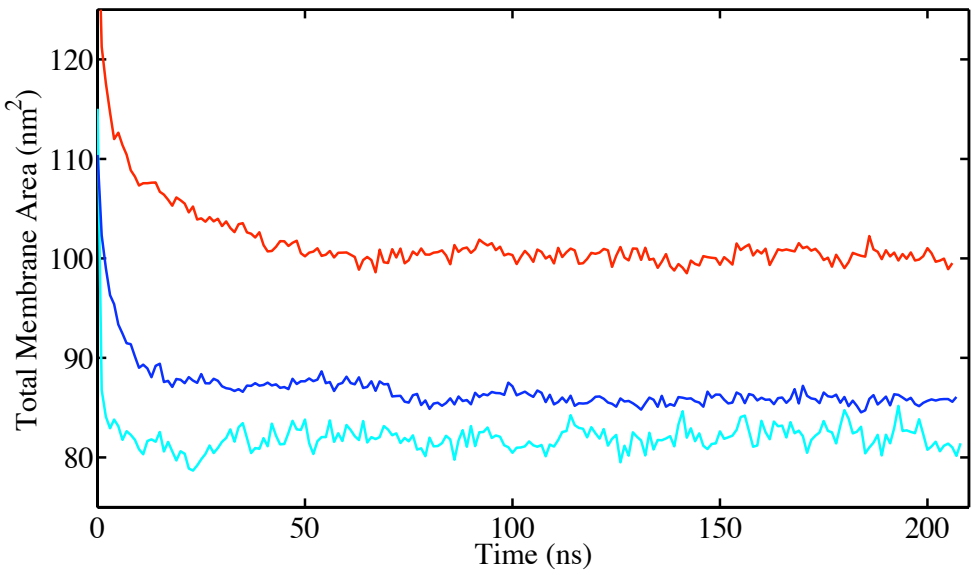

Figure 2.2: The total projected membrane area of the three membrane simulations — pure POPC (cyan), 30% mole fraction cholesterol (blue), and 30% mole fraction 25-hydroxycholesterol (red).

SASA Calculations

Solvent-accessible surface area (SASA) calculations for our systems were performed with APBS version 1.0.0, using a 1.4 Å radius solvent probe [1]. For these calculations, the systems were stripped of solvent and ion molecules and replicated 3×3 times in the xy plane to reduce edge effects. Only the central image of this replicated bilayer was used for analysis. The SASA of each atom in the central structure's lipids in the replicated system is calculated with APBS, and the contributions from each lipid's atoms summed to obtain a molecular surface area for each lipid.

2.3 Results

2.3.1 Equilibration

In order to determine whether a lipid simulation is sufficiently equilibrated (e.g., with observables sampling a stationary distribution), we would like to examine those properties of the system which are slow to converge to a steady-state value. For bilayer systems, the total cross-sectional area A_{tot} of the simulation is a useful metric; it generally drifts more slowly than other properties of the system. Furthermore, the area offers useful information about the bilayer structure that can be compared with experimental values.

The total system areas of our three simulations are shown in Figure 2.2. For equilibration purposes, it

is necessary to make an estimation of when the initial drift in the simulations has vanished. The length of this initial drift phase varies somewhat for each system. For the pure POPC membrane, this drift phase is relatively short, reaching steady-state values in under 5-10 ns. The cholesterol system relaxes slightly more slowly, approaching steady-state values after approximately 15 ns, although with a slight change at 70 ns. Finally, the 25-hydroxycholesterol system converges much more slowly, not approaching steady-state values until after 40 ns. Based on observation of these areas, as well as additional metrics described in the Appendix (Section sect:equilib), the first 80 ns of all simulations were removed as an equilibration phase. Subsequent "production" analyses were performed using only data from the final 128 ns of the 208 ns trajectories.

Statistical inefficiency tests were applied to the "production" 128 ns of these area plots to determine the relaxation time of our systems. Approximate area relaxation times of 3.0-4.0 ns were obtained. Thus for all later statistical analyses, each trajectory was conservatively treated as containing 32 independent bilayer conformations. For analysis of individual molecules, each lipid was treated independently for each independent frame.

2.3.2 Areas and Volumes

In simple bilayers consisting of only one type of lipid, the total area can be converted to an area per lipid A by simply dividing the total area by N, the number of lipids per monolayer. For more complex bilayers composed of a mixture of different lipids, the mean area per lipid will differ for each component, and the computation of the mean area of each component is not straightforward. Numerous techniques have been proposed for partitioning the area of a phospholipid/sterol bilayer: allocating all area evenly between the two components, allocating all area to the phospholipid, assuming a constant mean area for the sterol equal to that seen in a sterol monolayer [113], assuming a constant mean volume for the sterol equal to that observed in the crystal structure [48], partitioning the area of a slice through the membrane using VdW radii of the component atoms [29], among others [18,22,102]. Partial molecular areas have also been used to examine the effects of cholesterol on membranes [22,101]. However this type of analysis requires multiple simulations with different molar concentrations of the additional molecule and is beyond the scope of our current focus (or resources). One may also estimate phospholipid area by structural analysis based on volume and thickness information [48, 105, 110].

After removing the equilibration portion of our simulations, we calculated the average area per POPC by simply dividing the total system area by the number of POPC lipids in a monolayer, resulting in 64.0 $\pm$ 0.8 Å^2 per POPC for the pure POPC simulation, 67.1 $\pm$ 0.4 Å^2 for the cholesterol/POPC simulation, and 78.4 $\pm$ 0.5 Å^2 for the 25-hydroxycholesterol/POPC simulation. The pure POPC results agree with simulation

results of Róg *et al.*who obtained 63.5 ± 0.5 Å^2, while experimental data shows a somewhat larger area of 68.3 ± 1.5 Å^2 [67, 113]. Róg *et al.*also performed simulations of POPC/cholesterol mixtures, and the per-POPC area for a 22 mole percent cholesterol simulation can be calculated from their data as 70.2 ± 0.5 Å^2 [113].

The change in per-phospholipid area with the addition of small molecules can be partitioned into a *direct* increase of area due to additional molecules in the system and an *indirect* effect of the small molecules on nearby phospholipids. Cholesterol is known to have an area-decreasing effect on nearby phospholipids, but in simulations of relatively high cholesterol concentration, the direct increase in system area from the additional volume of the cholesterol molecules dominates and creates a slight increase in total area per phospholipid [29, 48, 56]. We observe a 3.1 Å^2 increase in area per phospholipid between the 0 and 30 mole percent cholesterol simulations. This change is consistent with previous results and shows a larger direct than indirect influence of cholesterol on membrane area. 25-hydroxycholesterol, however, shows a much larger increase of 14.4 Å^2 in per-POPC area between 0 and 30 mole percent 25-hydroxycholesterol simulations. Together with the solvent-accessible area data (below), this observation suggests that 25-hydroxycholesterol takes up much more area in the membrane than cholesterol.

In order to decompose the area-altering effect of cholesterol and 25-hydroxycholesterol on system area into direct and indirect contributions, the solvent-accessible surface area (SASA) of each snapshot from the three trajectories was calculated and partitioned into molecular SASAs. This decomposition gave distributions of SASA for each type of molecule, shown in Figure 2.3. This allows assessment of the indirect effect of sterols on system area through their perturbation of individual POPC area from the direct increase of area due to the additional molecules. Differences in distributions are compared using the Kolmogorov-Smirnov test, described in the Appendix (Section 6.1.2). In the cholesterol-containing simulation, the distribution of POPC molecular SASAs clearly shifts to smaller values by depletion of large area contributions. Conversely, in the 25-hydroxycholesterol-containing simulation, the distribution of POPC surface areas shifts to much larger areas. Even larger differences between distributions are seen for the cholesterol and 25-hydroxycholesterol molecule SASAs, where the mean area of cholesterol is much smaller than that of 25-hydroxycholesterol and the distribution of cholesterol SASA is much more tightly peaked.

The volumes of the membranes were calculated as the product of the system area with the thickness of the membrane, estimated as the mean phosphate-to-phosphate distance [113]. Volume distributions over the course of the three simulations are shown in Figure 2.4. We observed a large increase in membrane volume with the addition of 30% of either sterol, with a slightly larger increase in volume for 25-hydroxycholesterol as compared to cholesterol. This suggests that the perturbation of total volume by sterols is primarily

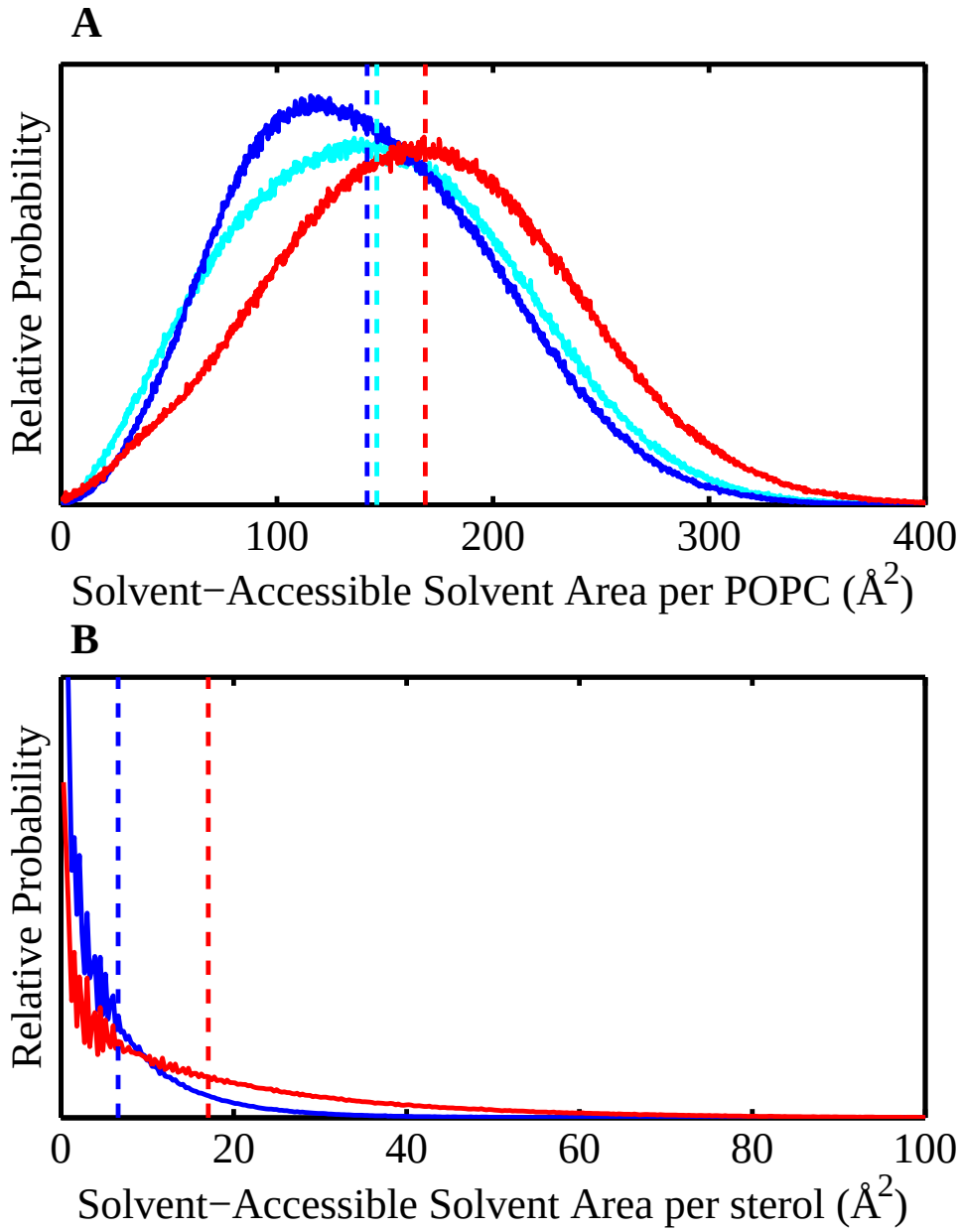

Figure 2.3: Membrane component solvent-accessible areas. (A) Solid colored lines show the probability distributions of per-POPC solvent-accessible surface area (SASA) in simulations of pure POPC (cyan), 30% mole fraction cholesterol (blue), and 30% mole fraction 25-hydroxycholesterol (red). The mean SASAs for these distributions are 150 ± 60, 140 ± 60, and 170 ± 60 Å^2, respectively. (B) Solid colored lines show the probability distributions and means of per-sterol SASA, cholesterol in blue and 25-hydroxycholesterol in red. Dashed vertical lines show the mean SASA for the whole distribution. Mean SASAs for these distributions are 10 ± 20 and 17 ± 20 Å^2, respectively. p-values for distribution differences are calculated using the Kolmogorov-Smirnov test (see Appendix, Section 6.1.2), and are all less than 0.1%.

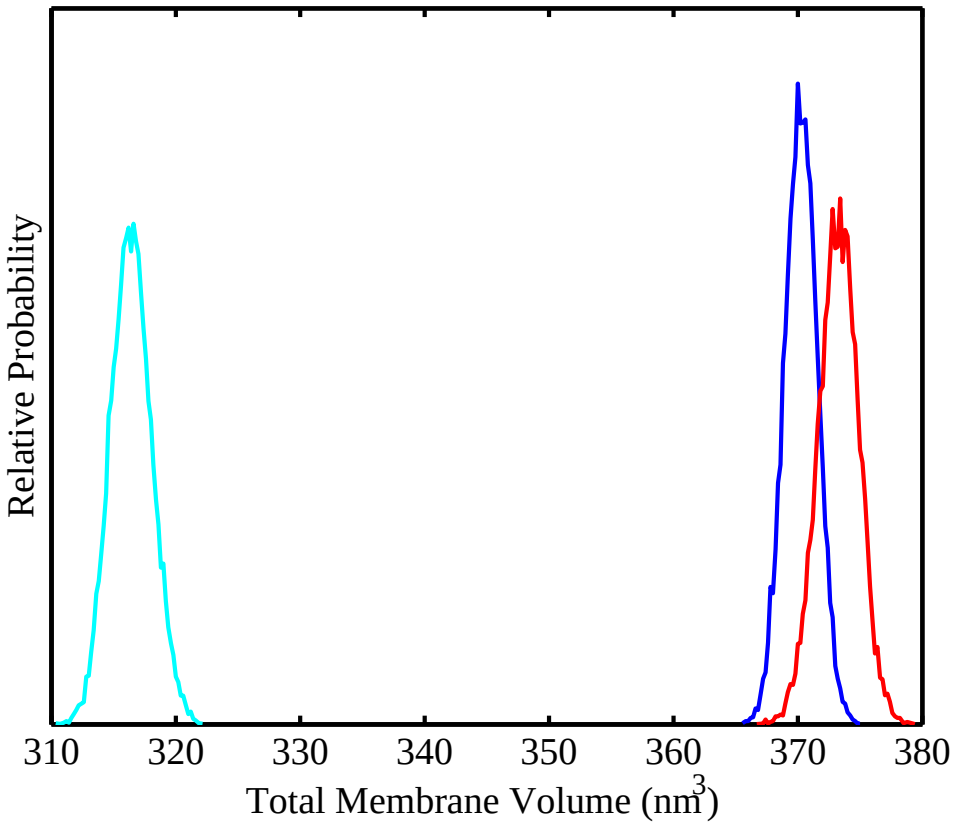

Figure 2.4: The distributions of total membrane volume for a pure POPC membrane (cyan), 30% mole fraction cholesterol (blue), and 30% mole fraction 25-hydroxycholesterol (red). Mean membrane volumes are 316 ± 2, 370 ± 1, and 373 ± 2 nm^3, respectively. p-values for distribution differences are calculated using the Kolmogorov-Smirnov test (see Appendix, Section 6.1.2), with the p-values for all distribution differences less than 0.1%.

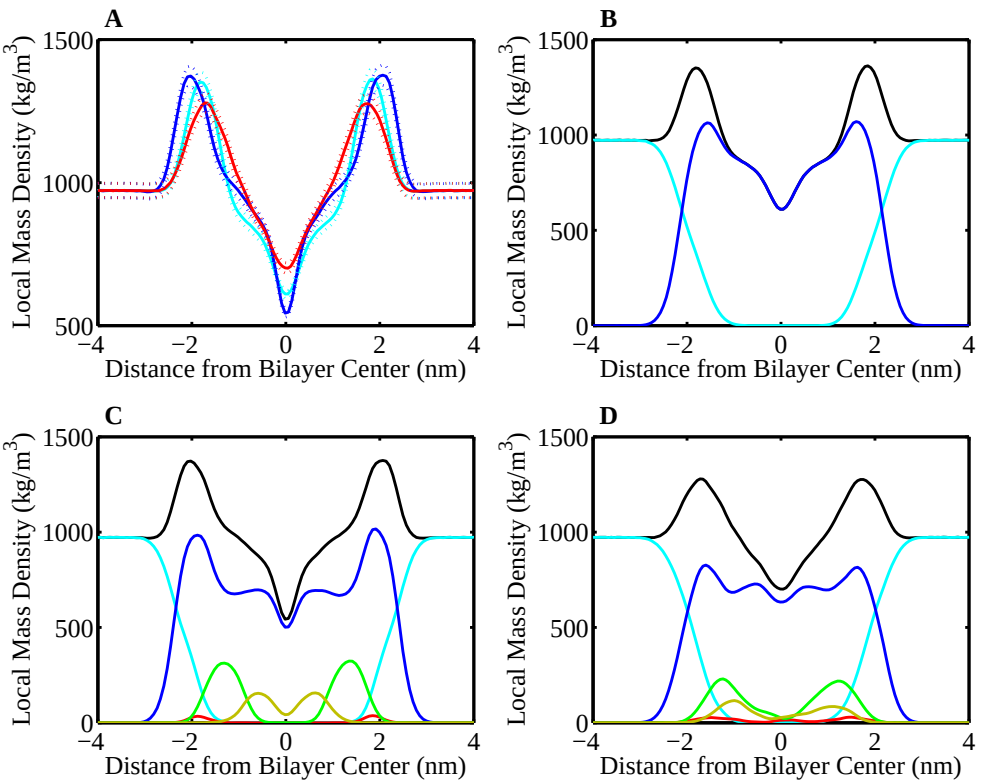

Figure 2.5: Mass density profiles of POPC bilayers. (A) Total electron density profiles for 256 POPC bilayer systems with 0% sterol (cyan), 30% mole fraction cholesterol (blue), and 30% mole fraction 25-hydroxycholesterol (red). Errors, calculated using a bootstrap sampling method (Sec. 2.2.3), are shown as dotted lines. (B), (C), and (D) Component densities for 0% sterol, 30% cholesterol, and 30% 25-hydroxycholesterol simulations, respectively. Water and ions (cyan), POPC (blue), sterol ring (green), sterol tail (yellow), and sterol hydroxyl groups (red).

due to the additional volume from the sterols themselves and that the differential effects of cholesterol and 25-hydroxycholesterol on total membrane area are compensated by changes in membrane thickness.

2.3.3 Densities

The cross-sectional mass densities of the simulations were calculated by taking each frame and dividing the system into slabs approximately 2 Å thick and calculating the mass density of each slab. These densities are averaged over the 128 ns of equilibrated simulation time. The total mass densities for all three simulations calculated this way are shown in Figure 2.5A. The general density profile is similar for all simulations: a symmetric profile where uniform bulk water density gives way to a strong peak, corresponding to the heavy phospholipid phosphate group, which in turn decays to a value lower than bulk water in the less-populated hydrophobic interior of the bilayer. The major effect of sterols on the total mass density profiles is seen

in the peak locations. In particular the peak-to-peak distance between the two largest peaks in the total mass density is 37 Å in the pure POPC bilayer, 41 Å in the cholesterol/POPC system, and 34 Å in the oxysterol/POPC system. The increased thickness of the cholesterol-containing bilayer is similar to that seen experimentally [56]; this increased and the decreased thickness of the oxysterol-containing bilayer are consistent with our observation of compensatory area and volume changes resulting in small overall volume differences between the two sterol-containing systems.

We also evaluated the contributions of the membrane components to the total mass density, examining the mass density profiles of water, POPC, and the sterol ring, tail and hydroxyls (Figures 2.5B, 2.5C, and 2.5D). Of particular interest is the correlation between the location of sterol density and its effect on POPC density. While the total density profiles are largely similar (Figure 2.5A), the component profiles change quite substantially, with shift of POPC density towards the bilayer center when sterols are present. This phenomenon is pronounced in the oxysterol simulation, and implies a displacement effect of sterols; by integrating themselves into the bilayer, they shift POPC density into other regions. Information about sterol organization can also be obtained from these component densities: the cholesterol density is quite ordered, with hydroxyl density furthest out, followed by ring, then tail density. Oxysterol density, on the other hand, shows significant overlap and spread, suggesting less ordered orientations.

2.3.4 Membrane Mechanical Properties

Mechanical properties of the membrane such as bending modulus, area compressibility, and volume compressibility, were also calculated. Bending moduli are evaluated as previously established [21,76,121]. Briefly, the height of each lipid is defined by the position of the first phospholipid glycerol carbon. The height of an evenly spaced grid of ≈5 Å was then fit based on the lipid positions. The undulatory motion of the system was estimated by taking the average of the top and bottom leaflet heights. The square of the 2-dimensional Fourier transform of the undulatory height grid was calculated, giving the spectral intensity at a given x-axis wavenumber m and y-axis wavenumber n. The 1-dimensional undulation mode spectrum was calculated by reducing m and n into a single wavenumber q:

$$q = 2\pi\sqrt{\left(\frac{m}{L_x}\right)^2 + \left(\frac{n}{L_y}\right)^2}. \tag{2.1}$$

Under conditions where the thickness of a bilayer is significantly smaller than the area, membrane mechanics can be modeled as an elastic sheet. At the zero surface tension conditions of our simulations, the relationship

Table 2.1: The results of linear regression on the logarithm of spectral intensity versus the logarithm of wavenumber (Eq. 2.2). Errors are calculated from the linear regression to the data using standard techniques [107].

System	Slope	Intercept	Pearson's R^2
No sterol	-4.06±0.09	-2.81±0.07	98.5%
Cholesterol	-4.09±0.13	-2.85±0.09	97.2%
Oxysterol	-4.09±0.14	-2.78±0.09	97.1%

between spectral intensity and wavenumber can be described as

$$\log(\langle u^2(q)\rangle) = -\log(\beta\langle A_{box}\rangle K_{bending}) - 4\log(\langle q\rangle), \tag{2.2}$$

where $u^2(q)$ is the spectral intensity at a given wavenumber q, β is the inverse thermal energy $1/k_BT$, and A_{box} the system area [21, 76, 121]. By performing a linear regression of $\log(\langle u^2(q)\rangle)$ and $\log(\langle q\rangle)$ over the trajectories, we can confirm that our system behaves quartically in $\langle q\rangle$ and thus that the elastic sheet model is valid over the scales we simulate. As shown in Table 2.1, these regressions give slopes not significantly different than -4.00, showing that the undulation intensity scales as expected to $\sim q^{-4}$. The bending modulus can be determined from the total spectral intensity as follows [21, 76, 121]:

$$K_{bending} \approx \frac{\langle A_{box}\rangle}{257\beta\left\langle\sum_q u^2(q)\right\rangle}. \tag{2.3}$$

The results of these calculations are shown in Figure 2.6A. The experimentally determined bending modulus for pure POPC membranes is 8.5 $\times$ 10^{-20} J [87], thus our calculated bending moduli are within a factor of 2 of the experimental values, similar to that seen in previous lipid simulations [121]. We see a small but significant increase in bending modulus upon the addition of cholesterol to the membrane, consistent with experimental results [85,86]. 25-hydroxycholesterol, however, has the opposite effect of lowering the bending modulus These changes in bending modulus mean that 25-hydroxycholesterol-containing bilayers are slightly easier to bend than pure POPC bilayers, while cholesterol makes the membrane more resistant to bending.

The area and volume compressibilities of a system can be calculated from the fluctuations in the total system area or volume by [32, 44, 121]:

$$K_{area} = \frac{\langle A_{box}\rangle}{\beta\sigma_A^2}. \tag{2.4}$$

$$K_{volume} = \frac{\langle V_{membrane}\rangle}{\beta\sigma_V^2}. \tag{2.5}$$

Using the projected area of the system (Figure 2.2A), the area compressibilities of our systems (Figure 2.6B), are calculated to be 320 ± 100, 1250 ± 370, and 870 ± 210 mN m^{-1} for the sterol-free, cholesterol, and

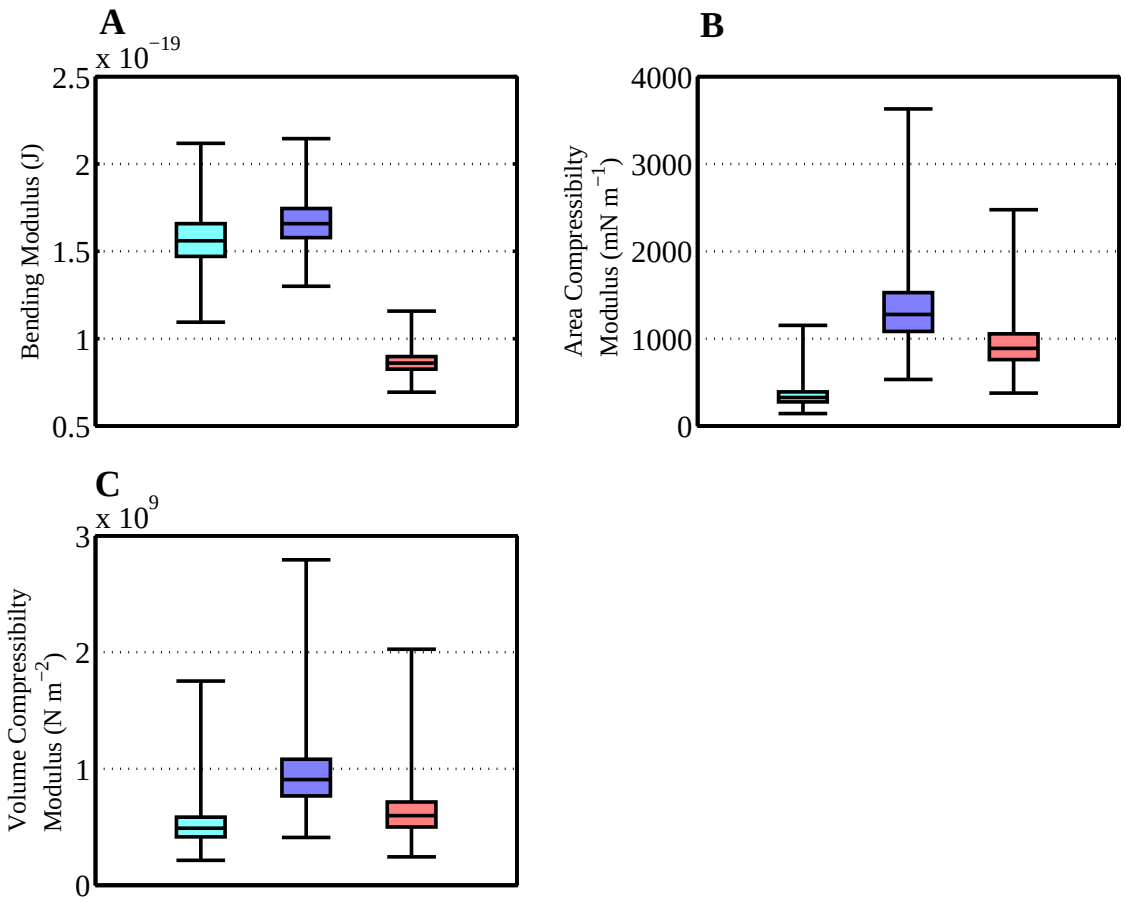

Figure 2.6: Calculated bulk membrane properties of our pure POPC (cyan), mixed POPC/cholesterol (blue), and mixed POPC/oxysterol (red) membranes. All errors were calculated using the bootstrap method described in Sec. 2.2.3. Box-and-whiskers plots are shown for bootstrapped distributions of calculated bulk membrane properties. The central box shows the interquartile range and median of the distribution, while the whiskers show the full range of calculated values. Membrane-to-membrane comparison of calculated properties are significant with p-values $< 0.1\%$ for all properties and membrane comparisons. (A) The bending modulus of the bilayers, calculated from the total power in the undulation spectrum as described in the text. (B) The area compressibility of the bilayers, calculated from the size of fluctuations in total system area. (C) The volume compressibility of the bilayer, calculated from the size of fluctuations in total system volume.

oxysterol simulations, respectively. The value for the sterol-free system is reasonably close to the experimental value for pure POPC membranes of 278 mN m^{-1} [87]. Cholesterol has been previously shown to increase the area compressibility modulus [93] in a manner consistent with our results. Compared to cholesterol, 25-hydroxycholesterol has a smaller but significant effect on the area compressibility. Volume compressibility moduli can be calculated the same way, from fluctuations in the total system volume as shown in Figure 2.4. Results are shown in Figure 2.6C, and behave similarly to the area compressibility moduli, with sterols increasing the compressibility modulus and 25-hydroxycholesterol having a smaller effect than cholesterol.

2.3.5 Lipid Structure

The tail order of membrane component lipids can be used to measure the ordering of the lipid acyl chains in the bilayer and provide a convenient comparison with experimental carbon deuterium order parameters measured by NMR spectroscopy [116]. Lipid order is normally characterized by the order parameter tensor for each tail atom i: [25, 104, 121]:

$$S_{\alpha\beta}(i) = \frac{1}{2}\left\langle 3\cos\theta_\alpha(i)\cos\theta_\beta(i) - \delta_{\alpha\beta}\right\rangle, \tag{2.6}$$

where $\alpha, \beta = x, y, z$ and $\theta_\alpha(i)$ is the angle between the z-axis and the α^{th} axis of the ith atom. In particular, $\theta_z(i)$ is estimated by the angle between the vector pointing from the $(i+1)$th atom to the $(i-1)$th atom and the z-axis. The experimentally relevant deuterium order parameter is related by $S_{CD}(i) = -\frac{1}{2}S_{zz}$ and we present $|S_{CD}|$ for closer comparison with experiment. Larger numbers indicate a more ordered orientation, with increased alignment of the chain at that position along the bilayer normal axis, while smaller numbers indicate a more disordered orientation. This analysis was applied to the atoms of the oleoyl unsaturated and palmitoyl saturated chains of POPC in the three simulations. The average results across all lipids in our simulations are shown in Figure 2.7. We see, as has been observed in other simulations, an increase in POPC tail order in the mixed cholesterol/POPC simulation as compared with the pure POPC simulation for all tail atoms except those directly around the double bond in the unsaturated oleoyl tail [100]. This has been attributed to packing of the phospholipid tails around the rigid cholesterol ring structure [41]. The effect of 25-hydroxycholesterol on POPC tail order is more ambiguous, with an moderate ordering of tail atoms near the head group region transitioning to a slight disordering of tail atoms away from the head groups.

Hydrogen bonding patterns among lipids were analyzed as well. Hydrogen bonds were defined based on geometric criteria among all potential acceptor (A), donor (D), and hydrogen (H) atoms: the acceptor-donor distance r_{AD}, the acceptor-hydrogen distance r_{AH}, and the angle formed by the hydrogen, donor, and

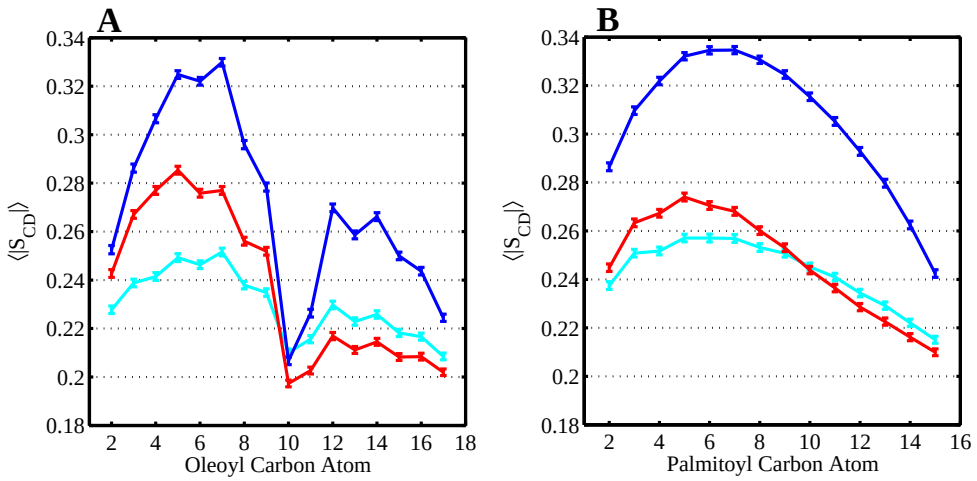

Figure 2.7: The mean tail order parameters for atoms in the oleoyl unsaturated chain of POPC (A) and the palmitoyl saturated chain of POPC (B). Order parameters for the pure POPC bilayer shown in cyan, the mixed POPC/cholesterol bilayer in blue, and the mixed POPC/oxysterol bilayer in red. Smaller atom indices are closer to the POPC headgroup. Errors calculated using a bootstrap method.

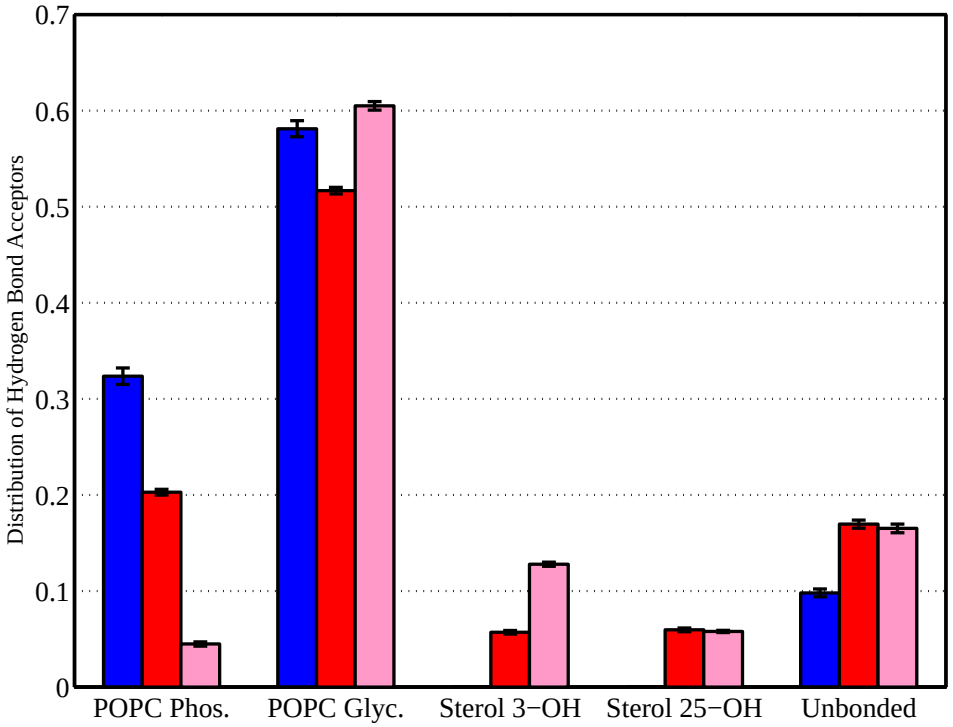

Figure 2.8: Hydrogen bonding distributions for sterol hydroxyl groups, shown as a fraction of sterol hydroxyls bonded to specific hydrogen bond acceptors. Hydrogen bond distributions of cholesterol 3-hydroxyl are shown in blue, oxycholesterol 3-hydroxyl in red, and oxycholesterol 25-hydroxyl in pink. The non-bonded category includes hydroxyl groups with no hydrogen bonds at all as well as those only bound to water. Errors are calculated using the bootstrap method described in Section 2.2.3.

acceptor atoms θ_{HDA}. When $r_{AD} < 3.4$ Å, $r_{AH} < 2.425$ Å, and $\theta_{HDA} < 30.0°$, the interaction is defined as a hydrogen bond [42, 80]. Of the lipids, the only potential hydrogen bond donors are the sterol hydroxyl groups, while both the sterol hydroxyl groups as well as POPC phosphate and glycerol groups can accept hydrogen bonds.

Each sterol hydroxyl group was analyzed to determine which of these potential partners it is bonded with, and total distributions calculated. The equilibrium distributions for the sterol simulations are shown in Figure 2.8. Hydrogen bonds between membrane components and waters were not considered; thus, molecules which hydrogen bond only to water are counted in the "unbonded" category. The cholesterol hydroxyl group is mostly bound to POPC, and about twice as likely to be bound to a POPC glycerol oxygen as to a POPC phosphate oxygen. Only about 10% of cholesterols were unbound or bound to only water. A negligible fraction of cholesterol hydroxyl groups hydrogen bonded to other cholesterol molecules. The oxycholesterol 3-hydroxyl group shows reduced propensity for POPC bonding. This compound has an increased likelihood to remain unbound from lipid or to form sterol-sterol hydrogen bonds. The 25-hydroxyl group at the end of the tail shows similar sterol-sterol hydrogen bond formation. An examination of the bilayer structures reveals that these sterol-sterol hydrogen bonds are often found as clusters of 2 to 4 sterols in the hydrophobic center of the bilayer. These clusters may have relevance for the increase in membrane permeability to polar and charged molecules observed upon addition of 25-hydroxycholesterol [49, 125].

We also performed radial distribution function calculations between the C9 atom of the POPC oleoyl chain and the C18 β-methyl atom of the sterols in a manner similar to Pandit *et al.* for cholesterol [101]. Plots of these distribution functions are shown in the Appendix, Section 6.1.5. There are two distinct peaks corresponding to packing of the oleoyl chain around the rough and smooth faces of the sterols. The oleoyl chains of POPC appear to pack evenly around both faces of cholesterol, while there is a slight bias towards packing of the unsaturated chains around the smooth rather than the rough face of 25-hydroxycholesterol.

2.3.6 Sterol Orientation and Organization

In order to investigate whether the distributions of sterol orientations within the membrane bilayer are related to the differential effects of sterols on membrane and lipid properties, we require a method to define sterol orientation. This is done with a series of Euler angles [69], shown in Figure 2.9. First, molecular axes are defined. The ring Z axis is defined from carbon 13 to carbon 3, pointing towards the head of the sterol along the ring structure. The ring X axis is defined from carbon 10 to 19, pointing outwards along the protruding methyl groups on one face of the ring. Finally, the tail Y axis is defined from carbon 25 to 17, from the end of the tail to the beginning.

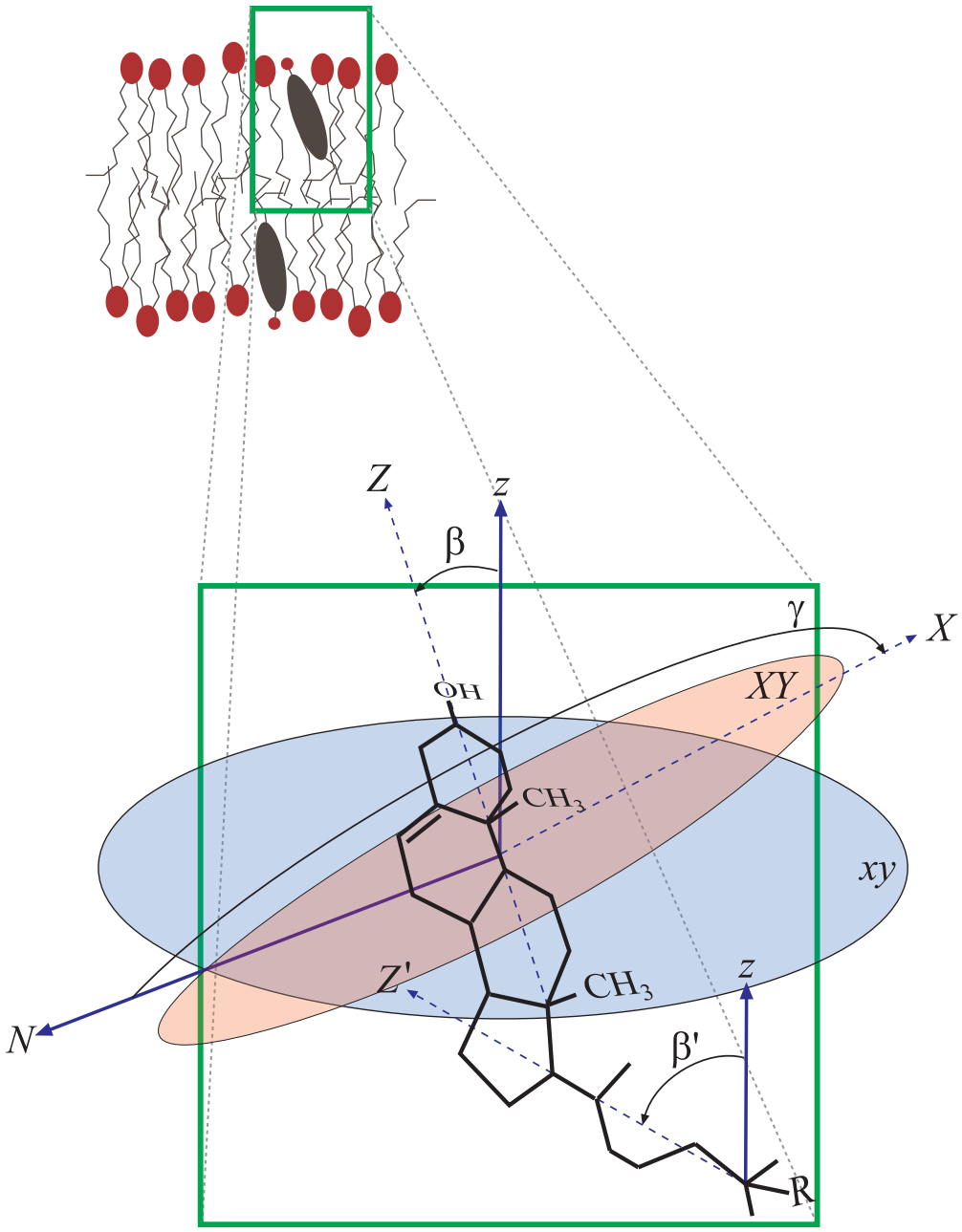

Figure 2.9: A diagram showing the methods by which individual sterol orientation is defined using Euler angles relating molecular axes of the sterol to reference axes of the bilayer as a whole. The reference z axis is defined along the membrane normal, while the reference xy is the plane of the bilayer. A molecular ring axis Z is defined from carbon 13 to 3 along the length of the ring, and a molecular tail axis Z' is defined from carbon 25 to 17 along the length of the tail. Finally, a ring normal axis X is defined from carbon 10 to 19, outward through the protruding methyl groups. Three Euler angles are then calculated. The sterol ring tilt β is defined as the angle between the reference z-axis and sterol ring Z-axis, the sterol ring twist γ is defined as the angle between the intersection N of the reference xy plane and sterol ring XY plane and the sterol ring X axis, and the sterol tail tilt β' is defined as the angle between the reference z-axis and sterol tail Z'-axis.

Euler angles defining the orientation of the sterol can be calculated using these molecular axes and their relationship to the reference bilayer axes (the box axes in the top leaflet, the negative of the box axes in the bottom leaflet). The ring tilt β is defined as the angle between the reference z axis and the sterol ring Z axis, and varies from 0° to 180°, where 0° indicates a parallel orientation, with the ring aligned so that the head points out of the bilayer and the tail inside, and 180° indicates an antiparallel orientation, with the head pointing inside the bilayer. The ring twist γ is defined as the angle between the sterol ring X axis and the reference xy plane, measured along the ring XY plane. This twist varies from -180° to 180°, where 90° indicates the sterol lying with the rough face facing out of the bilayer and -90° indicates the sterol lying with the rough face facing into the bilayer. Finally, the sterol tail tilt β; is defined as the angle between the reference z axis and the sterol tail Z'-axis, varying, as with the sterol ring tilt, from 0° to 180°. In addition to these angles, we also calculated an average ring height, as the mean distance of carbon 13 and 3 from the bilayer center.

The orientation of each sterol in each frame of the equilibrated region of our systems was analyzed and combined into a multidimensional orientation distribution for both cholesterol and 25-hydroxycholesterol. Contour plots of 2-dimensional slices through these distributions are shown for cholesterol in Figure 2.10 and for 25-hydroxycholesterol in Figure 2.11.

The cholesterol distribution contours show a relatively tight distribution. All parameters other than the ring twist are sharply peaked: ring tilt at $\approx$ 20°, ring height at $\approx$ 1.4 Å, and tail tilt at $\approx$ 20°. Ring twist does show a wider distribution, though with a definite peak at -120°. The main peak of the distribution corresponds to a sterol fully extended in the bilayer with the tail stretched out along the same angle as the rigid ring (Figure 2.12A).

The distribution of 25-hydroxycholesterol orientation is much more complicated. To aid with visualization, a variety of representative oxysterol orientations are shown in Figure 2.13. The orientations of oxysterols depicted in Figure 2.13 are marked on the distribution shown in Figure 2.11. Figure 2.11C plots height versus ring tilt and shows two distinct populations of molecules, one with ring tilts of about 20° to 70° and large ring heights of $\approx$ 1.0 - 1.5 Å, and another smaller population of ring tilts $\approx$ 150° and heights of $\approx$ 0 - 0.5 Å. The first population corresponds to normally-oriented sterols with rings tilted towards the bilayer interface and tails in the bilayer interior. The second population corresponds to inverted sterols with rings in the bilayer interior and the tails oriented towards the bilayer interface. Figure 2.11D, shows the relative orientation of the tail with respect to the ring. This figure includes the same inverted (in the top right corner) and normal (in the bottom left corner) orientations, but also indicates that the normally-oriented sterol distribution has a generally-larger tail than the ring tilt. We observe that many of the sterols adopt

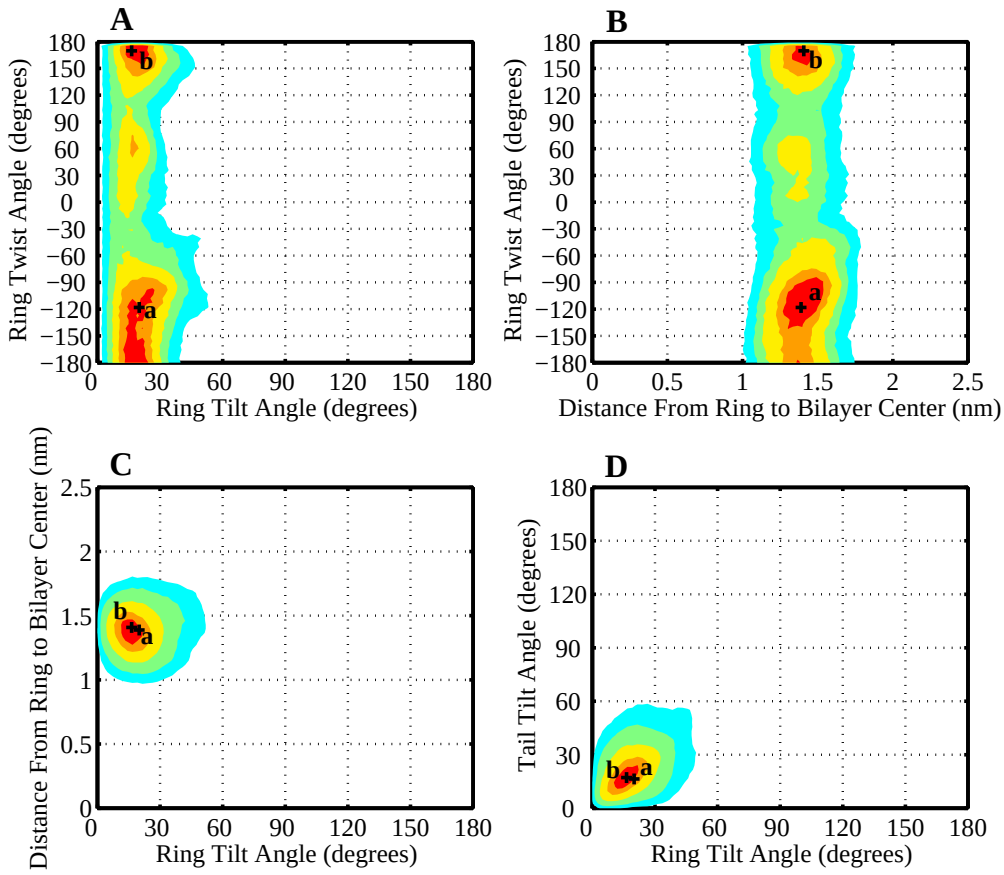

Figure 2.10: A contour plot showing the distribution of cholesterol orientations in mixed POPC/cholesterol bilayers. Regions containing the densest 10%, 25%, 50%, 75%, and 90% of the total probability density are shown by areas of red, orange, yellow, green, and cyan respectively. (A) Ring tilt β vs. ring twist γ. (B) Ring tilt β vs. ring height, calculated as the average distance of carbons 3 and 13 from the bilayer center. (C) Ring height vs. ring twist γ. (D) Ring tilt β vs. tail tilt β'. Labelled crosses show the orientations of the specific sterol molecules depicted in Figure 2.12.

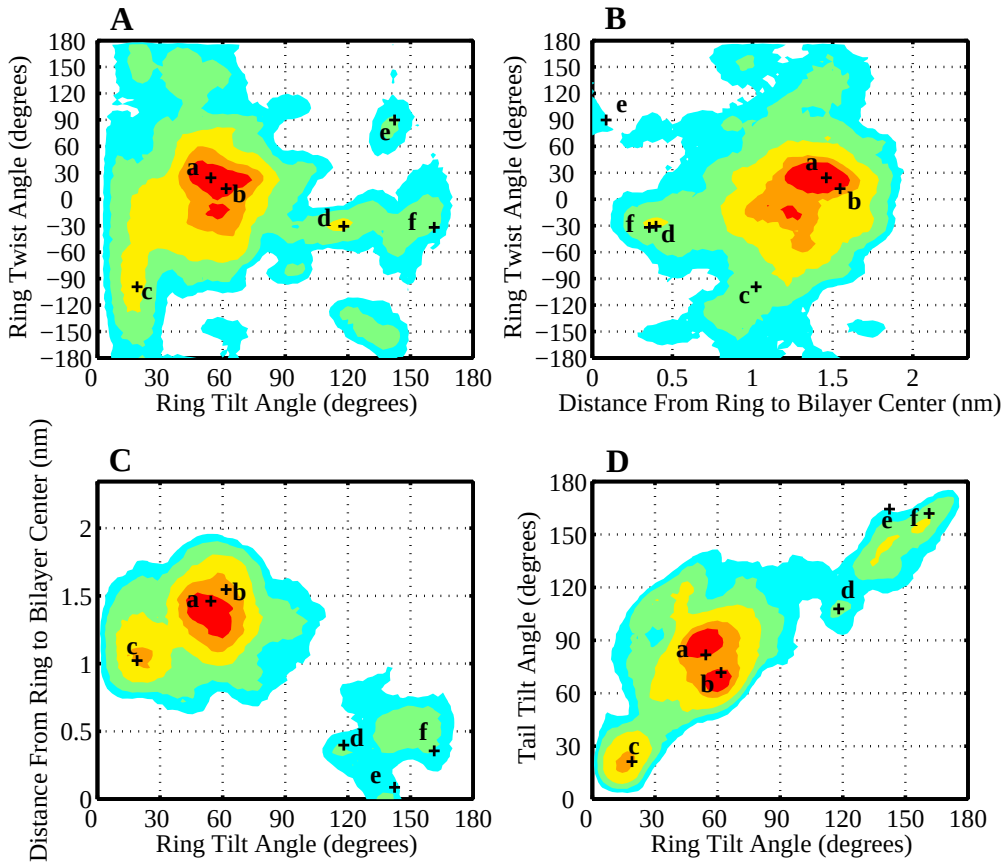

Figure 2.11: A contour plot as in Figure 2.10 showing the distribution of 25-hydroxycholesterol orientations in mixed POPC/oxysterol bilayers. Regions containing the densest 10%, 25%, 50%, 75%, and 90% of the total probability density are shown by areas of red, orange, yellow, green, and cyan respectively. (A) Ring tilt β vs. ring twist γ. (B) Ring tilt β vs. ring height, calculated as the average distance of carbons 3 and 13 from the bilayer center. (C) Ring height vs. ring twist γ. (D) Ring tilt β vs. tail tilt β'. Labelled crosses show the orientations of the specific sterol molecules depicted in Figure 2.13.

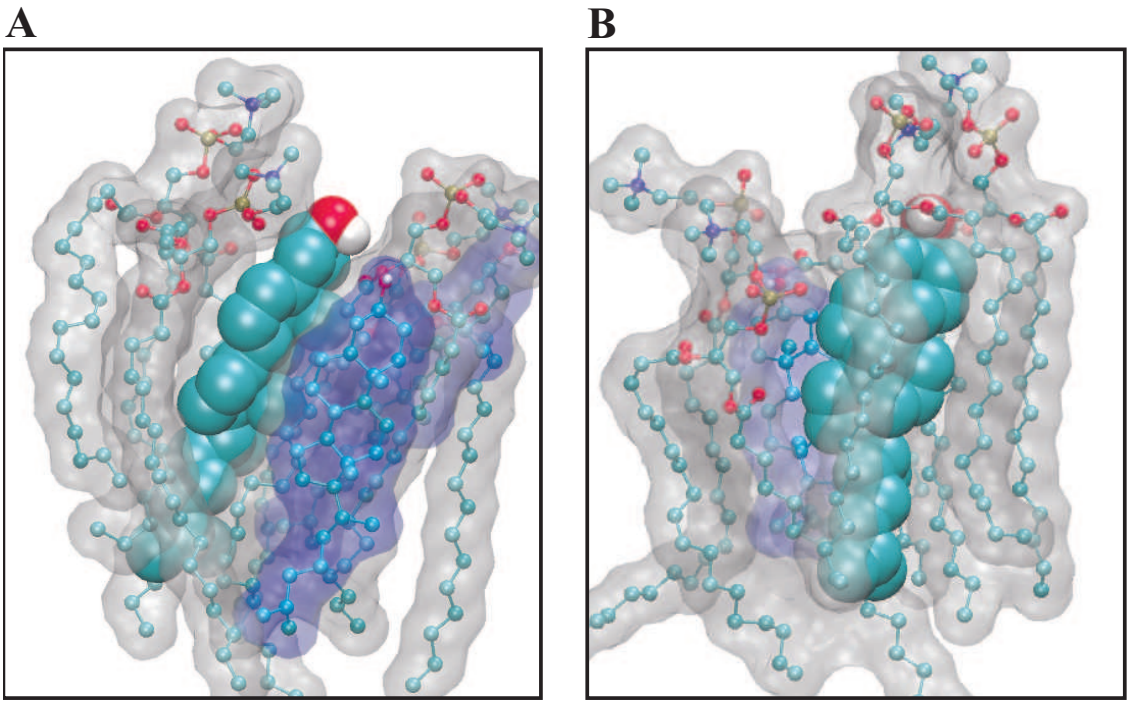

Figure 2.12: Depiction of cholesterol molecules from our molecular dynamics simulations. The cholesterol of interest is shown as a space-filling model, while nearby POPC molecules as ball-and-stick models with a gray molecular surface and nearby cholesterol molecules shown as ball-and-stick models with a blue molecular surface. Each subfigure shows a section from a single leaflet of the bilayer, with the lipid/water interface at the top of the figure. The sterol labels (A) through (B) correspond to the marked orientations shown in Figure 2.10.

an orientation in which one of their hydroxyl groups is buried in the bilayer interior form hydrogen bond interactions with other such buried sterol hydroxyl groups, forming clusters of polar hydroxyl groups in the hydrophobic interior of the membrane.

2.4 Discussion

We observe significant changes in the bulk properties of POPC membranes when relatively high concentrations of cholesterol or 25-hydroxycholesterol are added. Most obviously, the membrane volumes and areas increase upon the addition of these sterols. However, while the volume increase is similar in both sterol systems, the area increase is much larger for membranes containing 25-hydroxycholesterol as compared to cholesterol. We attribute the observed volume increases to the direct effects of additional sterol volume, which is largely the same between the two sterols. The large difference in area effects by these sterols suggest that they have altered interaction with the POPC lipids, and that indirect effects of sterols on POPC structure contribute to these changes. Examination of membrane density profiles shows that the choles-

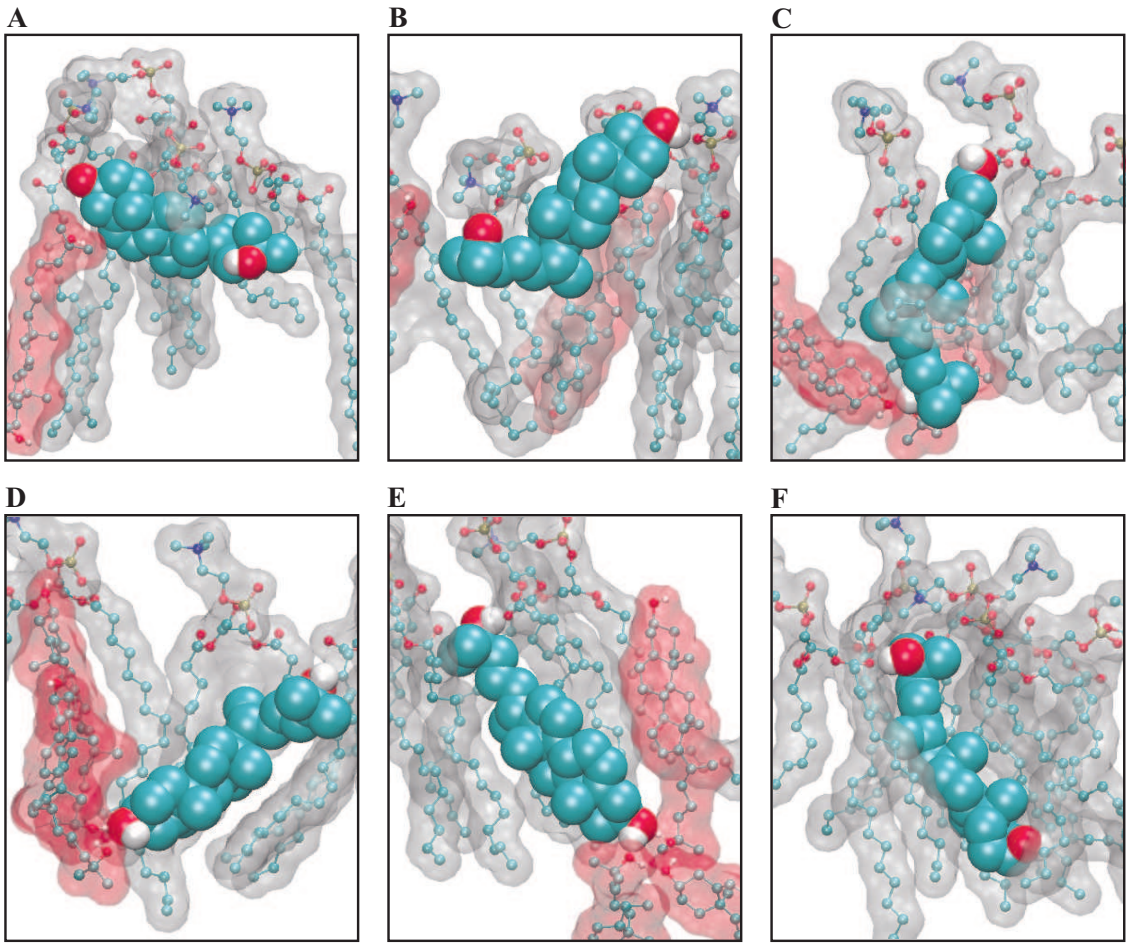

Figure 2.13: Depiction of 25-hydroxycholesterol molecules from our molecular dynamics simulations. The 25-hydroxycholesterol of interest is shown as a space-filling model, while nearby POPC molecules as ball-and-stick models with a gray molecular surface and nearby 25-hydroxycholesterol molecules shown as ball-and-stick models with a red molecular surface. Each subfigure shows a section from a single leaflet of the bilayer, with the lipid/water interface at the top of the figure. The sterol labels (A) through (F) correspond to the marked orientations shown in Figure 2.11.

terol system has thickened with respect to the sterol-free system, while the 25-hydroxycholesterol system has thinned. Cholesterol, as has been previously observed both in simulation and experiment [29,48,56,108,129], condenses and thickens membranes. On the other hand, we show 25-hydroxycholesterol to have an opposing effect, expanding the membrane laterally and thinning it. In addition to changes in gross membrane dimensions, the membrane's mechanical properties are altered. Sterol-containing systems show less resistance to bending, with a corresponding increase in membrane undulations. These systems also show increased volume and area compressibility modulus, making them more difficult to compress and with smaller area and volume fluctuations. In all of these mechanical properties, oxysterol-containing membranes show a larger deviation from pure phospholipid membranes than cholesterol-containing membranes.

The bulk membrane changes induced by cholesterol and 25-hydroxycholesterol necessarily have their roots in the altered molecular structure of the membranes, both through perturbations in POPC structure as well as addition of new molecules forming sterol-POPC interactions. Solvent-accessible surface area calculations for POPC show that POPC has a smaller surface area in cholesterol-containing membranes, while POPC in 25-hydroxycholesterol-containing membranes has a much larger surface area. These differences suggest a compression of POPC by cholesterol and an expansion by 25-hydroxycholesterol. Calculated POPC order parameters are consistent with this observation: cholesterol orders POPC acyl tails while 25-hydroxycholesterol has both ordering and disordering effects, with ordering dominant near the head group, and disordering dominant near the end of the tails. Looking at differences in sterol structure, we examined hydrogen bonding patterns for the sterol hydroxyl groups. Cholesterol engages in almost no cholesterol-cholesterol hydrogen bonding, preferring to hydrogen bond to the POPC headgroup. However, 25-hydroxycholesterol shows significant levels of sterol-sterol hydrogen bonding, with reduced sterol-POPC bonding. These hydrogen bonding patterns are rooted in the different orientations of sterols within the membrane bilayer.

We defined these sterol orientations with respect to the membrane normal axis and found that, while cholesterol was overwhelmingly found in a single orientation roughly parallel to the phospholipid tails, 25-hydroxycholesterol was found in a very wide range of orientations. Cholesterol adopts an orientation with its steroid ring at a slight tilt to the membrane normal axis and its iso-octyl tail fully extended into the center of the bilayer (Fig. 2.10 a and b). While this orientation is accessible to 25-hydroxycholesterol (Fig. 2.11c), only a small fraction of 25-hydroxycholesterol molecules are found in that orientation. This cholesterol-like orientation is presumably disfavored for the oxysterol because the 25-hydroxyl group would then be buried in the non-polar center of the bilayer with few hydrogen bonding partners. The preferred orientation for 25-hydroxycholesterol is, instead, with a relatively deep ring tilt of about 60° and the iso-octyl tail with its

hydroxyl group bent up towards the hydrophilic interfacial layer (Fig. 2.11 a and b). This orientation allows both hydroxyl groups to avoid the hydrophobic bilayer interior. Also accessible are inverted orientations, with the steroid rings buried in the bilayer interior and the iso-octyl tails extending into the interfacial layer (Fig. 2.11 d, e, and f).

The orientations of cholesterol and 25-hydroxycholesterol are relevant to the effects observed on bulk membrane and phospholipid properties. The parallel alignment of the rigid cholesterol ring in bilayer has been thought to order nearby phospholipid tails by inducing them to stretch out along its rigid structure [41]. This effect can not only produce the increased POPC order parameters we observe but also changes the thickness, density, and melting point of cholesterol-containing bilayers [56, 108, 129]. 25-hydroxycholesterol however, does not align neatly in the bilayer, but instead adopts a diverse array of orientations which cause it to have a more chaotic, disordering effect.

Given the varied responses of cells to oxysterols it seems appropriate to consider the possible consequences for oxysterol addition to membranes on membrane proteins. The change in membrane thickness and the disorder of the aliphatic chains are prominent effects observed in our simulations. Hydrophobic matching is a major mechanism of protein-membrane interaction and this has been proposed as one important role for cholesterols in biological membranes [83,91]. The difference we see between the cholesterol membrane and the oxysterol membrane represents a dramatic change in the hydrophobic matching region for many proteins [84, 88]. In addition, oxysterol-related changes in aliphatic chain order would be expected to influence the mobility of transmembrane portions of membrane transporters, channels and transmembrane receptors/signaling complexes [75, 134].

2.5 Conclusions

The change in cholesterol from an amphiphilic to bisamphiphilic character by the addition of the 25-hydroxyl group changes the energy landscape of orientational space. Specific regions of the space are disfavored, including the aligned cholesterol orientation, while other regions are favored, shifting the distribution of molecular orientations. We predict that the occupancy of these different regions of orientational space is what drives the biophysical effects observed on phospholipid membranes. In particular, the 25-hydroxyl group preferentially biases the molecule towards regions of orientational space that increase bilayer area and affect lipid order.

We can make predictions about how these sterols may interact with membranes of different lipid composition as well. Saturated lipids such as DPPC have more ordered lipid chains and thus the presence of

these lipids should promote more ordered and extended orientations of sterols, similar to those preferred by cholesterol. Unsaturated lipids or polyunsaturated lipids such as DOPC, however, have more disordered tail chains that will disfavor ordered sterol orientations and shift the equilibrium towards the tilted and clustered orientations observed in our 25-hydroxycholesterol simulation. These expected changes in the energies of various orientations would then show their effects in the perturbation of membrane structure by sterols, with cholesterol having stronger condensing effects on unsaturated lipids and 25-hydroxycholesterol conversely showing stronger expansive effects on saturated lipids. These different lipid sensitivities have been observed in a recent study examining the area expansive effects of 25-hydroxycholesterol on lipid bilayers [36]. Unsaturated DOPC membranes showed a larger area increase than POPC membranes upon the addition of 25-hydroxycholesterol, while DPPC membranes showed relatively little change.

25-hydroxycholesterol has previously been shown to increase the permeability of membranes to ions and small osmolytes [49,63,125]. Our understanding of how this sterol perturbs membrane structure suggests two potential mechanisms for this permeability. Firstly, the oxysterol directly thins the membrane. Secondly, the orientations of these sterols produces clusters of hydrogen-bonded hydroxyl groups in the hydrophobic interior of the bilayer. These hydroxyl clusters would allow limited hydrogen bonding interactions with polar molecules traversing the membrane, lowering the energy barrier to permeation. This mechanism is currently being tested in ongoing simulations.

These structural effects of 25-hydroxycholesterol on lipid membranes have biological relevance. A recent study has shown that the effects of 25-hydroxycholesterol on cellular cholesterol homeostasis are not enantioselective; the enantiomer of 25-hydroxycholesterol has identical effects on membrane biophysical properties and suppression of the cholesterol synthetic pathway [36]. This lack of stereospecificity suggests that 25-hydroxycholesterol does not act in this pathway through protein binding but rather that the signal is transduced through perturbation of the membrane, potentially through some of the mechanisms we have observed. This result reveals the role of the membrane in mediating signal cascades, and suggests that the biological effects of not only 25-hydroxycholesterol but potentially other signaling molecules as well may be effected through their perturbation of membrane structure.

Chapter 3

Interactions Between 25-Hydroxycholesterol and Cholesterol in POPC Bilayers

Abstract

Oxysterols are oxidation products of cholesterol that play major roles in mediating cholesterol homeostasis. Recent work has shown that oxysterols can change membrane structure in very different ways from cholesterol, suggesting a possible mechanism for how oxysterols regulate cholesterol homeostasis. Here we extend our previous work, using molecular dynamics simulations of 25-hydroxycholesterol (25-HC) and cholesterol mixtures in 1-palmitoyl-2-oleoyl-phosphatidylcholine (POPC) bilayers to examine interactions between 25-HC and cholesterol in the same bilayer. When added to cholesterol-containing membranes, 25-HC causes larger changes in membrane structure than when added to cholesterol-free membranes, demonstrating interactions between the two sterols. We also find that the presence of 25-HC changes the position, orientation, and solvent accessibility of cholesterol, shifting it into the water interface and making it more available to external acceptors. This is consistent with experimental results showing that oxysterols can trigger cholesterol trafficking from the plasma membrane to the ER. These interactions provide a potential mechanism for 25-HC regulation of cholesterol trafficking and homeostasis through direct modulation of cholesterol availability.

3.1 Introduction

Biological membranes are primarily composed of phospholipids, which provide the membrane's basic physical structure. However, other molecules, most notably proteins and sterols, serve to modulate membrane behavior. Cholesterol is the most prominent sterol in mammalian membranes, with some membranes containing up to 50% cholesterol [96,128]. Cholesterol is distributed asymmetrically within cells, with the plasma membrane containing a much higher concentration than internal membranes such as the endoplasmic reticulum (ER) and Golgi [78,96,128]. Cholesterol is required by all mammalian cells, and serves multiple functions: it regulates protein behavior through direct binding to sterol-sensing domains [13,27,68], it serves as a precursor for steroid hormone and bile acid synthesis [15], and it promotes the formation of lipid rafts [23,59]. In addition to the direct effects of cholesterol, it is also known to alter the structure and behavior of membranes themselves. Biophysical and simulation studies have shown that, even without forming distinct domains, the addition of cholesterol to membranes decreases membrane fluidity while increasing membrane thickness, bending modulus, and lipid order [26,56,86,94,108,129]. These indirect effects are also known to influence cellular behavior: increases in membrane thickness caused by high levels of cholesterol are thought to help sort membrane proteins between the plasma membrane and the ER [79], and membrane structural changes can alter ion channel properties [90] as well as influence protein signaling [23].

Because of its importance to cellular function, the levels of cholesterol in cellular membranes must be tightly controlled through a process known as cholesterol homeostasis. Control over cholesterol levels is achieved through regulating *de novo* cholesterol synthesis, cholesterol uptake from and efflux to circulating lipoproteins, and esterification of cholesterol through long-term storage [13, 14, 96, 124]. Transcriptional regulation has been shown to act through the sterol regulatory element (SRE), a promoter that can upregulate transcription from a number of genes involved in cholesterol homeostasis, including HMGCoA reductase, the enzyme which performs the rate-limiting step in cholesterol synthesis [39,117]. Activation of the SRE is triggered by cholesterol depletion through a complex series of protein activation events. SREs are activated by a family of transcription factors called SRE binding proteins (SREBPs) [11,52]. SREBPs are transmembrane proteins and, under cholesterol-rich conditions, they are located in the ER, where they form a complex with another transmembrane protein, the SREBP cleavage-activating protein (SCAP) [11,52]. SCAP also binds to ER-resident Insig proteins, and the complete complex is retained in the ER [131,133]. When cholesterol is depleted, the SCAP/Insig complex is disrupted, and the SREBP/SCAP complex migrates to the Golgi [131,133]. In the Golgi, two specific proteases cleave the transcription factor domain of SREBP from its transmembrane domain, freeing it to move to the nucleus and activate transcription [11,52,131,133].

While cholesterol alone can block SREBP maturation, oxysterols such as 25-hydroxycholesterol (25-HC)

and 27-hydroxycholesterol (27-HC) are over 50 times more effective at suppression of SRE activation than cholesterol itself [40, 55]. These oxysterols are also binding partners and activators of the liver X receptor (LXR) transcription factors, which in turn up-regulate the expression of genes involved in cholesterol efflux, offering another role for oxysterols in cholesterol homeostasis [60, 61]. Recent work has shown that, while enantiomeric oxysterols do not activate LXR-responsive elements as natural oxysterols do, they do suppress SRE activation just as effectively as natural oxysterols [36]. Because protein-small molecule interactions are enantiospecific, this suggests that, while oxysterol activation of LXRs is clearly protein-dependent, oxysterol suppression of SREBP cleavage likely does not occur through stereospecific protein-binding events.

Much like cholesterol, oxysterols have biological effects not only through direct protein binding, but also through membrane property changes. However, oxysterols affect membranes very differently than cholesterol. While cholesterol orders phospholipids and condenses membranes, reducing membrane area and permeability, oxysterols increase membrane permeability and area [49, 63, 125]. Recent computational work from our group has shown that molecular dynamics simulations can recapitulate experimentally observed effects of cholesterol and 25-HC on membrane structure [97]. We found that cholesterol and 25-HC orient themselves very differently within membranes, and proposed that these different distributions of orientations were the drivers of sterol effects on membranes [97]. However, the simulations from which we drew these conclusions were necessarily limited, containing membranes composed of only single sterol and phospholipid species. This limits the applicability of these conclusions to biological systems, as 25-HC does not act on single-phospholipid membranes but rather on more complex mixtures. In particular, because 25-HC is enzymatically produced from cholesterol, membranes that contain 25-HC will always contain cholesterol as well. The presence of this cholesterol may change 25-HC behavior by altering the initial structure of the membrane and component phospholipids. Therefore, we chose to extend our earlier work by examining how the presence of cholesterol changes the effect of 25-HC on membranes using membrane mixtures composed of POPC, cholesterol, and 25-HC.

3.2 Methods

3.2.1 Parameters and Structures

Sterol and phospholipid parameters and charges were described in our previous work [97]. To prepare our mixed sterol simulations, four structures were taken from the converged regions of our previously described 256 POPC/112 cholesterol and 256 POPC/112 25-HC simulations: two from the 30% cholesterol system and two from the 30% 25-HC system [97]. Water and ions were first removed from these structures. Next, half

of the cholesterol or 25-HC was removed from each leaflet of all structures. 25-HC or cholesterol molecules, with conformations randomly sampled from the converged simulations, were then inserted into the newly created empty positions, resulting in four bilayers which contained 256 POPC, 56 cholesterol, and 56 25-HC molecules, evenly distributed between leaflets.

These structures could not be used as starting points for simulations because of steric clashes between the newly-inserted molecules and the existing phospholipids and sterols. In order to resolve these clashes, the bilayer was expanded laterally by approximately a factor of 3, resulting in very widely spaced sterols and lipids. This expansion was followed by serial iteration of conjugate-gradient energy minimization and compression in the plane of the bilayer to bring the structures back to near their original sizes but with steric clashes resolved. These final bilayer structures were solvated with 17426 SPC water molecules and 36 K^+ and Cl^- for an approximate molar concentration of 115mM KCl, and used as the starting structures for the 256 POPC and 112 mixed sterol systems.

Low concentration sterol systems with 256 POPC lipids and 56 sterols were prepared as controls. These low concentration systems allow us to directly compare the effect of 56 cholesterol or 56 25-HC in the presence and absence of other sterols. Two structures from the converged region of our previously described 256 POPC/112 cholesterol and 256 POPC/112 25-HC simulations were taken, one from the 30% cholesterol system and one from the 30% 25-HC system, and non-lipid (water and ion) molecules removed. Half of the sterols in each system were randomly removed from each leaflet, resulting in final compositions of 256 POPC lipids and 56 sterols. These bilayers were re-solvated with 15850 SPC water molecules and 33 K^+ and Cl^- for an approximate molar concentration of 115mM KCl, and used as the starting structures for the 256 POPC, 56 sterol systems.

Previously published 256 POPC, 256 POPC/112 cholesterol, and 256 POPC/112 25-HC simulations were also extended to provide further controls for our mixed sterol simulations [97]. A full list of simulations is summarized in Table 3.1.

3.2.2 Simulations

All molecular dynamics (MD) simulations were performed using GROMACS version 3.3.1 or 4.0 [4, 77]. All simulations followed the same molecular dynamics protocol. Conjugate gradient energy minimization was first performed on the initial structures to relax any unfavorable contacts between molecules. The systems were then gradually warmed with a series of 30 ps constant temperature, constant pressure MD simulations from 0 to 300 K in 15 K increments. Production systems were then run from the warmed structures. Anisotropic pressure coupling was applied at 1 bar using the Parrinello-Rahman method with

Table 3.1: A summary of all simulations performed and analyzed in this work.

Composition	# of Initial Simulations	# of Replica Simulations	Cumulative Simulation Time (ns)
256 POPC	1	4	1200
256 POPC, 56 Cholesterol	1	4	1200
256 POPC, 112 Cholesterol	1	4	1200
256 POPC, 56 25-HC	1	4	1200
256 POPC, 112 25-HC	1	4	1200
256 POPC, 56 Cholesterol, 56 25-HC	4	16	4800

a time constant of 1 ps [103]. Temperature coupling was applied independently to lipids and solvent using the Nosé-Hoover algorithm with a time constant of 0.2 ps [51]. Electrostatic interactions were calculated using the particle-mesh Ewald method (PME), with both the direct space PME cutoff and the Lennard-Jones cutoffs set to 1 nm [20]. Constraints were applied to all bonds [29, 102] using the LINCS algorithm incorporated in GROMACS to allow 2 fs timesteps [47]. Initial production simulations were run for 400 ns of total simulation time, as summarized in Table 3.1. In order to obtain better sampling and statistical confidence, replica simulations for each initial simulation were prepared by first taking snapshots from the initial simulations at 150, 200, 250, and 300 ns. These snapshots were taken as the starting point for new systems after resampling particle velocities from a 300K Maxwell-Boltzmann distribution, resulting in independently evolving systems. Each of these replica simulations was run for 200 ns of total simulation time. Snapshots of each simulation were taken every 100 ps for analysis.

3.2.3 Analysis Methods

SASA Calculations

Solvent-accessible surface area (SASA) calculations for our systems were performed with APBS version 1.0.0, using a 1.4 Å radius solvent probe [1]. For these calculations, the systems were stripped of solvent and ion molecules and replicated 3×3 times in the xy plane. To remove edge effects, only the central image of this replicated bilayer was used for analysis. The SASA of each atom in the central structure's lipids in the replicated system was calculated with APBS, and the contributions from each lipid's atoms were summed to obtain a molecular surface area for each lipid.

Density and Depth Calculations

Cross-sectional mass density profiles for our simulations were calculated by first taking each frame of the simulation and centering the center of mass of the bilayer in the middle of the periodic box. The box was then divided into approximately 2Å thick slabs, the mass of all atoms within each slab summed, and the local mass density calculated. This was done for multiple subsets of atoms to obtain separate profiles for phospholipids, solvent, and sterols. Solvent mass density profiles were also used to calculate the positions of the water/bilayer interfaces. The solvent mass density profile for each frame of the simulation was calculated as above and smoothed using a local moving average. The water/bilayer interfaces were considered to be the two points at which the solvent mass density reached 50% of the bulk density value. The interface positions were then used to calculate bilayer thicknesses as the distance between the two interfaces and atomic depths as the distance between an atom and the closest interface.

Hydrogen Bonding Calculations

Hydrogen bonds were calculated using geometric criteria. First all potential acceptor (A), donor (D), and donor hydrogen (H) atoms were identified in solvent and lipid molecules in the simulations. Hydrogen bonds were considered to be present when an acceptor-donor distance was less than 3.4Å, the acceptor-hydrogen distance was less than 2.425Å, and the hydrogen-donor-acceptor angle was less than 30.0°. Of the molecules present in our simulations, the only potential hydrogen bond donors are the sterol hydroxyl groups and solvent molecules, while solvent molecules, sterol hydroxyl groups, as well as POPC phosphate and glycerol groups can accept hydrogen bonds.

Sterol Orientation Calculations

Sterol orientations were calculated by defining molecular axes through the rigid sterol ring and evaluating angles of these molecular axes with respect to reference axes defined by the bilayer plane and normal axis. The molecular Z axis was defined from carbon 13 to carbon 3, thus pointing from the tail towards the head of the sterol through the sterol ring. The molecular X axis was defined from carbon 10 to carbon 19, pointing outwards along the protruding methyl groups on the rough face of the ring, and then orthonormalized with respect to the molecular Z axis. Finally, the molecular Y axis was calculated as the cross product of the orthonormal Z and X axes. Reference axes were taken as either the normalized system axes, for sterols in the top leaflet of the bilayer, or the negative of the system axes, for sterols in the bottom leaflet of the bilayer. This ensures that the reference z axis points out of the leaflet in which the sterol to be analyzed is located. Two angles were calculated to define a sterol orientation. The sterol tilt β was defined as the

angle between the reference z axis and the sterol ring Z axis, and varies from 0 to 180°, where 0° indicates a parallel orientation, with the ring aligned so that the head points out of the bilayer and the tail inside, and 180° indicates an antiparallel orientation, with the head pointing inside the bilayer. The sterol twist γ was defined as the angle between the sterol ring X axis and the reference xy plane, measured along the ring XY plane. The twist varies from -180° to 180°, where 90° indicates the sterol lying with the rough face facing out of the bilayer and -90° indicates the sterol lying with the rough face facing into the bilayer.

Significance Tests

The Kolmogorov-Smirnov (K-S) test is used to compare continuous univariate distributions, such as the distributions of surface areas for a molecule in two different molecular dynamics simulations [107]. These distributions can be converted into cumulative distribution functions $S_N(x)$, where $S_N(x)$ is the fraction of the total distribution that has a value less than x. These $S_N(x)$ are monotonically increasing functions which vary from zero to one over the range of the data. The K-S statistic is simply the ℓ_∞ norm of the difference between two cumulative distribution functions:

$$D = \max_{-\infty<x<\infty} \left| S_{N_1}(x) - S_{N_2}(x) \right|. \tag{3.1}$$

The significance statistic for this test requires calculation of the effective number of data points, N_e:

$$N_e = \frac{N_1 N_2}{N_1 + N_2}, \tag{3.2}$$

where N_1 and N_2 are the number of independent data points in each distribution.

The p-value for significance is [107]:

$$p_{KS} = 2 \sum_{j=1}^{\infty} (-1)^{j-1} e^{-2j^2\lambda^2}, \tag{3.3}$$

where

$$\lambda = D \left(\sqrt{N_e} + 0.12 + \frac{0.11}{\sqrt{N_e}} \right). \tag{3.4}$$

Replica simulations were used to calculate the number of independent data points. For evaluating the statistical significance of differences in whole-membrane properties, each replica simulation was treated as a single independent bilayer conformation, giving 4 independent conformations for all one- and two-component systems and 20 independent conformations for the three-component system. For examining differences in lipid properties, each lipid was treated independently for each simulation.

3.3 Results

3.3.1 Equilibration

Based on examination of the total projected area of each system over time, as well as other metrics including total system energy, we chose to discard the first 100 ns of each initial simulation as "equilibration" time, leaving 300 ns of steady-state simulation time for analysis. Based on similar analyses, 50 ns of each replica simulation was discarded, leaving 150 ns of steady-state simulation time. Therefore, each initial structure produced 900 ns of equilibrium simulation.

3.3.2 Membrane Effects

We began our analyses by examining how cholesterol and 25-HC change membrane structure, individually and in mixtures. We are particularly interested in knowing whether the effects of cholesterol and 25-HC on membranes are independent of each other. In other words, we wish to examine whether the changes induced upon addition of a given amount of 25-HC are the same in membranes containing and lacking cholesterol.

Areas

The simplest membrane structural property to examine is the total membrane area. The projected area of each system is calculated from the periodic system box, taking the product of its size along the x and y axes at each frame of the simulation. Changes in the projected area induced by addition of small molecules can be divided into two effects. First, the added small molecules must take up some area themselves, thus increasing the projected membrane area. Secondly, the added small molecules can alter the structure of the membrane, either through changing the configuration of membrane phospholipids or changing the amount of empty area in the bilayer. This second effect can either increase or decrease the membrane area, depending on the actual effect of the small molecule.

Figure 3.1 shows the range of projected areas obtained for membranes of six different compositions. These are shown as box-and-whisker plots. The central box shows the interquartile range and median of the area distributions, while the whiskers show the minimum and maximum area reached. We first note how concentration changes the marginal effects of cholesterol and 25-HC on projected membrane area. The addition of 56 cholesterol molecules to a 256 POPC bilayer decreases the projected membrane area by 0.2 nm^2, while an additional 56 cholesterol molecules increases it by 2.8 nm^2. Cholesterol is well known [56, 129] to cause condensation of nearby phospholipids, decreasing their per-lipid area. When comparing a pure POPC bilayer with one containing a low concentration of cholesterol, we see an approximate balance

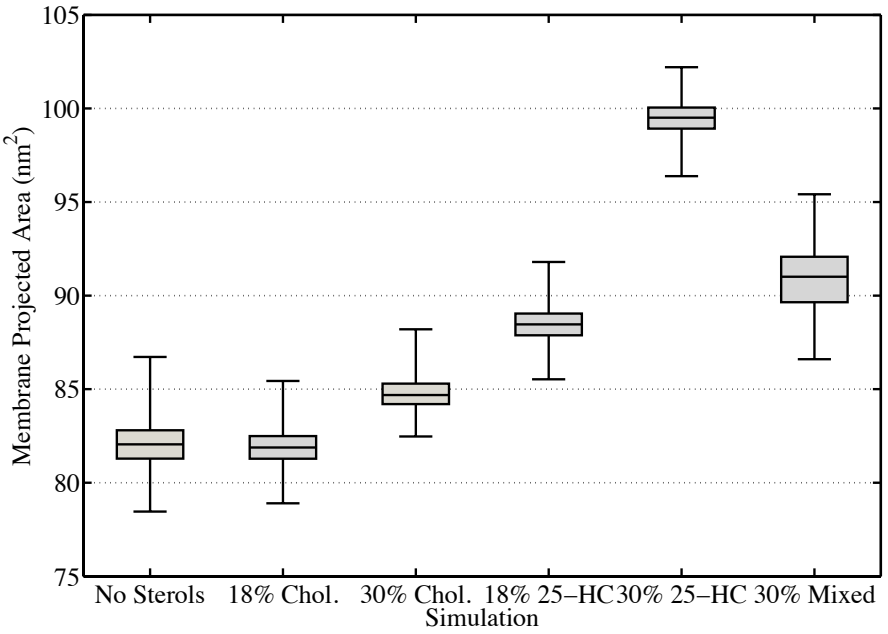

Figure 3.1: Box-and-whisker plots showing the distributions of projected system areas for each set of simulations. Differences between all pairs of distributions are significant at 1% except for those between the pure POPC and 18% cholesterol simulations (not significant) and between the pure POPC and 30% cholesterol simulations (significant at 2%). Median membrane areas are 82.0 nm^2 (pure POPC), 81.9 nm^2 (18% cholesterol), 84.7 nm^2 (30% cholesterol), 88.5 nm^2 (18% 25-HC), 99.5 nm^2 (30% 25-HC), and 91.0 nm^2 (30% mixed sterols).

between this condensation effect and the direct area taken up by the cholesterol molecules themselves, resulting in a small net decrease in projected area. When comparing bilayers containing low and high concentrations of cholesterol, the indirect area-decreasing effect is limited because the phospholipids are already partially condensed in the low cholesterol system and therefore the direct area taken up by the additional cholesterol dominates, resulting in a net increase in projected area. The observed saturation of phospholipid condensation at cholesterol concentrations between 18% and 30% is consistent with previous experimental and simulation results [18, 36, 101]. In the case of 25-HC, we see a more linear response of membrane expansion with increasing oxysterol concentration. The addition of 56 25-HC molecules to the 256 POPC bilayer increases projected membrane area by 6.4 nm^2 and 56 additional 25-HC molecules increases projected membrane area further by 11.0 nm^2. Unlike cholesterol, 25-HC causes area expansion of nearby phospholipids [63, 97]. Therefore the direct and indirect effects of 25-HC on membrane area are not opposed. Instead, both effects increase projected membrane area, resulting in a more linear response.

The mixed sterol simulations show how cholesterol and 25-HC interact. By comparing the mixed sterol system to the 18% 25-HC system, we see that the addition of cholesterol increases projected membrane area by 2.5 nm^2. However, comparing the pure POPC system to the 18% cholesterol system shows that in the absence of 25-HC, the same amount of cholesterol causes a decrease in projected membrane area of 0.2 nm^2. This demonstrates that the presence of 25-HC alters the marginal effect of cholesterol, reducing its ability to condense membrane bilayers. Using similar comparisons to compare the marginal effect of 25-HC, we find that in the absence of cholesterol, 56 25-HC molecules increase projected membrane area by 6.4 nm^2, while adding the same amount of 25-HC in the presence of cholesterol results in an even larger projected area increase of 9.1 nm^2. In other words, 25-HC shows larger effects on projected membrane area in the presence of cholesterol. A potential mechanism for this increased expansion could be that phospholipids condensed by the presence of cholesterol can be expanded more than phospholipids which are already partially disordered.

A better understanding of interactions between the two sterols can be obtained by breaking down the total membrane areas into areas associated with each membrane component using solvent-accessible surface area (SASA) calculations. This deconvolution allows us to attribute changes in total membrane area to changes in the areas of specific membrane components. The SASA for each lipid in the bilayer was calculated and the total SASA due to POPC, cholesterol, or 25-HC was summed for each type of lipid in each snapshot of the systems. These cumulative SASA contributions were divided by two to obtain the mean per-leaflet SASA of POPC, cholesterol, and 25-HC. Results are shown in Figure 3.2 as bar plots, with the height of each bar denoting the mean contribution of POPC, cholesterol, and 25-HC to membrane SASA.

Both the 18% and 30% concentrations of cholesterol reduce the POPC contribution to surface area by

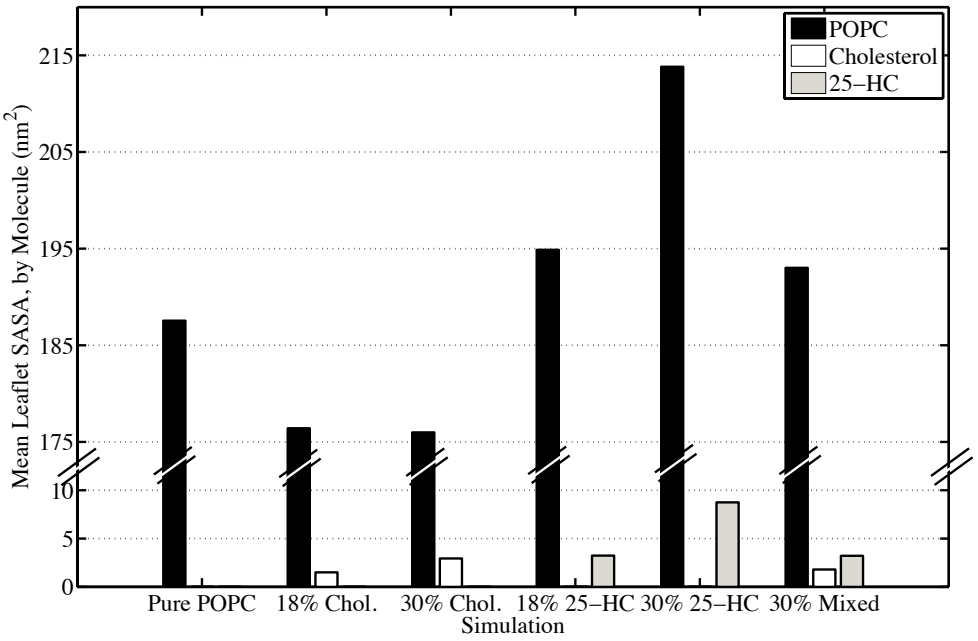

Figure 3.2: Bar plots showing the total mean per-leaflet solvent-accessible surface area for each set of simulations, divided into contributions from POPC (black), cholesterol (white), and 25-HC (gray).

11-12 nm^2; the difference between the area of POPC in the two different cholesterol concentrations is not statistically significant. Because no further decrease in POPC SASA is observed at the higher concentration of cholesterol, a limit in phospholipid condensation by cholesterol must be reached between 0 and 30% cholesterol [18, 101]. The contribution of cholesterol itself to leaflet surface area doubles from 1.5 nm^2 in the 18% cholesterol system to 2.9 nm^2 in the 30% system. Because the number of cholesterol molecules doubles as well, this indicates that cholesterol in POPC/cholesterol bilayers has a constant molecular SASA, regardless of concentration.

The solvent-accessible surface area does not necessarily change in the same way as the projected area, because the surface has varying degrees of "roughness" as its composition is varied. Changes in membrane structure that create bumps or pockets in the membrane surface can increase the SASA for a given projected area. This roughness can be quantified by examining the ratio of leaflet SASA to membrane projected area. The ratio is a dimensionless number greater than one. A perfectly flat surface would have an identical SASA and projected area, giving a ratio of one, while rougher surfaces would have larger SASAs than projected areas, giving ratios greater than one. Cholesterol decreases the roughness of the membrane. The pure POPC systems show a roughness ratio of 2.29, while the 18 and 30% cholesterol systems have roughnesses of 2.17 and 2.11, respectively.

The addition of 25-HC to a POPC bilayer causes significant increases in the POPC solvent exposure. The 128 POPC molecules in each leaflet take up 7.3 nm^2 more surface area in the presence of 18% 25-HC and 26.3 nm^2 more in the presence of 30% 25-HC. Unlike cholesterol, the effect of 25-HC does not saturate at higher concentrations. Rather, the expansion of POPC induced by 25-HC continues up to 30% 25-HC. Unlike cholesterol, 25-HC appears to not have a consistent mean molecular SASA over the range of concentrations examined. The contribution of 25-HC to leaflet surface area increases by a factor 2.8, significantly greater than two, indicating that at higher concentrations of 25-HC, the sterol becomes more exposed to solvent.

The mixed system SASA analysis shows the same synergy between cholesterol and 25-HC that is observed in projected areas. Adding both cholesterol and 25-HC to a POPC membrane results in larger POPC leaflet SASA than would be expected from their independent effects on POPC membranes. As with projected areas, this interaction can be ascribed to 25-HC disrupting the cholesterol-induced condensation of POPC. Examining membrane SASA shows that the effects of this interaction are driven by changes in phospholipid structure rather than by changes in direct area contributions by sterols.

Densities

Membrane density profiles show membrane thickness and how mass is distributed within the membrane. Mass density profiles for all simulations were calculated as described in Section 3.2.3, and the densities for all simulations of the same composition were averaged. These total mass density profiles are shown in Figure 3.3. The general shape of all the profiles is indicative of phospholipid membranes. Further than approximately 3 nm from the bilayer center, we see bulk water density of 975 kg/m^3. Major peaks occur at 1.7-2.2 nm from the bilayer center, showing the position of the heavy phosphorus atom of the phospholipids. The density then drops to a minimum at the bilayer center, with densities 30-40% lower than that of bulk water, where the acyl chains of the phospholipids interact.

While the general shape of the profile for all membrane compositions is similar, some differences are seen that give insight into how the membrane structure is changed. Cholesterol thickens the membrane in a dose-dependent manner, shifting the major phosphate peak further from the bilayer center. It also narrows the phosphate peak, indicating more homogeneity in the position of the phosphate and thus a more ordered membrane. At the same time, the minimum at the center of the bilayer deepens, showing less intercalation between acyl chains of the two separate leaflets. On the other hand, 25-HC thins the membrane, widens the major phosphate peak, and raises the minimum at the center of the bilayer. These changes show membrane collapse, a disordering of the phospholipid headgroups, and an increase in acyl chain intercalation. The simulations containing both cholesterol and 25-HC show a mixture of these effects. The bilayer thickens

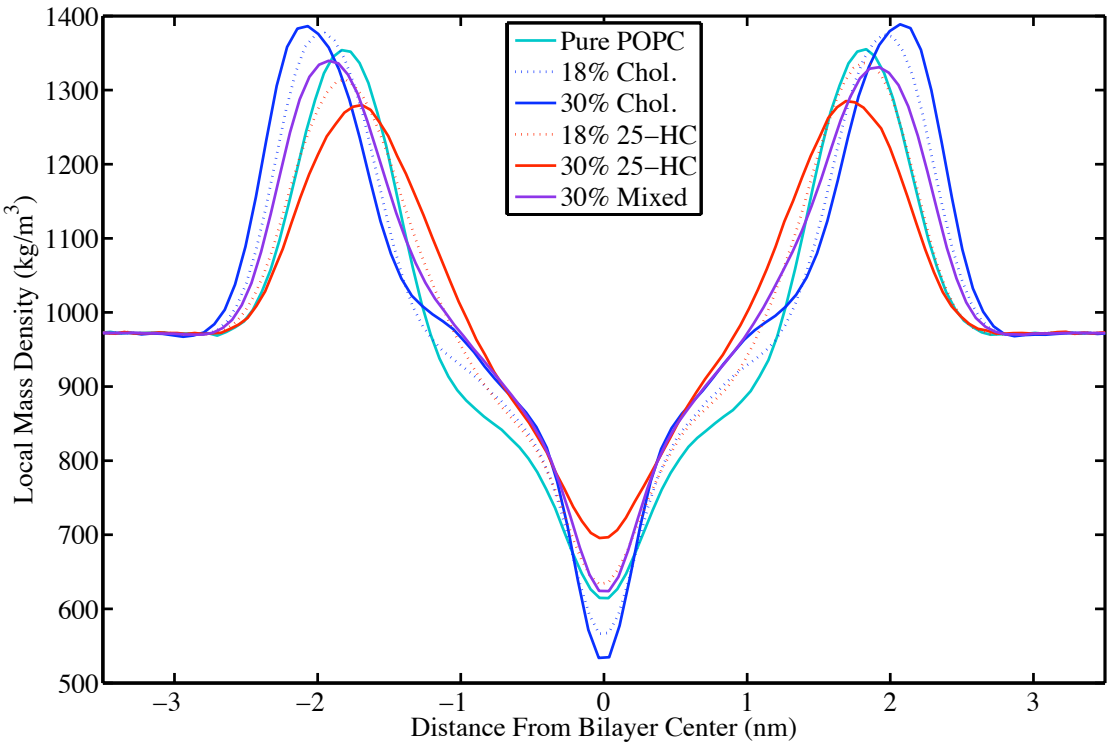

Figure 3.3: Mean mass density profiles for all POPC bilayer simulations.

slightly while the phosphate peak is widening, and the opposing effects of 25-HC and cholesterol on acyl chain intercalation results in no change with respect to the pure POPC bilayer.

Membrane thicknesses were calculated using solvent density profiles, as the distance between the half bulk water density positions in each leaflet. These thicknesses were then multiplied by projected areas to estimate membrane volume over the course of each simulation (data not shown). Both 18% sterol systems show identical increases in volume as compared to the pure POPC system, and the 30% 25-HC, 30% cholesterol, and 30% mixed sterol all show identical increases as well. This independence to sterol structure demonstrates that cholesterol and 25-HC have approximately the same molecular volume, as one would expect from their molecular structures.

3.3.3 Molecular Effects

In addition to looking at how 25-HC and cholesterol affect total membrane structure, we also wished to examine how the behavior of individual cholesterol molecules changes in membranes of different compositions.

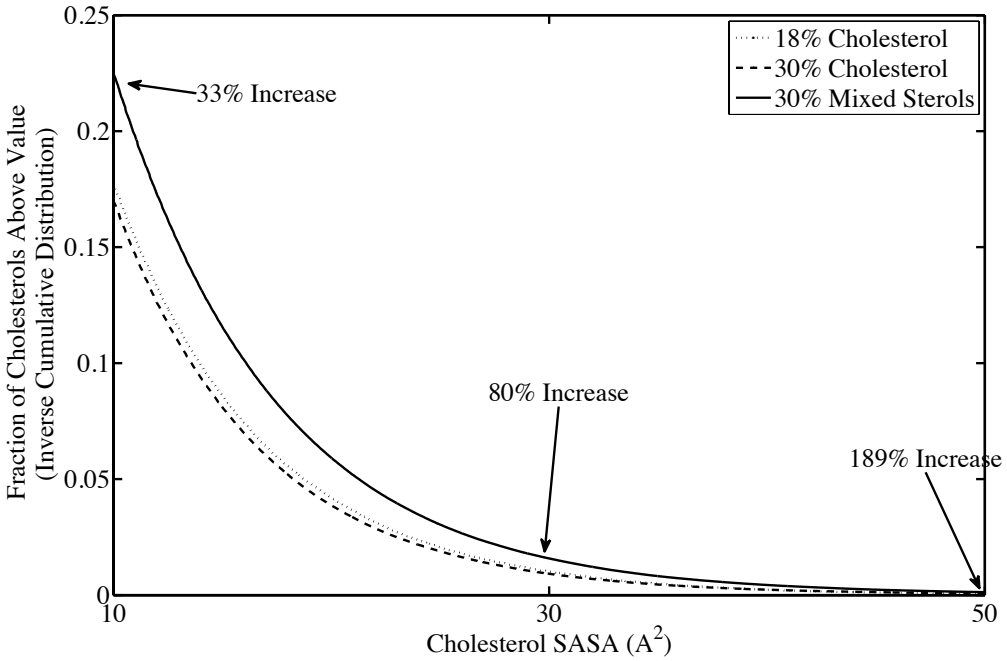

Figure 3.4: Inverse cumulative probability distributions for cholesterol solvent-accessible surface area in the 18% cholesterol (dotted), 30% cholesterol (dashed) and 30% mixed sterol (solid) simulations. For each solvent-accessible surface area, the plot shows the fraction of cholesterol molecules with an area greater than that value.

Molecular SASA

Solvent-accessible surface area calculations can be used to calculate individual molecular areas as well as total membrane areas. We calculated the SASA for each cholesterol molecule in every snapshot of our simulations. Cholesterol SASAs cluster around zero, making the probability of finding cholesterol molecules with very high surface areas quite low. To best compare SASA distributions for cholesterol in membranes of different composition, we used an inverse cumulative probability distribution. At a range of threshold SASAs, this distribution shows the fraction of all cholesterol molecules with SASAs larger than the threshold. Inverse cumulative probability distributions for cholesterol in 18% cholesterol, 30% cholesterol, and 30% mixed sterol simulations are shown in Figure 3.4.

There is no significant difference in the solvent exposure of cholesterol in the 18% and 30% cholesterol simulations. In the 30% mixed sterol simulation, cholesterol becomes significantly more exposed to solvent, with over 20% of cholesterols having SASAs greater than 10 Å^2. While the fraction of cholesterols with high SASAs is still not large, it becomes significantly larger when cholesterol is exposed to 25-HC. We see a 33%, 80%, and 189% increase in the fraction of cholesterols with SASAs above thresholds of 10, 30, and 50 Å^2, respectively.

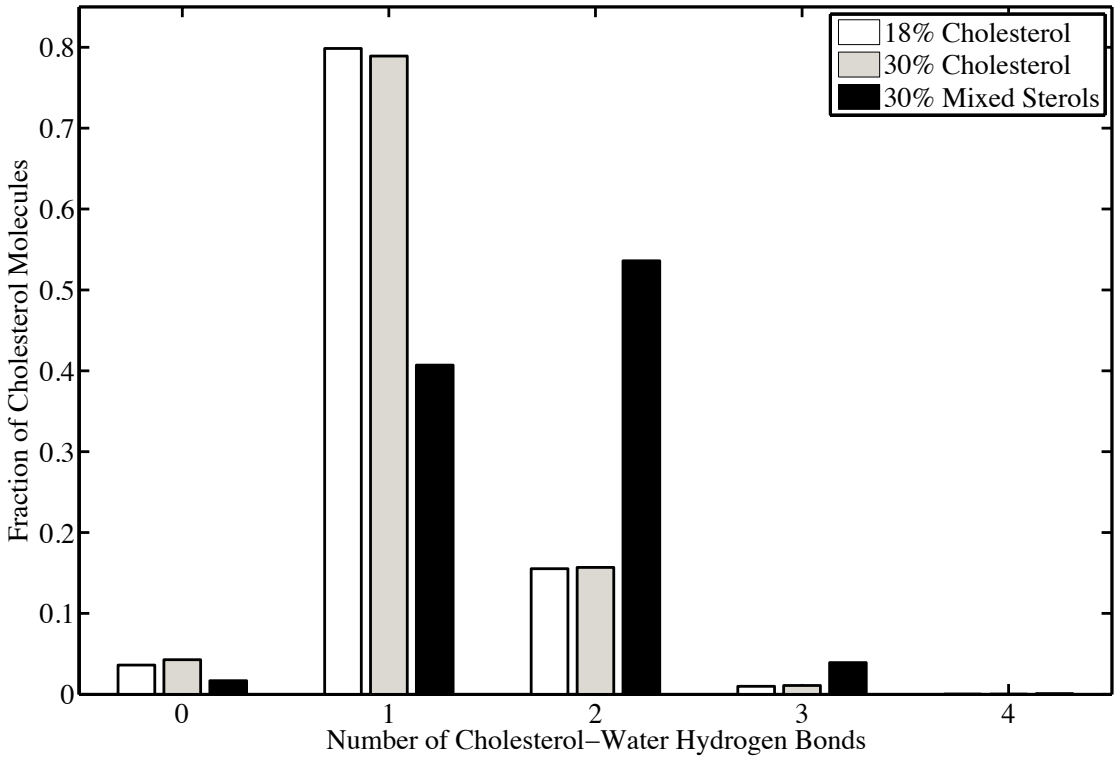

Figure 3.5: Histograms showing the number of cholesterol-water hydrogen bonds for cholesterol molecules in the 18% cholesterol (white), 30% cholesterol (gray), and 30% mixed sterol (black) simulations.

Hydrogen Bonding and Solvation

SASA results show that the presence of 25-HC causes cholesterol to become more exposed to solvent. We wished to examine how this increased exposure to solvent changed the distribution of cholesterol-solvent interactions. Hydrogen bonds were calculated between cholesterol hydroxyl groups and all solvent molecules, with hydrogen bonds defined geometrically as described earlier. The total number of cholesterol-solvent hydrogen bonds was calculated for each individual cholesterol and pooled to find the fraction of all cholesterols forming each number of solvent hydrogen bonds was calculated for all three cholesterol-containing system compositions. Histograms showing probabilities of cholesterol-solvent hydrogen bonds are shown in Figure 3.5.

As with cholesterol SASA, we find no significant differences in cholesterol-solvent hydrogen-bonding between in the 18% and 30% cholesterol. Cholesterol in these cholesterol/POPC simulations prefers to mostly hydrogen bond with a single water molecule, with less than 5% forming no solvent hydrogen bonds and only about 15% forming more than one. In the 30% mixed sterol simulations, cholesterol forms significantly more hydrogen bonds with water. In the presence of 25-HC, most cholesterol molecules prefer to hydrogen bond with multiple water molecules, rather than only one in the absence of 25-HC. This demonstrates that the

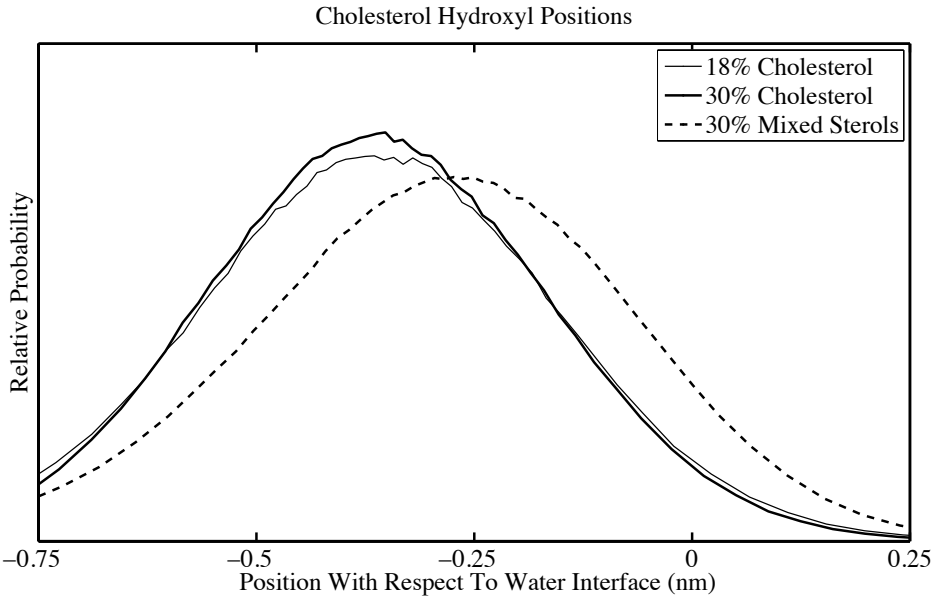

Figure 3.6: Probability distributions for finding the oxygen of the cholesterol hydroxyl at a given position with respect to the water/bilayer interface. Shown for cholesterol in the 18% cholesterol (thin solid), 30% cholesterol (thick solid), and 30% mixed sterol (dashed) simulations.

increase in cholesterol solvent-accessible surface area observed in the presence of 25-HC is accompanied by increased interactions with solvent molecules.

Sterol Positions

While examination of individual cholesterol SASA and hydrogen bonding shows that cholesterol becomes more exposed to solvent in the presence of 25-HC, it does not reveal how this increased exposure occurs. Increased exposure may be due to movement of cholesterol out of the bilayer into the solvent, or it may be due to an opening of the bilayer structure allowing solvent to penetrate. In order to examine this, the positions of cholesterol molecules were calculated with respect to the interface between solvent and the bilayer. The interface positions were calculated as the two positions along the normal axis at which the water density is 50% of the bulk water density. The probability distributions for cholesterol hydroxyl positions with respect to the interface are shown in Figure 3.6.

Much like our other cholesterol analyses, we find that the distributions of cholesterol positions in the 18% and 30% simulations are not significantly different. Cholesterol prefers to position its hydroxyl group in the bilayer somewhere between 2.5 and 5 Åbelow the water interface, with a median depth of 3.6 Åfor both 18% and 30% cholesterol systems. In the 30% mixed sterol simulations, cholesterol shifts significantly closer to the water interface, with a median depth of 2.8 Å. While the shift is small compared to the width of the

distributions, it results in a large change in the fraction of cholesterol molecules positioned above the water interface, with only 3-4% of cholesterols in the 18% and 30% cholesterol simulations that exposed but over 8% in the 30% mixed sterol simulations. The cholesterol position results show that the increased exposure of cholesterol to solvent induced by 25-HC, as shown in the cholesterol SASA and hydrogen bonding data, is due to movement of cholesterol out of the bilayer rather than a change in bilayer structure that allows increased solvent penetration.

Sterol Orientations

In previous work examining the differential effects of 25-HC and cholesterol on membrane behavior, we found significant differences in the orientations of the two sterols within bilayers and suggested that these differential orientations may be responsible for their effects on membrane structure [97]. In particular, we suggested that the interfacial orientations adopted by 25-HC could be responsible for the drastic increase in membrane area observed in 25-HC-containing membranes. In order to examine this further, we have calculated distributions of the orientations of both cholesterol and 25-HC in the 18% single sterol, 30% single sterol, and 30% mixed sterol simulations. We calculated sterol tilt and twist for each sterol molecule in these simulations, as described in Section 3.2.3. These tilt and twist angles were projected onto a spherical surface, using sterol tilt angle as the spherical inclination and sterol twist angle as the spherical azimuth. This puts parallel and anti-parallel orientations at two opposite poles of the sphere, with perpendicular orientations with different facings along the equator. Contour plots of these spherical distributions are shown in Figure 3.7 for cholesterol and Figure 3.8 for 25-HC, as viewed from the "parallel" pole of the sphere. The radiating circles from the center denote 30°, 60°, and 90° sterol tilt angles, and the radiating lines denote sterol twist angles.

Examination of cholesterol results shows few differences in cholesterol orientations among the three sets of simulations. In all cases, cholesterol prefers parallel orientations, with over 60% of cholesterol molecules having ring tilts of less than 30°. There is a slight shift towards a tighter distribution around the preferred parallel orientation at higher sterol concentrations. At the lower cholesterol concentration, only 65% of cholesterol molecules have ring tilts of less than 30°, while 78% and 77% of cholesterol molecules in the 30% cholesterol and 30% mixed sterol simulations, respectively, occupy this region. Because this shift is seen in both the 30% cholesterol simulations as well as the 30% mixed sterol simulations, it appears to be caused by general sterol concentration and is not dependent on sterol identity.

Examination of 25-HC orientations shows significant differences. At the low 18% concentration, 25-HC prefers to adopt primarily interfacial orientations. The dominant orientation has a sterol tilt of 60° with a

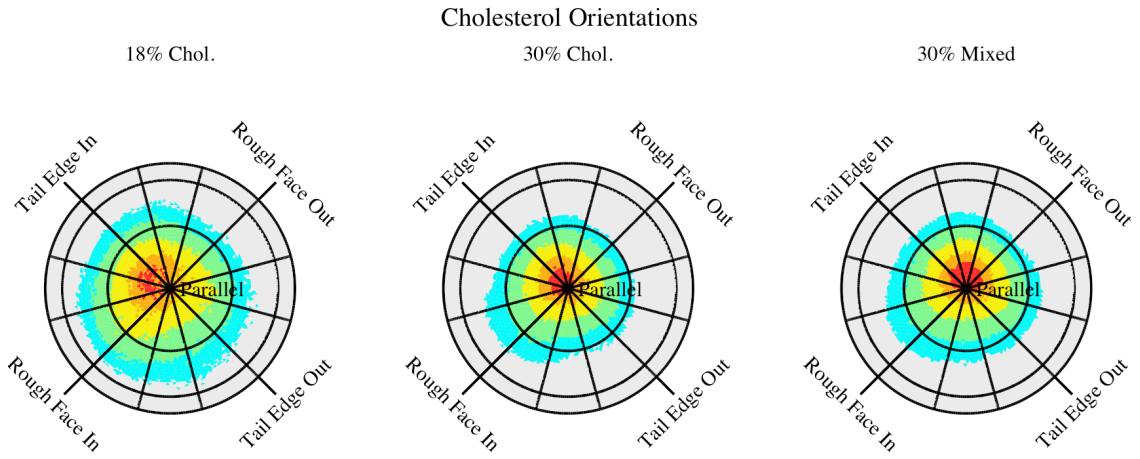

Figure 3.7: Spherical distribution plots of cholesterol orientations in the 18% cholesterol, 30% cholesterol, and 30% mixed sterol simulations. Regions containing the densest 10%, 25%, 50%, 75%, and 90% of the total probability density are shown by areas of red, orange, yellow, green, and cyan respectively. Parallel orientations are found at the center pole, and perpendicular orientations with different facings are found along the perimeter.

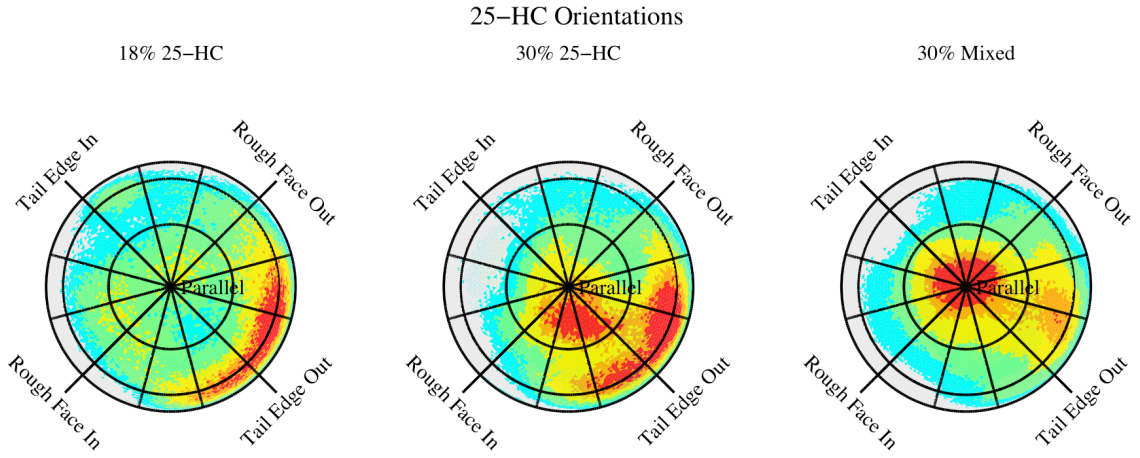

Figure 3.8: Spherical distribution plots of 25-HC orientations in the 18% 25-HC, 30% 25-HC, and 30% mixed sterol simulations. Regions containing the densest 10%, 25%, 50%, 75%, and 90% of the total probability density are shown by areas of red, orange, yellow, green, and cyan respectively. Parallel orientations are found at the center pole, and perpendicular orientations with different facings are found along the perimeter.

sterol twist such that the edge of the ring containing the hydroxylated tail faces towards the water interface. This orientation allows both hydroxyl groups to interact with solvent. While this interfacial orientation is dominant, the distribution is broad, with a wide variety of other available orientations, including (data not shown) inverted orientations with the sterol tail at the water interface and the steroid ring buried in the bilayer. If we define a parallel orientation as one with a ring tilt of less than 30° and an interfacial orientation with a ring tilt between 40° and 80° and a ring twist between -45° and 60°, then we find that only 13% of 25-HC molecules are found in parallel orientations, while 35% are found in interfacial orientations, with the remainder in these alternative conformations. At the higher 30% 25-HC concentration, there is a shift from alternative to parallel conformations, with 19% of 25-HC molecules adopting parallel orientations similar to that of cholesterol, while the fraction in interfacial orientations does not significantly change. This may be due to saturation of possible occupancy sites that prevents further alternative orientations, and leading excess 25-HC to adopt alternative orientations. In the 30% mixed sterol simulation, we find a larger shift towards parallel conformations, with 31% of 25-HC molecules adopting parallel orientations. In this case, the increase in parallel orientations is compensated by a decrease in interfacial orientations, with only 24% of oxysterols adopting interfacial orientations.

Based on our earlier work, we expected the presence of 25-HC interfacial orientations to correlate with membrane expansion. This appears to be the case in the absence of cholesterol: in the 18% and 30% 25-HC simulations, the fraction of oxysterols in interfacial orientations is approximately the same. Thus, at the low concentration, roughly a third of 56 total oxysterols are in interfacial orientations, while at the higher concentration, a third of 112 total oxysterols are in interfacial orientations. This increase in total interfacial oxysterols correlates with the increase in membrane expansion between the low and high 25-HC concentration simulations. In the presence of cholesterol, this correlation is no longer seen. Roughly a quarter of the 56 total oxysterols in the mixed sterol simulations are found in interfacial orientations, while these oxysterols cause a larger increase in membrane area than they would in the absence of cholesterol. The reasons for the shift in 25-HC orientations in the presence of cholesterol are still unclear. The loss of correlation between interfacial oxysterol concentration and membrane expansion in the presence of cholesterol suggests that either interfacial oxysterols do not cause area expansion but are instead signals of it or that cholesterol increases the ability of interfacial oxysterols to induce area expansion.

3.4 Discussion

We have found that adding both cholesterol and 25-HC to POPC membranes results in membrane effects that are significantly different from what would be expected in the absence of interactions between the two sterols. When added to POPC bilayers at low concentrations, 25-HC expands bilayers, increasing the solvent exposure of nearby phospholipids. However, when the same concentration was added to POPC bilayers that already contain cholesterol, an even larger increase in POPC expansion was seen. Results from phospholipid surface area calculations clarify this by demonstrating that the addition of cholesterol causes a much smaller decrease in phospholipid surface area in membranes containing 25-HC than in membranes without 25-HC, suggesting that the interaction between 25-HC and cholesterol interferes with the ability of cholesterol to condense bilayers. A better understanding of this effect could be gained by further simulations comparing the effect of cholesterol on 25-HC-induced membrane expansion over a range of cholesterol concentrations. If the increase in oxysterol membrane expansion is caused by a disruption of the ability of cholesterol to condense bilayers, then the increase should be proportional to cholesterol concentration.

In our earlier work, we predicted this effect and hypothesized that it would be driven by conformational shifts in 25-HC [97]. We proposed that 25-HC causes membrane expansion through its adoption of interfacial conformations, and that the presence of cholesterol would cause 25-HC to favor these interfacial conformations, thus increasing its expansive effect. We suggested that membranes contain a limited number of available occupancy sites for upright sterols, and that cholesterol would compete with 25-HC for access to these sites, driving 25-HC towards interfacial orientations. However, we find that this predicted conformational shift does not occur. Instead, 25-HC shifts away from interfacial orientations in the presence of cholesterol. This suggests that at the sterol concentrations studied, the number of available occupancy sites for upright sterols is not limiting. Thus, rather than competing with 25-HC for access to these sites, cholesterol alters membrane structure in such a way as to energetically favor upright conformations.

A potential consequence of these shifts in 25-HC orientation may be a change in oxysterol-induced membrane permeability. We have previously speculated that the hydrogen bonded oxysterol clusters formed by upright 25-HC molecules are the cause of oxysterol-induced increases in membrane permeability [97]. The clusters of oxysterol hydroxyl groups in the center of the bilayer would lower the desolvation penalty of passing small polar molecules through the bilayer by offering alternative hydrogen bonding sites. The shift in oxysterol orientations from interfacial to upright conformations we have observed in the presence of cholesterol would also cause an increase in the number of available hydrogen bonding sites in the interior of the bilayer, further lowering the barrier to small molecule permeation of the bilayer. Thus we hypothesize that the observed increase in membrane permeability induced by 25-HC will be larger in membranes containing

cholesterol than in those without.

We have proposed that the oxysterol-induced expansion of membrane bilayers may be a biologically-relevant signaling mechanism [97]. While 25-HC is only present at low concentrations in the cell, in the direct region around 25-HC-producing enzymes, it may be present at locally high concentrations similar to what we have simulated here. Locally elevated concentrations of 25-HC could cause changes in membrane structure sufficient to alter membrane protein structure and activity. The ability of cholesterol to increase the expansive effect of side-chain oxysterols on membranes may be biologically relevant. The concentration of cholesterol in the ER would then control not only the local concentration of 25-HC but also the local expansion caused by 25-HC, increasing the signaling capacity of a given concentration of 25-HC.

We also examined cholesterol behavior in mixed membranes and found significant changes when compared to cholesterol in the absence of 25-HC. In the absence of 25-HC, the cholesterol hydroxyl group has a mean position slightly below the bilayer/water interface. The addition of 25-HC to the membrane shifts this position towards the interface by nearly an angstrom. This shift suggests that cholesterol is less tightly bound to nearby phospholipids and may be linked to the reduced ability of cholesterol to condense bilayers. The change in cholesterol position is accompanied by an increased exposure of cholesterol to solvent, as measured by cholesterol solvent-accessible surface area and cholesterol-solvent hydrogen bonding. This demonstrates a reduction in the shielding of the largely hydrophobic cholesterol by surrounding phospholipid headgroups.

It has been hypothesized that cholesterol in membranes exists in both complexed and free or activated forms [71]. While the complexed cholesterol is tightly bound to phospholipids and unavailable to enzymes or binding partners, activated cholesterol is available to partners such as cholesterol oxidase, cyclodextrin, and lipoproteins [71]. Under normal conditions, the availability of cholesterol is determined by the capacity of membrane phospholipids to form complexes with cholesterol. Addition of cholesterol past membrane capacity leaves a pool of uncomplexed free cholesterol with higher activity [71]. A wide range of amphipaths including alcohols, fatty acids, and ketones have been shown to increase the fraction of activated cholesterol when added to membranes [72].

We suggest that the shifts in cholesterol position and exposure induced by the presence of 25-HC are consistent with an activation of membrane cholesterol. Oxysterol-induced cholesterol activation provides another potential mechanism through which 25-HC can signal in a non-enantioselective manner. Increases in activated cholesterol may be responsible for the increased trafficking of cholesterol from the plasma membrane to the ER that has been observed when large amounts of 25-HC are added externally to cells [71]. Under physiological conditions, 25-HC is largely present in the ER, where its effect on cholesterol activity could increase cholesterol's availability to proteins such as ACAT, HMGCoAR, and SREBP. Based on this signaling

model, we predict that 25-HC activation of SREBP should be dependent on the presence of cholesterol, and be greatly diminished in cholesterol-starved cells. We would also anticipate that 25-HC should increase the availability of cholesterol to cholesterol oxidase and cyclodextrin in a dose-dependent manner.

Chapter 4

Influence of Phospholipid Acyl Chains on 25-Hydroxycholesterol Membrane Interactions

Abstract

Oxysterols are oxidation products of cholesterol that help regulate cholesterol homeostasis. Recent work has shown that oxysterols alter membrane behavior and structure in very different ways than cholesterol, and that oxysterol-induced changes in membrane structure may be important for the regulatory behavior of oxysterols. We have extended our previous work to examine how phospholipid structure alters oxysterol interactions with membranes using molecular dynamics simulations of 25-hydroxycholesterol and cholesterol in DMPC, DPPC, POPC, and DOPC bilayers. We have identified novel binding modes of 25-HC within DMPC bilayers. A small fraction of oxysterols in DMPC bilayers stretch across the entire bilayer, and drive membrane expansion. We have further found significant differences in interactions of oxysterols with saturated and unsaturated lipids, finding that oxysterols cause larger changes in membrane properties in unsaturated than saturated lipids. Finally, we have identified correlations between structural properties of both oxysterols and phospholipids and the magnitude of oxysterol-induced membrane expansion that provide insight into the mechanisms of 25-HC modulation of membrane structure.

4.1 Introduction

While the basic building blocks of biological membranes are phospholipids, sterols and proteins regulate membrane structure and behavior. Cholesterol is the most common sterol, and is essential to the proper functioning of mammalian cells. Cholesterol regulates cell behavior both through binding to sterol-sensing domains of membrane proteins [13,27,68] and through modulation of membrane structure and behavior. The addition of cholesterol to membranes broadens the liquid-disordered to gel phase transition, and can induce the formation of cholesterol-dependent liquid ordered phases [30,128]. Both biophysical and simulation studies have shown that the addition of cholesterol to membranes decreases membrane fluidity while increasing membrane thickness, bending modulus, and lipid order [26, 56, 86, 94, 108, 129]. The effect of cholesterol on membrane structure influences cellular behavior. Increases in membrane thickness caused by cholesterol are thought to help sort membrane proteins between the plasma membrane and the ER [79]. Membrane phase and structure can also alter signaling and behavior in proteins such as adenylate cyclase, G-proteins, and diacylglycerol kinase [53, 74, 132].

Cellular cholesterol levels are tightly regulated by a number of feedback pathways. One of the best understood feedback pathways involves the regulation of the rate-limiting enzyme in the cholesterol synthesis pathway, HMGCoA reductase [39]. Transcription of HMGCoAR is triggered by cholesterol depletion, promoting cholesterol synthesis to restore cholesterol levels. A drop in ER cholesterol levels disrupts binding between the ER membrane proteins Insig and Scap, freeing Scap to translocate into the Golgi, carrying the transcription factor SREBP along with it [11, 52, 133]. Once in the Golgi, endogenous proteases cleave SREBP, releasing an active transcription factor that induces the production of HMGCoAR [11, 52].

While cholesterol itself can suppress SREBP activation, it has been known for over 30 years that oxysterols, oxygenated derivatives of cholesterol, can suppress SREBP activation more than 50 times as strongly [40, 55]. Oxysterols have also been found to be activators of the liver X receptor (LXR) transcription factors, which up-regulate expression of cholesterol efflux proteins [60, 61]. While oxysterols play a role in regulation of both the SREBP and LXR feedback pathways, the mechanisms of interaction are distinct. Recent work using enantiomers of natural oxysterols has shown that while the ent-oxysterols suppress SREBP activation as effectively as natural oxysterols, they are unable to activate LXRs [36]. Protein-small molecule interactions are enantiospecific, suggesting that while oxysterol directly binds and activates LXRs, oxysterol suppression of SREBP activation is mediated through some non protein-dependent pathway.

Like cholesterol, oxysterols perturb membrane structure and behavior, although the changes oxysterols make are very different. While cholesterol orders and condenses membranes, reducing their area and permeability, oxysterols instead increase membrane area and permeability [49,63,125]. Our previous computational

work has shown that molecular dynamics simulations of cholesterol and 25-HC in phospholipid membranes can capture experimentally observed changes in membrane structure induced by these sterols [97]. The atomic detail of molecular dynamics simulations allowed us to see molecular differences in how cholesterol and 25-HC orient themselves within membranes and correlate those orientations with their mesoscopic effects on membrane structure [97]. Specifically, we found that while cholesterol prefers to orient upright in POPC membranes, 25-HC adopts interfacial orientations that avoid the desolvation penalty of burying the additional 25-hydroxyl group in the hydrophobic interior of the bilayer [97].

Experimental work from our collaborators has demonstrated that the effects of 25-HC on membrane behavior is highly dependent on the structure of its component phospholipids. They found that while 25-HC causes significant expansion in monolayers composed of fully or partially unsaturated phospholipids, its effects on membranes composed of saturated phospholipids are much smaller [36]. We would like to examine how the phospholipid composition of bilayers alters its interactions with 25-HC. In order to do this, we have prepared simulations of cholesterol and 25-HC in bilayers of four different phospholipids. We chose two different saturated phospholipids, the short-chain dimyristoylphosphatidylcholine (Figure 4.1A) and the long-chain dipalmitoylphosphatidylcholine (Figure 4.1B). While both of these lipids are fully saturated, they have different chain lengths, allowing us to observe the effect of chain length on 25-HC/membrane interactions. We also chose a partially unsaturated lipid, 1-palmitoyl-2-oleoyl-phosphatidylcholine (Figure 4.1C), and a fully unsaturated lipid, dioleoylphosphatidylcholine (Figure 4.1D).

4.2 Methods

4.2.1 Parameters and Structures

Cholesterol and 25-hydroxycholesterol parameters and charges were used as described in our previous work [97]. 1-palmitoyl-2-oleoyl-phosphatidylcholine (POPC), di-palmitoyl-phosphatidylcholine (DPPC), di-oleoyl-phosphatidylcholine (DOPC), and di-myristoyl-phosphatidylcholine (DMPC) lipids were simulated using the united atom parameters of Berger and Lindahl [5], along with SPC water [3] and Straatsma-Berendsen potassium and chloride ion parameters [123]. Lipid topologies and initial bilayer structures with 128 DPPC, DMPC, or DOPC phospholipids were obtained from Tieleman and coworkers [127]. These 128 lipid bilayers were replicated in the bilayer plane and trimmed to produce larger 256 lipid bilayers with approximate dimensions of 10 $\times$ 10 nm in the bilayer plane. These 256 lipid bilayers prepared above were solvated with 14276 SPC water molecules and 30 K^+ and Cl^- ions for an approximate KCl concentration of 110 mM. The solvated DPPC, DMPC, and DOPC bilayers were then used as starting structures for the sterol-free

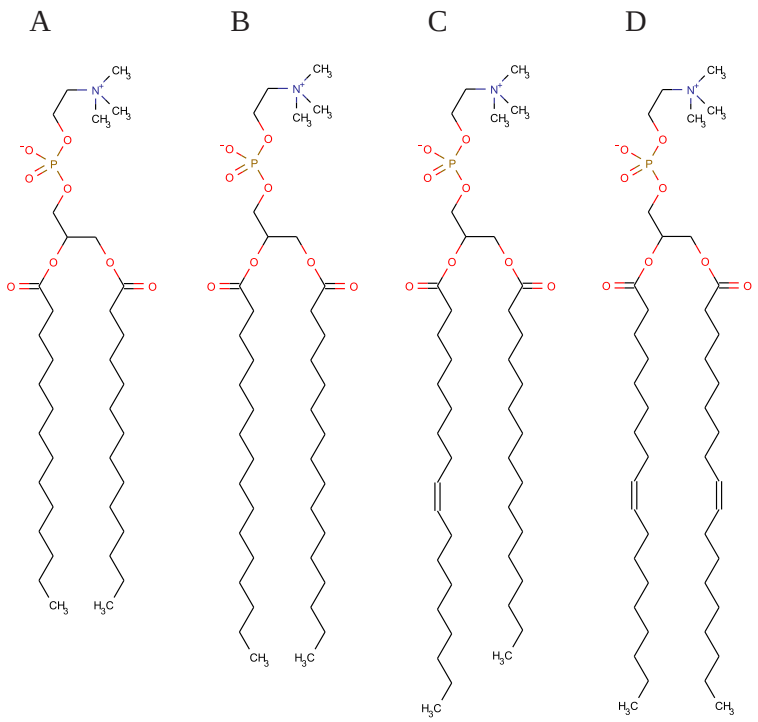

Figure 4.1: Structures of the four simulated phospholipids. A) DMPC b) DPPC c) POPC d) DOPC.

simulations.

To obtain cholesterol and 25-hydroxycholesterol configurations, a single molecule of cholesterol or 25-hydroxycholesterol was placed 1-2 nm from the surface of each monolayer in the solvated structures. These systems were simulated for 50 ns to allow the sterols to associate with the lipid bilayers. All sterols inserted themselves in the lipid bilayers in the first 25 ns of the simulation. The last 25 ns of these simulations were used to provide configurations of sterols for preparation of 30 mole percent sterol structures.

92 DMPC, DPPC, and DOPC lipid bilayers were prepared from the 256 lipid bilayers described above by selecting an appropriate rectangular patch of membrane and excluding lipids outside the patch. 14 phospholipids in each leaflet of the 92 lipid bilayers were then removed and replaced with cholesterol or 25-hydroxycholesterol structures taken from the 256 lipid/2 sterol simulations, resulting in bilayers containing 64 phospholipids and 28 sterols evenly divided between the two leaflets. These structures could not yet be used as starting points for simulations due to steric clashes between the newly-inserted sterols and the existing phospholipids. In order to resolve these clashes, the bilayer was expanded laterally by approximately a factor of 3, resulting in very widely spaced sterols and lipids. This expansion was followed by serial iteration of conjugate-gradient energy minimization and compression in the plane of the bilayer to bring the structures back to near their original size, but with steric clashes resolved. These minimized structures were then replicated 2 $\times$ 2 in the bilayer plane to produce 256 phospholipid, 112 sterol systems, or bilayers containing

approximately 30 mole percent sterols. The final bilayer structures were solvated with 17414 SPC water molecules and 36 K^+ and Cl^- ions for an approximate KCl concentration of 115 mM and used as starting structures for the 30% sterol simulations.

Previously published 256 POPC, 256 POPC/112 cholesterol, and 256 POPC/112 25-hydroxycholesterol simulations were extended to provide additional controls to the newly prepared DMPC, DOPC, and DPPC systems.

4.2.2 Simulations

All molecular dynamics (MD) simulations were performed using GROMACS version 3.3.1 or 4.0 [4, 77]. All simulations followed the same molecular dynamics protocol. Conjugate gradient energy minimization was first performed on the initial structures to relax any unfavorable contacts between molecules. The system was then gradually warmed with a series of 30 ps constant temperature, constant pressure MD simulations from 0 to 300 K in 15 K increments, with 2 fs time steps. Production simulations were then run from the warmed structures. Anisotropic pressure coupling was applied at 1 atm using the Parrinello-Rahman method with a time constant of 1 ps [103]. Temperature coupling was applied independently to lipids and solvent using the Nosé-Hoover algorithm with a time constant of 0.2 ps [51]. DMPC, DOPC, and POPC bilayers were simulated at a temperature of 300K, while DPPC bilayers were simulated at 323K in order to maintain the DPPC bilayer in a fluid phase. Electrostatic interactions were calculated using the particle-mesh Ewald method (PME), with both the direct space PME cutoff and the Lennard-Jones cutoffs set to 1 nm [20]. Constraints were applied to all bonds [29, 102] using the LINCS algorithm incorporated in GROMACS to allow 2 fs timesteps [47].

Twelve different system compositions were simulated: bilayers composed of 256 DMPC, DOPC, POPC, or DPPC phospholipids with no added sterols, added 112 cholesterol molecules, or added 112 25-HC molecules. Initial production simulations for each of these systems were run for 400 ns. In order to obtain better sampling and statistical confidence, replica simulations for each initial simulation were prepared by first taking snapshots from the initial simulations at 150, 200, 250, and 300 ns. These snapshots were taken as the starting point for new systems after resampling particle velocities from a 300K (for DMPC, DOPC, and POPC bilayers) or 323K (for DPPC bilayers) Maxwell-Boltzmann distribution, resulting in independently evolving systems. Each of these replica simulations was run for 200 ns of total simulation time. Snapshots of each simulation were taken ever 100 ps for analysis.

4.3 Results

4.3.1 Membrane Effects

Projected Areas

The most straightforward membrane property to examine is the total membrane area. The projected membrane area of each system is simply calculated as the area of the periodic box containing the system along the xy axis. This is calculated for each frame of the simulation, and replica simulations pooled to produce a distribution for each system composition. These distributions are shown in Figure 4.2.

We would first like to examine whether the pure phospholipid systems accurately capture the experimentally observed area per lipid. First examining only the simulations performed at 300K (the DOPC, POPC, and DMPC simulations) to avoid the complicating effect of temperature, we note that area per lipid increases in progressively more unsaturated lipids, with DMPC having a smaller projected area than POPC which in turn is smaller than DOPC. By dividing the total projected area of the pure phospholipid bilayer by the number of phospholipids in each leaflet, we can calculate an area per lipid comparable with experimental results. The mean area per lipid for our DOPC bilayers is 65.0 $Å^2$. While earlier experimental results for DOPC gives a much larger area of 72.4 $Å^2$ [67], new methods have revised the area per lipid downward to 67.4 $Å^2$, closer to our results [65]. As discussed in our previous work, our simulated POPC bilayers give an area per lipid, 64.1 $Å^2$, smaller than the experimental value of 68.3 $Å^2$ [67]. However, this result has not been updated using the new methods as for DOPC, and we are hopeful that the experimental result for POPC will similarly shift towards our simulation results when updated. Our DMPC simulation gives an area per lipid of 62.9 $Å^2$, which is slightly larger than the experimental value of 60.6 $Å^2$ [64]. Finally, the DPPC simulation is run at a higher temperature of 323K. This is done in order to keep it above the gel to liquid transition temperature and in the liquid disordered phase. Here we find an area per lipid of 65.2 $Å^2$, somewhat larger than the experimental value of 63.0 $Å^2$ [65]. Our simulation results are reasonably close to experimental results, with what appears to be a slight underestimate of the area of unsaturated lipids and a slight overestimate of the area of saturated lipids.

We next turn to examining the effects of cholesterol on projected membrane area. Membrane area changes due to the addition of cholesterol can be divided into the direct area increase caused by the addition of new molecules and the indirect area decrease caused by the cholesterol-induced condensation of phospholipids. While the direct area increase should be roughly similar for the same concentration of cholesterol in membranes of different phospholipid composition, the phospholipid condensation effect will be dependent on lipid saturation and tail length. In all phospholipids, we see that the addition of 30% cholesterol causes either an

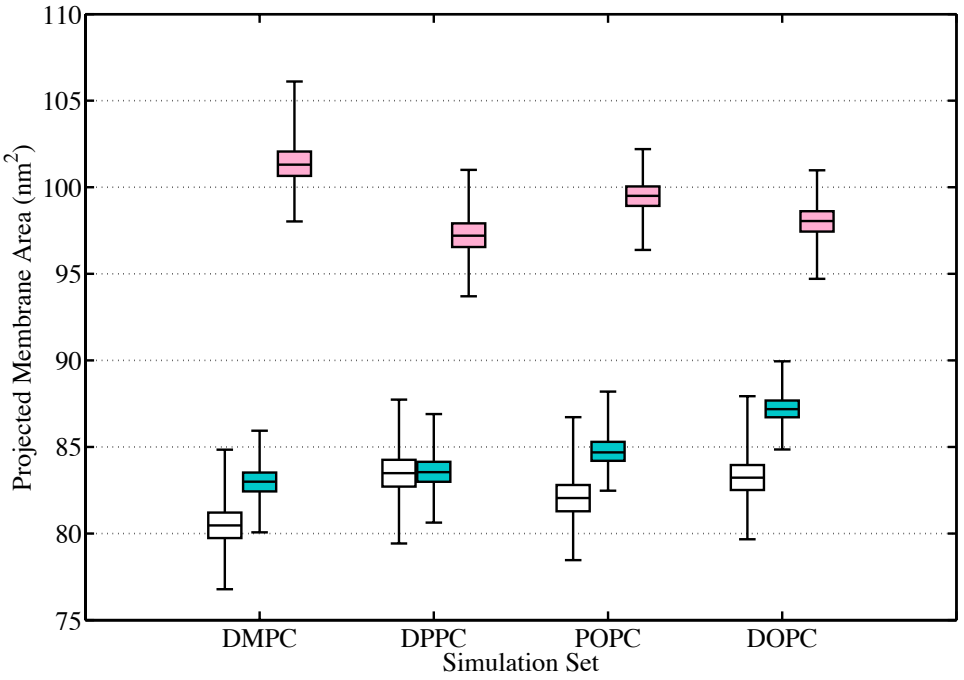

Figure 4.2: Box and whisker plots showing projected area distributions for phospholipid/sterol bilayers. The central box shows the median and interquartile range of the area distribution while the whiskers show the minimum and maximum. The phospholipid composition of each bilayer is given on the x axis, and for each phospholipid we show the distributions for three different systems: the 256 phospholipid bilayer (white), the 256 phospholipid/112 cholesterol bilayer (cyan), and the 256 phospholipid/112 25-HC bilayer (pink).

increase or no change in total membrane area. This indicates that the condensation effect of cholesterol at a 30% concentration is smaller or equal to the direct area effect in all four phospholipids.

First comparing the effects of lipid tail length, we see that the addition of 30% cholesterol to DPPC bilayers causes no change in the mean projected membrane area of 83.6 nm^2, while the same addition to DMPC bilayers causes an increase of 2.5 nm^2 from 80.5 nm^2 to 83.0 nm^2. This suggests that cholesterol has a stronger condensation effect on DPPC phospholipids than on DMPC phospholipids, in agreement with other simulation and experimental results [66, 111, 114]. This difference has been attributed to relative lengths of phospholipid acyl chains and cholesterol causing intercalation of cholesterol between leaflets in the shorter-chain DMPC bilayers but not in longer-chain DPPC bilayers [114].

Next, we compare the effects of cholesterol on DPPC, POPC, and DOPC bilayers to see how acyl chain saturation affects phospholipid condensation. The addition of 30% cholesterol to saturated DPPC bilayers causes no change in mean projected membrane area of 83.6 nm^2. The same addition to partially unsaturated POPC bilayers increases projected membrane area by 2.7 nm^2, from 82.1 nm^2 to 84.8 nm^2, and cholesterol addition to fully unsaturated DOPC bilayers increases projected membrane area by 3.9 nm^2, from 83.3 nm^2 to 87.2 nm^2. Thus we see a progression of membrane response, with cholesterol having the strongest condensation effect on saturated phospholipids, intermediate levels of condensation on partially unsaturated phospholipids, and the weakest condensation on fully unsaturated phospholipids. This is in good agreement with experimental results showing that cholesterol interacts more strongly with and has larger effects on unsaturated lipids [99].

25-hydroxycholesterol, like cholesterol, has both indirect and direct effects on membrane area. Unlike cholesterol, it does not condense nearby phospholipids but instead expands them [49, 63, 125]. Because both its direct and indirect effects on membrane area tend towards membrane expansion, addition of 25-HC to membranes causes much larger increases in total projected area than cholesterol. Comparing the effects of 25-HC on DMPC and DPPC bilayers, we find that the addition of 30% 25-HC to DPPC bilayers increases projected membrane area by 13.6 nm^2 from 83.6 nm^2 to 97.2 nm^2, while in DMPC bilayers 25-HC increases projected membrane area by 20.9 nm^2 from 80.5 nm^2 to 101.4 nm^2. This suggests that the expansive effect of 25-HC on DMPC bilayers is significantly larger than its effect on DPPC bilayers. Comparing the effects on saturated versus unsaturated bilayers, we see smaller effects in fully saturated and fully unsaturated bilayers, with the largest projected area increase in the partially saturated POPC bilayers. While 30% 25-HC increases the projected area of DPPC bilayers by 13.6 nm^2, it increases the projected area of DOPC bilayers from 83.3 nm^2 to 98.0 nm^2, a difference of 14.7 nm^2. The effect of 25-HC on POPC bilayers is significantly larger, increasing projected membrane area from 82.1 nm^2 to 99.5 nm^2, an increase of 17.4 nm^2. These differences

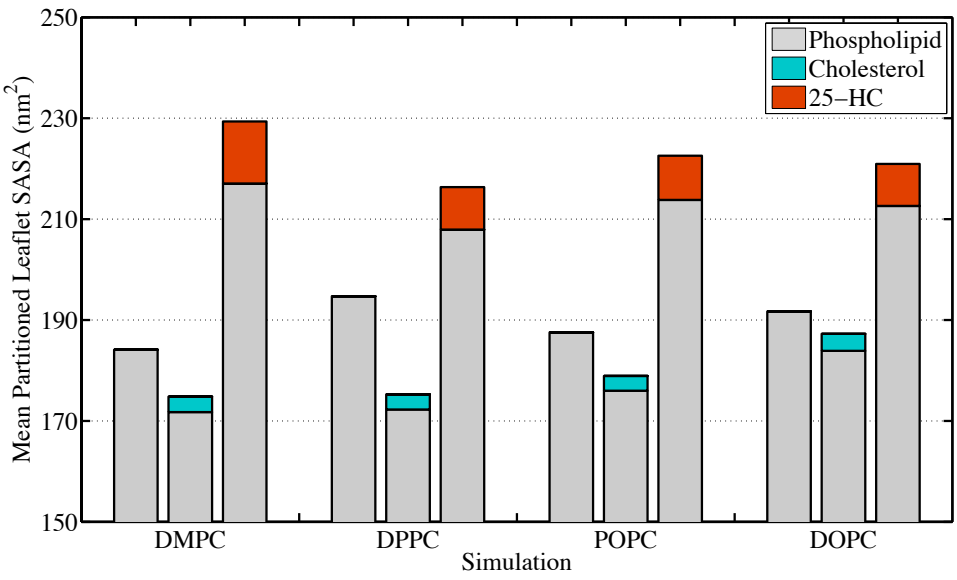

Figure 4.3: Stacked bar plots showing the mean leaflet solvent-accessible surface area and division into contributions from phospholipid (gray), cholesterol (cyan), and 25-HC (red).

demonstrate that oxysterol/membrane interactions are not purely driven by lipid saturation. First, we find significant differences in 25-HC interactions with two saturated lipids of different length. Secondly, we do not see increases in oxysterol-induced membrane expansion in fully saturated DOPC bilayers as compared with partially unsaturated POPC bilayers.

Leaflet SASA

In order to more closely examine the effects of sterols on membrane area, we break down the changes in total membrane area into changes associated with each membrane component. We do this using solvent-accessible surface area (SASA) calculations. The SASA of each molecule in the bilayer was calculated and the total SASA attributed to phospholipid, cholesterol, or 25-HC summed for each type of lipid in each snapshot of all systems. These contributions are divided by two and averaged over all equilibrated frames of the simulations to give mean per-leaflet SASAs, partitioned between phospholipid, cholesterol, and 25-HC. Results can be seen in Figure 4.3 as stacked bar plots. These areas are significantly larger than the projected areas shown in Figure 4.2 because they take into account the roughness of the surface, with rougher surfaces producing a larger SASA for a given projected area.

First examining the SASAs in the cholesterol-containing bilayers, we find that the differences in area attributed to cholesterol in the four different phospholipid bilayers are not significant, with SASA values from 2.9 to 3.4 nm^2. Differences in cumulative phospholipid SASAs are significant between the different

phospholipids. We see the largest decrease in cumulative phospholipid SASA in DPPC, which decreases from 194.7 to 172.3 nm^2. Progressively smaller decreases are seen in POPC, which decreases from 187.5 to 176.0 nm^2 and in DOPC, which drops from 191.7 to 183.9 nm^2. We also find differences due to acyl chain length, with DMPC showing less condensation than DPPC, dropping in area from 184.4 to 171.8 nm^2. These SASA results are consistent with the projected area results, showing that cholesterol condensation is stronger in saturated than unsaturated lipids and is dependent on chain length.

Examining 25-HC SASAs, we first note that the surface area of 25-HC in DMPC bilayers is significantly larger than in DPPC, POPC, or DOPC bilayers. While the mean cumulative SASA for 25-HC in DMPC is 12.3 nm^2, it ranges from 8.3 to 8.7 nm^2 in the other three phospholipids. This suggests that oxysterols may have significantly different conformations when present in DMPC bilayers that exposes them to solvent. Examining cumulative phospholipid area demonstrates that in all bilayers, 25-HC causes expansion of phospholipids. However, the size of this effect varies greatly between phospholipids. The largest expansion is seen in DMPC bilayers, where phospholipid SASA increases from 184.4 to 217.1 nm^2, a 17.7% increase in surface area. The smallest expansion is found in DPPC bilayers, with an increase of only 6.8%. This again demonstrates that acyl chain length has a significant effect on how oxysterols interact with phospholipids. The fully saturated DOPC shows intermediate levels of expansion, increasing in surface area by 10.9%, while the partially unsaturated POPC increases by 14.0%.

Membrane Density

Membrane density profiles show membrane thickness and how mass is distributed within the membrane. Mass density profiles for all simulations were calculated, obtaining results for phospholipid, sterol, and solvent densities. The mass density profiles for bilayers, *i.e.* all non-solvent molecules, are shown in Figure 4.4. The general shape is similar across all bilayer compositions, and is indicative of phospholipid membranes. The peaks of the distributions lie at 1.5-2.0 nm from the bilayer center, where the heavy phosphate groups lie. The distributions then taper off to zero as we get further from the bilayer and begin entering the bulk solvent region. The density drops to a local minimum at the bilayer center, with densities 30-40% lower than that of the peak region, where the acyl chains of the phospholipids of each leaflet interact with each other.

The effects of cholesterol and 25-HC on membranes are qualitatively similar in membranes of different phospholipid compositions. Cholesterol tends to thicken the membrane, pushing the main phosphate peak further from the bilayer center. It also lowers the density in the center of the membrane, likely due to a decrease in acyl chain interdigitation. 25-HC has the opposite effect, thinning the membrane and increasing the density in the membrane interior. While these effects are broadly similar across different phospholipid

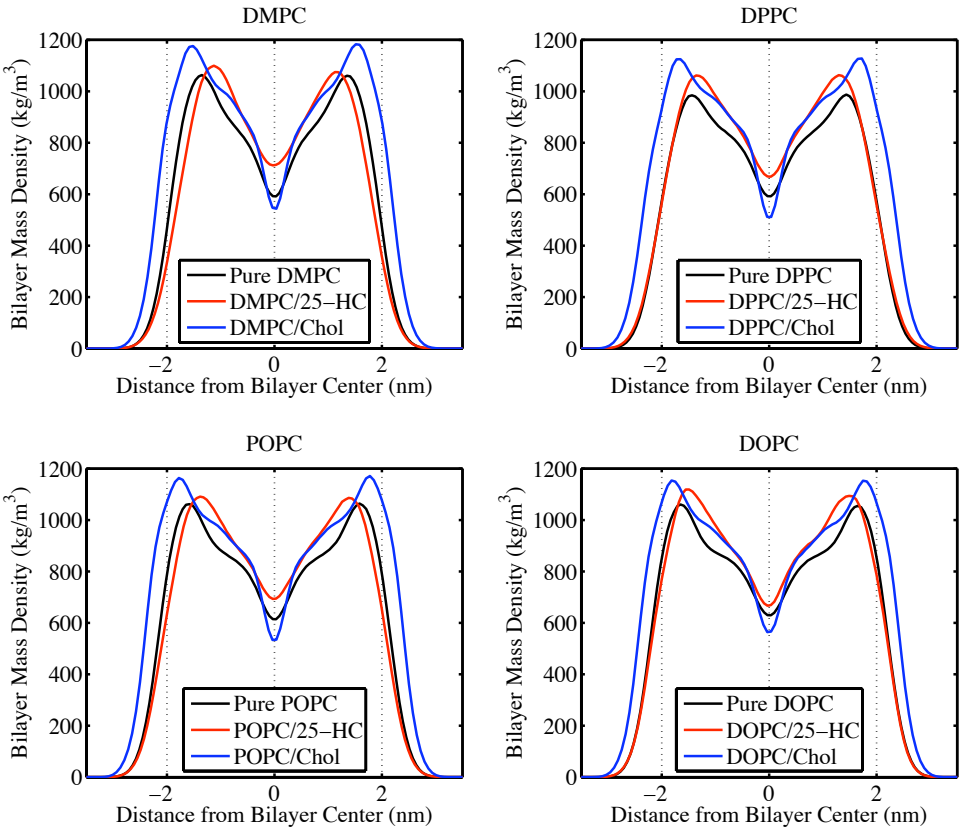

Figure 4.4: Bilayer mass density profiles for DMPC, DPPC, POPC, and DOPC bilayers. Consists of both phospholipid and sterol mass densities. Pure phospholipid bilayers in black, 30% 25-HC bilayers in red, and 30% cholesterol bilayers in blue.

membranes, there are quantitative differences. In particular, the effects of 25-HC on density profiles are correlated with its effects on membrane area. While in all bilayers, 25-HC causes membrane thinning, the thinning can be distinguished as to whether it is caused by a general shift in the density profile towards the bilayer center or whether it is caused by an independent increase in density closer to the bilayer center. In the case of DPPC, we see almost complete overlap between the pure DMPC and DMPC/25-HC density profiles at the solvent interface, and the bulk of the membrane thinning is caused by an increase in interior density. We see progressively larger shifts in DOPC, POPC, and DMPC bilayers, tracking their progressively larger effects on phospholipid surface area. These effects are likely due to conservation of membrane volume in these highly incompressible systems. The addition of sterols to membranes necessarily increases membrane volume, and this increased volume can take the form of increases in membrane area or increases in membrane thickness. In the case of cholesterol, the condensation of membrane area is compensated by large increases in membrane thickness. For 25-HC, membrane lateral expansion is compensated by membrane thinning, with larger amounts of thinning necessary to compensate for larger area expansions.

4.3.2 Lipid Effects

Order Parameters

Order parameters for the acyl chains of DMPC, DPPC, POPC, and DOPC phospholipids in our simulations were calculated as in our previous work [97]. Order parameters are calculated for each carbon in the acyl chain. Larger numbers indicate a more ordered orientation, with increased alignment of the chain at that position along the bilayer normal axis, while smaller numbers indicate a more disordered orientation. Tails are ordered near the headgroup and become increasingly disordered towards the end of the tail, indicating less conformational freedom near the attachment site to the glycerol backbone and increased freedom further away. The large drop in tail order seen at carbon 10 in the POPC sn2 chain and both DOPC chains is due to the oleoyl *cis* double bond causing a kink in the chain and interfering with its ability to align along the bilayer normal axis.

Examining the effects of sterols, we see that cholesterol causes an increase in tail order in both chains of all phospholipid bilayers. This is consistent with experiment, and has been attributed to packing of the phospholipid tails around the rigid sterol ring structure. 25-HC, however, causes significant amounts of ordering near the headgroup and differential effects near the end of the tails in the four different phospholipid bilayers. These effects appear to correlate well with 25-HC-induced phospholipid expansion. DPPC bilayers, which show the least expansion in the presence of 25-HC, also have some slight ordering or no change in acyl chain order in carbons 10-15 near the tail end upon the addition of 25-HC. DOPC bilayers, with slightly

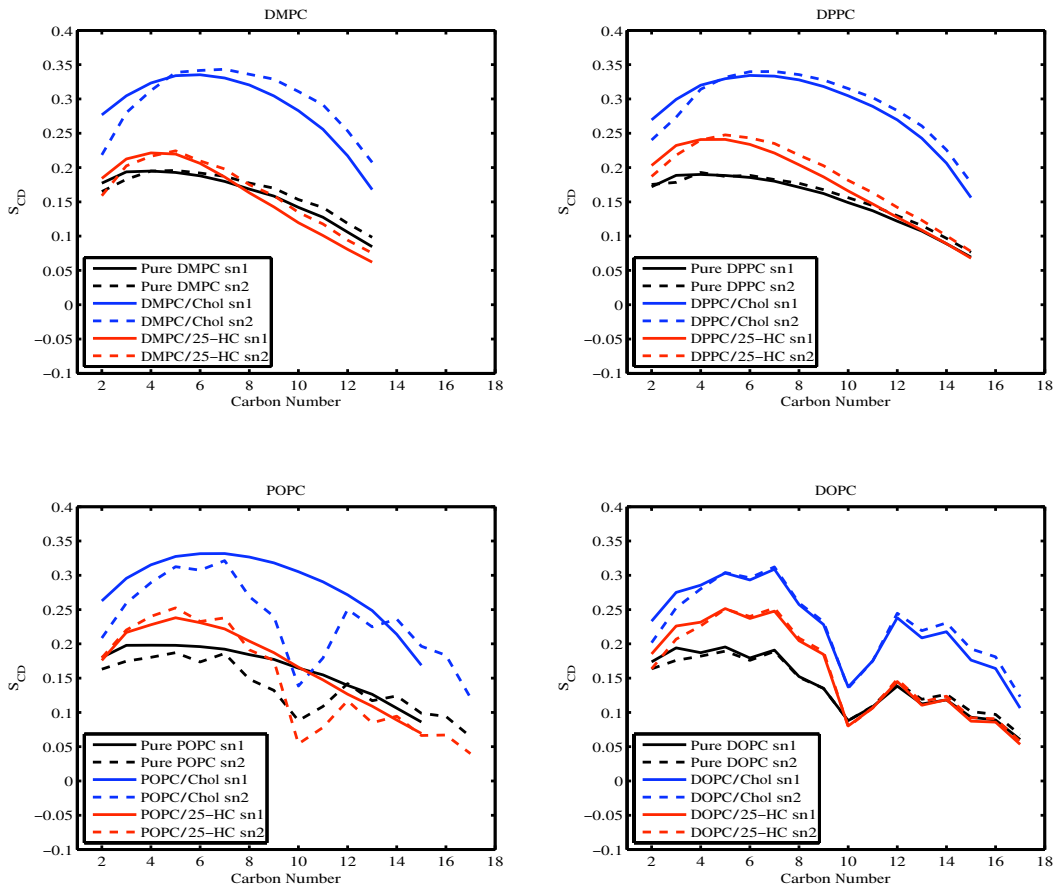

Figure 4.5: Order parameters for the SN1 (solid) and SN2 (dashed) acyl chains of DMPC, DPPC, POPC, and DOPC bilayers. Pure phospholipid results in black, phospholipid/cholesterol results in blue, and phospholipid/25-HC results in red.

more expansion, show almost no change in chain order in carbons 10-17 near the tail end. POPC and DMPC bilayers, which have the largest amounts of expansion, both show significant disordering of acyl chains near the end of the tail in the presence of 25-HC. This suggests that high levels of oxysterol-induced membrane expansion is linked with a disordering of the ends of phospholipid acyl chains.

Sterol Orientations

We have calculated distributions of the orientations of both cholesterol and 25-HC in DMPC, DPPC, POPC, and DOPC bilayers. We calculated sterol tilt and twist for each sterol molecule in these simulations, as described in our earlier work [97]. These tilt and twist angles were projected onto a spherical surface, using sterol tilt angle as the spherical inclination and sterol twist angle as the spherical azimuth. This puts parallel and anti-parallel orientations at two opposite poles of the sphere, with perpendicular orientations with different facings along the equator. No significant differences in cholesterol orientations were found between the four cholesterol/phospholipid simulations (data not shown). Contour plots of the spherical distributions are shown Figure 4.6 for 25-HC in all four bilayers. Lines of latitude and longitude are taken at 30° increments.

The distributions for oxysterol orientations are quite broad, but two major centers can be seen: parallel orientations, with ring tilts less than 30°, and interfacial orientations, with ring tilts between 40° and 80° and ring twists between -45° and 60°. While the parallel orientations are similar to the preferred orientation of cholesterol, the interfacial orientations are specific to 25-HC, and allow the polar hydroxylated tail access to the hydrophilic bilayer/water interface, preventing energetically costly desolvation of the 25-hydroxyl group. We have quantified the fraction of 25-HC molecules in the parallel and interfacial orientations, using the angles described above. A bar graph showing these results can be seen in Figure 4.7. There are significant differences in oxysterol distribution between the four different phospholipids. DMPC and POPC favor interfacial over parallel orientations for 25-HC, while DOPC and DPPC favor parallel orientations. In DMPC, 36% of oxysterols are found in interfacial orientations, while only 21% are in parallel orientations. POPC shows a similar distribution, with 33% interfacial oxysterols and 19% parallel oxysterols. DPPC has a slight bias towards parallel orientations, with 30% in parallel and 27% in interfacial orientations, while DOPC is strongly biased towards parallel orientations, with 37% in parallel and 18% in interfacial orientations. These results correlate with oxysterol-induced membrane expansion, with larger membrane expansions correlating with a higher fraction of interfacial oxysterol orientations. This suggests that either interfacial oxysterols are partially responsible for membrane expansion or that membrane expansion and thinning drives oxysterols towards interfacial orientations.

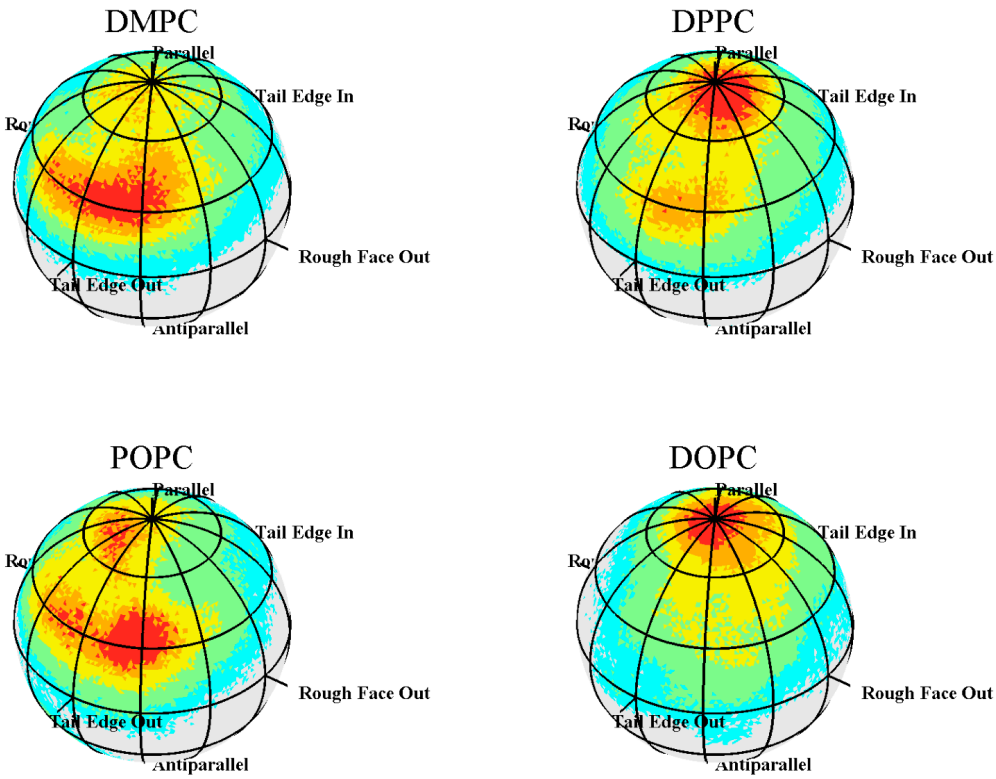

Figure 4.6: Spherical distribution plots of 25-HC orientations in DMPC, DPPC, POPC, and POPC bilayers. Regions containing the densest 10%, 25%, 50%, 75%, and 90% of the total probability density are shown by areas of red, orange, yellow, green, and cyan respectively. Parallel orientations are found at the top pole, and perpendicular orientations with different facings are found along the equator.

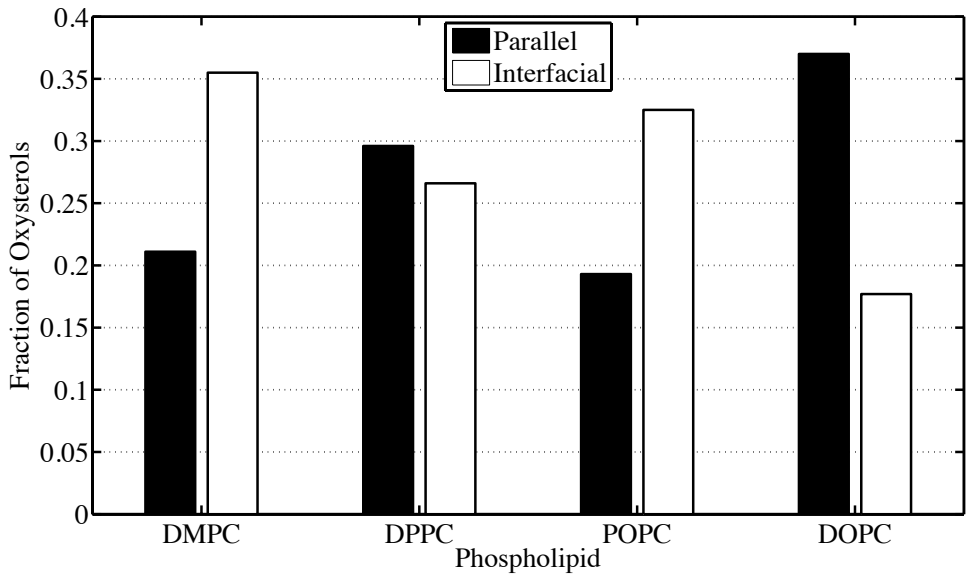

Figure 4.7: A bar graph showing the fractions of 25-hydroxycholesterol molecules found in parallel and interfacial orientations, as described in the text.

25-HC in DMPC

The very large differences in how 25-HC perturbs DMPC and DPPC bilayers was initially somewhat surprising. The expansion induced in DMPC bilayers was the largest observed, while that induced in DPPC bilayers was the smallest. This was surprising because the acyl chains of the two phospholipids differ by only 2 carbons, and that change was not expected to cause major changes in oxysterol arrangements within the bilayer. In order to understand this, we investigated the interactions between 25-HC and phospholipids in DMPC bilayers and found approximately 1-5% of 25-HC molecules forming "bridges" between the two leaflets of the bilayer. These bridges are formed by a single 25-HC molecule stretching across the hydrophobic interior of the bilayer, such that the 3-hydroxyl group hydrogen bonds with phospholipids of one leaflet while the 25-hydroxyl group bonds with those of the other, as seen in Figure 4.8. We believe that these bridges are the cause of the unexpected expansion induced by 25-HC. By pulling the two leaflets of the bilayer together through hydrogen bonding interactions, they directly thin the bilayer and indirectly drive area expansion.

4.4 Discussion

We have found that the effects of both cholesterol and 25-hydroxycholesterol on membrane bilayers are highly dependent on the structure of the phospholipid acyl chains. Cholesterol induces condensation of phospholipids when incorporated into bilayers, with saturated lipids showing more condensation than unsaturated

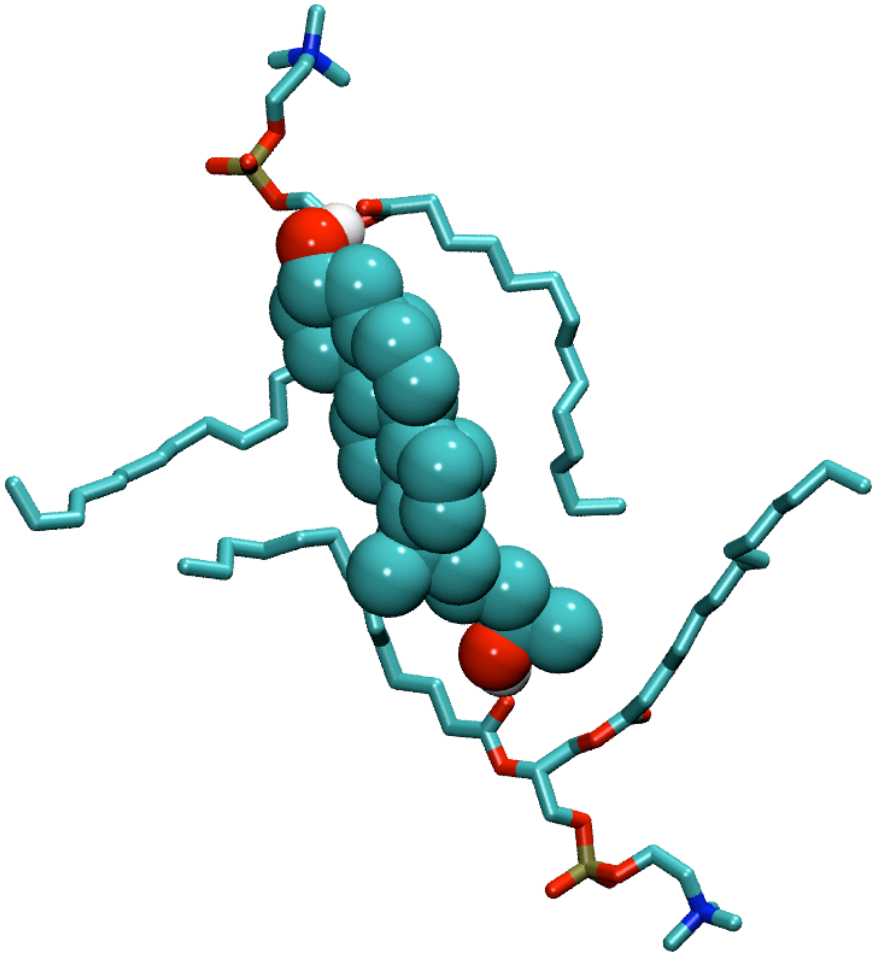

Figure 4.8: A representative structure of 25-HC bridging DMPC bilayers by forming hydrogen bonds to DMPC headgroups in both leaflets of the bilayer. Taken from a snapshot of the DMPC/25-HC simulations. DMPC molecules are shown as sticks, while 25-HC is shown as space-filling VdW atoms.

lipids, in agreement with experimental results [99]. We also see that cholesterol has a stronger condensation effect on DPPC phospholipids than on DMPC phospholipids, in agreement with other simulation and experimental results [66, 111, 114]. This is likely due to the relative lengths of cholesterol versus the palmitoyl or myristoyl chains of the phospholipid, with the shorter myristoyl chains causing intercalation of cholesterol between leaflets [114].

25-hydroxycholesterol, in turn, causes expansion of membrane bilayers. The largest expansion is seen in DMPC bilayers. This appears to be caused by a small number of 25-HC molecules bridging DMPC bilayers, forming hydrogen bonds to DMPC headgroups in both leaflets of the bilayer. These bridges then pull the leaflets of the bilayer together, thinning the bilayer and driving lateral expansion. Oxysterol bridges are not seen in DPPC bilayers, which show the least expansion of the four phospholipids tested. This presumably is because DPPC bilayers are thick enough that oxysterols can no longer bridge the entire bilayer, but are constrained to either bury a hydroxyl group in the bilayer center or form interactions with only one leaflet. This mechanism of oxysterol bridges driving membrane expansion could be experimentally tested using DMPC monolayers. Because there is no second leaflet with polar headgroups in a monolayer geometry, we would expect to find no oxysterol bridges in DMPC monolayers thus predict that DMPC monolayers would show only small amounts of expansion, comparable to what has been seen in DPPC monolayers [36].

In 25-HC/phospholipid bilayers with no oxysterol bridges, we find that while unsaturated lipids expand the least, the most expansion is seen not in fully saturated bilayers but in partially saturated bilayers. This result may have biological relevance as partially unsaturated lipids are the most common within biological membranes, suggesting that the 25-HC structure is tuned to elicit maximum effect from biological membranes [96, 128]. This is not in agreement with monolayer experiments, where 25-HC was found to cause slightly more expansion in DOPC monolayers than in POPC bilayers [36]. Differences between our simulation results and these monolayer experiments may be due to the altered geometry in monolayers versus bilayers. In particular, monolayer geometries may alter the favorability of parallel oxysterol orientations and internal hydrogen bonding between 25-HC molecules, causing slight changes in monolayer expansion relative to bilayer expansion.

We have identified correlations between lipid and oxysterol structure and behavior and membrane expansion. Membrane expansion is correlated with 1) disordering of the ends of phospholipid acyl chains and 2) oxysterol adopting interfacial orientations. The underlying mechanism of these correlations is not yet clear. We have hypothesized in previous work that oxysterol interfacial orientations directly drive membrane expansion [97]. An alternative hypothesis is that the adoption of interfacial orientations is instead driven by membrane expansion: the expansion exposes additional interfacial sites that can be occupied by

the 25-hydroxyl groups of the oxysterols. The hypothesis that interfacial orientations are secondary rather than primary effects is particularly compelling in the case of DMPC bilayers, where expansion appears to be primarily driven by bilayer compression due to oxysterol bridging. Acyl chain disordering in turn is likely secondary as well. It appears to be due either to thinning of the bilayer forcing acyl chain interdigitation or splaying or to oxysterols predominantly locating near the water interface, leaving free space in the bilayer center and allowing more flexibility in acyl chains. These mechanisms will be tested in future simulation and experimental work.

Chapter 5

Conclusions

5.1 Summary of Simulations

We have demonstrated that we can replicate experimentally observed effects of cholesterol and 25-hydroxycholesterol on phospholipid membranes using molecular dynamics simulations. We have run multiple simulations of cholesterol and 25-hydroxycholesterol in phospholipid bilayers, examining 15 different membrane compositions using a cumulative 21.6 microseconds of simulation time. These simulations give us dynamic atomic-level details of membrane structure that are currently inaccessible through any experimental procedure. However, the simulations are necessarily limited: the accuracy of the structural details is dependent on the parameters used for the simulations, and we are limited to examining membranes over relatively small length and time scales. We thus use simulations to calculate observables that can be compared with experimental results in order to validate our simulations as accurate representations of the modeled system.

In agreement with previous experimental and simulation experiments, we find that phospholipid membranes condense when exposed to cholesterol. The amount of condensation is concentration dependent. 30% cholesterol causes more condensation than 18% cholesterol in POPC membranes. However, the dependence is not linear; the marginal effect of a given amount of cholesterol is greater when added to membrane without cholesterol than when added to a membrane already containing 18% cholesterol. These results are similar to those obtained by Pandit *et al.*, who found that the condensing effect of cholesterol on phospholipid area is strongest up until approximately 20% cholesterol in POPC bilayers [101]. We also found significant differences in cholesterol interactions with membranes of different phospholipid compositions. The most condensation was found in fully saturated DPPC membranes, intermediate levels in partially saturated POPC membranes, and the least amount in unsaturated DOPC membranes. Our observation that saturated lipids

are more condensed by cholesterol than unsaturated lipids is in agreement with experimental results [99]. We also find differences due to lipid acyl chain length, with DMPC being less susceptible to condensation than DPPC, which we attribute to hydrophobic mismatching between the myristoyl chains of DMPC and cholesterol [66, 111, 114]. The source of cholesterol-induced membrane condensation was examined using solvent-accessible surface area calculations. This allows us to separate the direct increase in area due to the added cholesterol taking up space in the membrane from the indirect decrease in area due to phospholipid condensation. We found that per-cholesterol surface area is constant across all system compositions, with all variation in membrane area coming from changes in phospholipid surface area.

The hydroxylation of cholesterol at the 25 position causes major changes in both its effects on membranes and its conformation and interactions within membranes. Experimental studies have shown that 25-hydroxycholesterol increases the permeability of membranes to polar and charged molecules [49, 125] as well as expanding both monolayers and bilayers laterally [36]. We have replicated the oxysterol-induced expansion of membranes in our simulated bilayers. Like cholesterol, the effects of oxysterols are dependent on both oxysterol concentration and membrane composition. Unlike cholesterol, oxysterol concentration appears to be proportional to bilayer expansion over the range of oxysterol concentrations examined. Insofar as we see deviations from a linear dose response, oxysterols appear to have larger marginal effects when added to membranes which already contain 25-hydroxycholesterol. Oxysterol effects are also highly dependent on phospholipid structure: DMPC bilayers show the largest expansion, DPPC bilayers the least, with POPC and DOPC bilayers intermediate. The very large expansion of DMPC bilayers by 25-HC appears to be driven by the short myristoyl chains. The thin DMPC bilayers allow oxysterols to adopt bridging conformations, forming hydrogen bonds with phospholipids in both leaflets of the bilayer. This bridging then further thins the bilayer, inducing membrane expansion. In thicker bilayer which prevent the formation of oxysterol bridges, we find only small effects in saturated lipids and larger effects in partially or fully unsaturated lipids. This is in qualitative agreement with results from 25-HC on DOPC, POPC, and DPPC monolayers [36]. However, we find that POPC is slightly more affected by 25-HC than DOPC, while the monolayer experiments show the reverse. While such discrepancies can always be attributed to the limitations of classical molecular simulation, it is also possible that monolayer experiments do not fully capture the behavior of oxysterols in membranes. This is most obvious in the case of DMPC, where oxysterol bridges are necessarily precluded from forming in monolayers, but is present in other systems as well due to the lack of inter-leaflet interactions, both between oxysterols and between phospholipids.

We have been able to identify structural metrics for individual cholesterol and oxysterol molecules that correlate with the effects of sterols on gross membrane behavior. We have quantified the orientation of sterols

within bilayers, describing sterol orientation in terms of ring tilt and ring twist. Ring tilt defines as the angle between the long axis of the rigid steroid ring and the normal axis to the bilayer, while ring twist defines the rotation through the long axis of the ring, and for tilted orientations, describes how the steroid ring faces into the bilayer. Cholesterol molecules uniformly, in all system compositions examined, orient primarily along the normal axis, with ring tilts generally less than 30°. Oxysterol molecules have a much more diverse distribution of orientations, but two major peaks stand out. One is similar to that of cholesterol, with the ring aligned along the normal axis. The other, which we call an "interfacial" orientation, is moderately tilted with a facing such that the hydroxylated tail is pointed towards the bilayer interface. This orientation allows burial of most of the hydrophobic steroid ring within the bilayer, while also allowing both hydroxyl groups the ability to hydrogen bond with the phospholipid headgroups.

We have identified a strong correlation between the fraction of oxysterols in interfacial orientations and the expansive effect of oxysterols on membrane area. This suggests that either interfacial oxysterols drive membrane expansion or that membrane expansion favors interfacial orientations. Both of these explanations have plausible physical mechanisms. Interfacial oxysterols could directly push phospholipids apart by competing for access to the water interface. Alternatively, membrane expansion could favor interfacial oxysterols, either by lowering the free energy of interfacial orientations through increased access to solvent or by raising the free energy of parallel orientations through hydrophobic mismatching between bilayer and sterol. The presence of parallel orientations for oxysterols helps explain how they increase membrane permeability. Some of the increase in permeability is likely due merely to bilayer thinning. However, parallel oriented oxysterol bury their 25-hydroxyl group in the center of the bilayer. We have found that these buried hydroxyl groups interact, forming clusters of hydrogen-bonded hydroxyl groups within the normally hydrophobic bilayer. The presence of these clusters would likely lower the energetic barrier of polar molecules passing through the bilayer by providing potential hydrogen bonding opportunities.

Examination of mixed phospholipid/cholesterol/oxysterol simulations has provided insights into how cholesterol and 25-HC interact within the same membrane. In particular, we found that the presence of 25-hydroxycholesterol significantly alters the behavior of cholesterol within the bilayer. In the presence of 25-HC, cholesterol moves away from the bilayer center towards the water interface, increases in solvent-accessible surface area, and forms more hydrogen bonds with solvent molecules. We interpret these changes in cholesterol behavior as indicative of cholesterol activation. It has been hypothesized that cholesterol exists in membranes in both complexed and free or activated forms [71]. Activated cholesterol is more accessible to enzymes such as ACAT and cholesterol oxidase, and thus activities of these enyzmes as well as transfer of cholesterol from membranes to acceptors like cyclodextrin and lipoproteins are largely driven by activated

cholesterol concentration [71].

5.2 Mechanisms of Oxysterol Signaling

The effects of oxysterols on membrane and lipid behavior may have implications for the mechanisms of oxysterol signaling. While oxysterol activation of LXR transcription factors is mediated through oxysterol/LXR binding, oxysterol suppression of the SREBP pathway is not enantioselective, and thus likely not mediated through protein interactions [36]. We believe that oxysterol/membrane interactions provide non-enantioselective mechanisms through which oxysterols can alter cellular signaling. There are two mechanisms through which we propose oxysterols may signal to membrane proteins. First, oxysterols directly alter membrane behavior, changing membrane thickness and phospholipid order. Changes in membrane structure and behavior can in turn alter protein activity and protein sorting, as has been documented for a number of membrane proteins [53, 74, 132]. 25-hydroxycholesterol also alters cholesterol behavior in ways consistent with cholesterol activation. If oxysterols activate cholesterol in membranes, this would promote the interaction of cholesterol with sterol-sensing proteins. In ER membranes, where 25-HC-producing enzymes are located, the activation of cholesterol through 25-HC production could increase the binding affinity of cholesterol with sterol-sensing domain proteins like Scap and HMGCoAR, thus indirectly suppressing SREBP activation and promoting HMGCoAR degradation. This effect would also explain why application of large amounts of 25-HC to cells promotes trafficking of cholesterol from the plasma membrane to the ER [71]. First incorporating into the plasma membrane, 25-HC would activate cholesterol and increase its accessibility to trafficking enzymes responsible for moving cholesterol from the plasma membrane to the ER.

Although our simulations have been performed at relatively high concentrations of 25-HC compared to their extremely low concentrations in cells, this does not necessarily mean that these observed effects would not be observed in cellular systems. First, 25-hydroxycholesterol is normally produced locally by ER resident enzymes. Although total cellular oxysterol concentration may be low, the local concentration in the vicinity of productive ER enzymes may be significantly higher, high enough to observe the membrane changes and cholesterol activation that we have seen in 18% oxysterol simulations. Secondly, oxysterol signalling through cholesterol activation amplifies signals much more than signalling through protein binding. While production of one hundred 25-HC molecules can only bind to and activate one hundred LXR proteins, if concentrated enough to activate cholesterol in its vicinity, the same molecules may promote cholesterol binding to many more than one hundred SSD-containing proteins.

5.3 Future Work

Several experimental studies have been suggested by our work. We have proposed that oxysterol-induced expansion of DMPC bilayers is driven by oxysterols bridging the full bilayer, hydrogen bonding to phospholipids in both bilayer leaflets, and directly thinning the bilayer. This suggests that expansion in DMPC bilayers is largely dependent on the bilayer structure and that, unlike DOPC or POPC, monolayers of DMPC would not show large amounts of expansion. We predict while DMPC monolayers will undergo low levels of oxysterol-induced expansion similar to DPPC bilayers, while DMPC liposomes would show much larger levels of expansion.

We have also proposed that oxysterols suppress SREBP activation by activation of cholesterol through alteration of membrane structure, freeing cholesterol to more efficiently bind to sterol sensing domains of proteins. This suggests multiple experiments that could be used to test this hypothesis. If oxysterol effects are mediated by cholesterol activation, then they should be directly dependent on cholesterol concentration. Therefore, oxysterol effects on SREBP activation should be significantly ablated in cells starved of cholesterol. It is also possible to directly measure cholesterol activation, using accessibility to cholesterol oxidase or cyclodextrin as a proxy. We anticipate that low concentrations of 25-HC would cause significant increases in cholesterol transfer to cyclodextrin in both cells and model membranes. Further, we anticipate that oxysterol-induced cholesterol activation should be identical between normal 25-HC and enantiomeric 25-HC. We should also be able to find a correlation between the effectiveness of various side-chain oxysterols at suppressing SREBP activation and their ability to activate cholesterol.

We are interested in the mechanisms by which oxysterols perturb membrane structure. To date, all of our simulations have used 25-hydroxycholesterol as a representative side-chain oxysterol. However, there may be important differences in how different side-chain oxysterols affect membranes, and there are certainly differences between side-chain oxysterols and main ring oxysterols. In order to examine the impact of slight changes in oxysterol structure on membrane/oxysterol interactions, examination of a wider range of oxysterols would be useful. Two important oxysterols would be particularly interesting: 7-ketocholesterol and 27-hydroxycholesterol. Both are enzymatically produced, as is 25-HC, so their effect on membranes may have biological significance. Experimental studies have shown that 27-HC has expansive effects on lipid monolayers similar to that of 25-HC, although there appear to be differences in their comparative effects on saturated versus unsaturated lipids [36]. 7-ketocholesterol, however, has condensing effects on lipid monolayers, similar to but smaller in magnitude than that of cholesterol [36]. Based on our simulations with 25-HC and other groups' simulations of 6-ketocholesterol [120], we would predict that 27-HC occupies similar interfacial configurations to that of 25-HC, while 7-ketocholesterol would adopt an intermediate

position with a tilted ring structure but a buried iso-octyl tail.

We have so far only examined the concentration dependence of cholesterol and 25-HC on POPC membranes. Similarly, studies of 25-HC and cholesterol interactions within bilayers have only been performed using POPC membranes. Because we have seen that the effects of cholesterol and oxysterols on membrane behavior and structure are heavily dependent on phospholipid composition, we propose extending the analysis of mixed sterol interactions to membranes of different phospholipids. Simulations of both cholesterol and 25-HC in DMPC, DOPC, and DPPC bilayers would allow us to better understand the mechanisms through which 25-HC expands membrane bilayers and compare its effectiveness at activating cholesterol in different membranes. We believe that the increased effects of 25-HC in the presence of cholesterol are due to a disruption of cholesterol-phospholipid interactions which ablate the ability of cholesterol to condense bilayers, resulting in an increased marginal expansion for a given concentration of 25-HC. This suggests that bilayers in which cholesterol has stronger condensing effects should show the largest change in 25-HC-induced expansion between oxysterol only and mixed sterol bilayers.

Experimental results using enantiomeric 25-HC have shown that oxysterol suppression of SREBP activation is not enantiospecific. This suggests that suppression is not caused by protein-oxysterol interactions but by some non-enantiospecific mechanism. We have proposed changes in membrane structure as a potential mechanism for this signaling. However, while phospholipids do not contain as many chiral centers as proteins, they do contain at least one – the central glycerol carbon. Because we have found that interactions between oxysterol hydroxyl groups and the sn2 ester group are common, we would like to examine whether there are chiral effects on oxysterol/phospholipid interactions. In order to do this, simulation of ent-25-hydroxycholesterol in POPC membranes would be used. We predict that ent-25-HC would cause similar expansive effects on membranes, as has been seen in monolayer experiments [36]. However, we anticipate slight differences in hydrogen bonding between 25-HC and ent-25-HC hydroxyl groups in bilayers due to chiral interactions with the sn2 acyl chain.

Chapter 6

Appendix

6.1 Supporting Information, Chapter 2

6.1.1 Statistical Inefficiency

When sampling conformational states using molecular dynamics, successive system conformations will be highly correlated with each other [33,81]. To calculate properties of the trajectory as a whole, it is necessary to know the relaxation time after which a conformational state is independent of previous states. This allows estimation of the number of independent states across the trajectory. In order to calculate this relaxation time, we use a statistical inefficiency method [95].

Given a set of n sequential, evenly spaced data points:

$$A = \{a_1, a_2, \ldots, a_n\} \tag{6.1}$$

we break A into b blocks $A_1, A_2, \ldots, A_b$ of equal length n_b. The block average for some property $\langle A \rangle_i$ for each block A_i and the average $\langle A \rangle$ for all data points contained in the blocks are calculated. We then calculate the block average for a given block size n_b and total variance for all points contained in the blocks:

$$\sigma^2_{n_b} = \frac{1}{b-1} \sum_{i=1}^{b} \left(\langle A \rangle_i - \langle A \rangle \right)^2 \tag{6.2}$$

$$\sigma^2_{n} = \frac{1}{n-1} \sum_{i=1}^{n} \left(a_i - \langle A \rangle \right)^2 \tag{6.3}$$

The statistical inefficiency can then be defined as a function of n_b:

$$s(n_b) = \lim_{n_b \to \infty} \frac{n_b \sigma^2_{n_b}}{\sigma^2_n} \tag{6.4}$$

We can determine the relaxation time by plotting the statistical inefficiency versus the block size. The relaxation time is the value of s at which a plateau is asymptotically approached for large values of the block size n_b.

6.1.2 Kolmogorov-Smirnov Test

The Kolmogorov-Smirnov (K-S) test is used to compare continuous distributions which are functions of a single variable, such as the distributions of surface areas for a molecule in two different molecular dynamics simulations [107]. These distributions can be converted into cumulative distribution functions $S_N(x)$ where $S_N(x)$ is the fraction of the total distribution that has a value less than x. These are monotonically increasing functions which range from zero to one over the range of the data. The K-S statistic is simply the maximum value of the absolute difference between two cumulative distribution functions:

$$D = \max_{-\infty < x < \infty} \left| S_{N_1}(x) - S_{N_2}(x) \right|. \tag{6.5}$$

The significance statistic for this test requires calculation of the effective number of data points, N_e:

$$N_e = \frac{N_1 N_2}{N_1 + N_2}, \tag{6.6}$$

where N_1 and N_2 are the number of independent data points (as determined by a statistical inefficiency test) in each distribution.

The p-value for significance is [107]:

$$p_{KS} = 2 \sum_{j=1}^{\infty} (-1)^{j-1} e^{-2j^2 \lambda^2}, \tag{6.7}$$

$$\lambda = D \left(\sqrt{N_e} + 0.12 + \frac{0.11}{\sqrt{N_e}} \right). \tag{6.8}$$

6.1.3 Equilibration

Fig. 6.1 shows simple time series of several different membrane properties with 1ns running averages overlaid to emphasize general trends. Simulation time from 0 to 80 ns was cut off as equilibration, and the 80 to 208

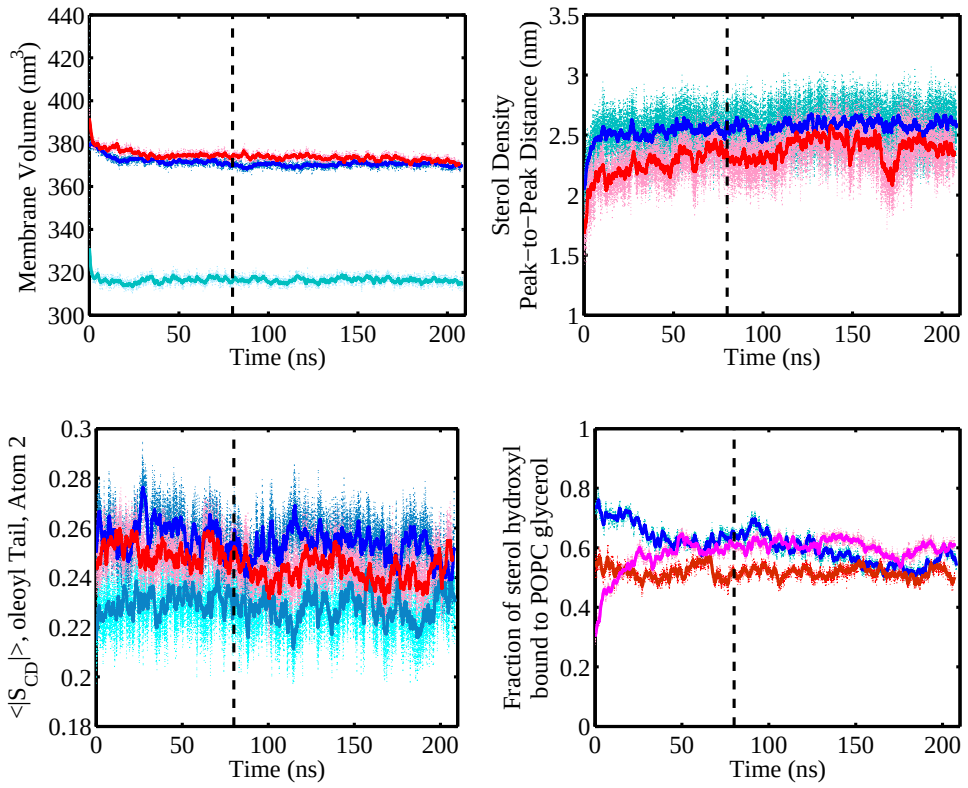

Figure 6.1: Time series of membrane properties (dashed lines), overlaid with a 1ns running average (solid line). The cutoff for equilibration time is shown in dashed black. (A) Total membrane volume. POPC (cyan), POPC/cholesterol (blue), and POPC/oxysterol (red). (B) Peak-to-peak distance between leaflets of sterol density. POPC/cholesterol (blue), POPC/oxysterol (red). (C) Mean order parameter of atom 2 in the oleoyl tail, averaged across all POPC molecules for each frame. POPC (cyan), POPC/cholesterol (blue), and POPC/oxysterol (red). (D) Fraction of sterol hydroxyl groups hydrogen bonded to the POPC glycerol group. Cholesterol 3-hydroxyl (blue), oxysterol 3-hydroxyl (red), oxysterol 25-hydroxyl (pink).

ns region was used as the "production" region for all analyses in the body of the paper. Four analyses are shown. First, membrane volume, calculated as the product of mean phosphate-to-phosphate distance with projected membrane area. Secondly, the peak-to-peak distance between the peaks of the sterol mass density in each bilayer leaflet. Third, the mean order parameter of the second methylene group in the oleoyl tail, averaged across all phospholipids. Fourth, the fraction of sterol hydroxyl groups that form hydrogen bonds to the phospholipid glycerol oxygens.

6.1.4 Membrane System Construction

High-concentration sterol/POPC structures were prepared from the converged portions of these low-concentration simulations as follows. 7 sterol and 16 POPC molecules were extracted from the converged low-concentration

Table 6.1: Structural properties of simulated and experimental membranes.

Bilayer Property	PL	PL/Cholesterol	PL/25-Hydroxycholesterol
Per-PL Area (simulation) (Å^2)	64.0 ± 0.8	67.1 ± 0.4	78.4 ± 0.5
(experimental)	68.3 [67], 68.5 (SOPC) [56]	73 (SOPC) [56]	—
Bending Modulus (simulation) (10^{-20} J)	15.5 ± 1.3	16.5 ± 1.2	8.6 ± 0.6
(experimental)	8.5 [87], 15.4 [46]	34.7 [46]	—
Area Compressibility (simulation) (mN m^{-1})	320 ± 100	1250 ± 370	870 ± 210
(experimental)	278 [87], 213 [46]	354 [46]	—
Volume Compressibility (simulation) (10^8 N m^{-2})	4.8 ± 1.4	8.8 ± 2.6	5.8 ± 1.6
(experimental)	—	—	—

simulation and arranged in a 5 × 5 array to form an oriented monolayer. This monolayer was then stacked on an inverted copy of itself to produce a 14 sterol, 32 POPC bilayer. These very small bilayers were simulated for 10 to 15 ns to allow them to relax. The relaxed structure was then copied 3 × 3 in the plane of the bilayer and 16 POPC and 7 sterols removed from each monolayer of the resulting structure. This process, illustrated in Fig. 6.2, produced final structures consisting of 256 POPC and 112 sterols, or bilayers of about 30 mole percent of sterols. These structures were solvated with 17541 (cholesterol) or 17325 (oxysterol) SPC water molecules and 36 K^+ and Cl^- ions for an approximate molar concentration of 110mM KCl.

6.1.5 Radial Distribution Functions

Radial distribution calculations were performed between the C9 atom of the POPC oleoyl chains and the C18 β-methyl atom of the sterols. Distances were calculated within the xy-plane (ignoring height differences) between all POPC and sterol molecules in the same leaflet of the bilayer. Sterol positions were mirrored into neighboring periodic boxes to avoid edge effects. Distances were binned into 0.01 nm bins, and radial density was calculated by dividing the population of each bin by $\pi\Delta r\,(2r + \Delta r)$, the area of each circular ring. These density functions were then normalized such that they tail off to 1 at large r. Bootstrapped errors were calculated using 32 independent frames as described in the text. We see two immediate peaks corresponding to tail packing around the rough (smaller r) and smooth (larger r) faces of the sterol, followed by tailing off to bulk density at 3nm. Cholesterol shows no large bias in which face is preferred for tail packing, while 25-hydroxycholesterol shows a slight bias towards packing around the smooth face, as well as broader peaks indicating less strong packing.

6.1.6 Bilayer Structural Properties

Table 6.1 lists computed structural properties for our simulated systems along with available experimental results for comparison.

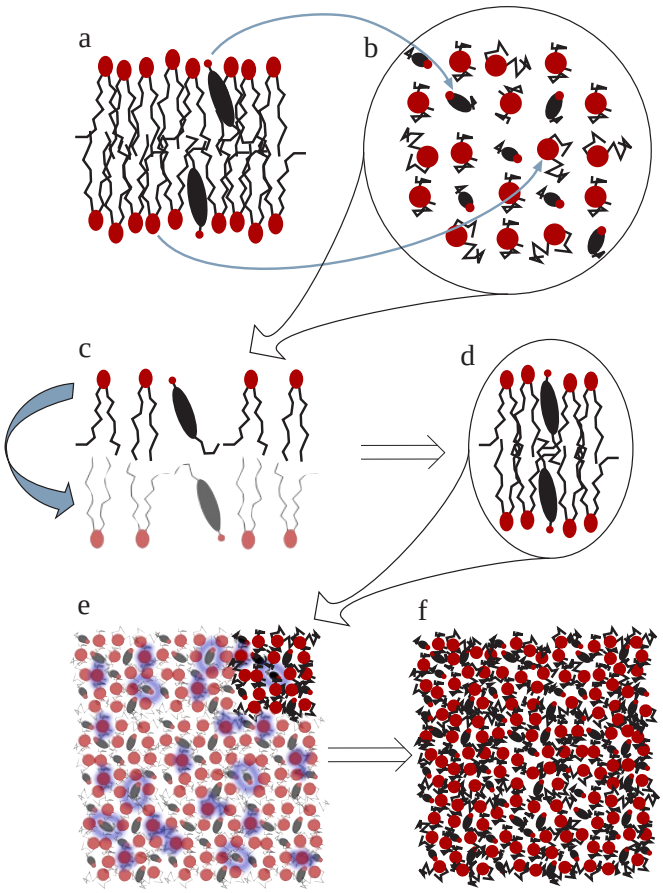

Figure 6.2: Conformations for 7 sterols and 16 POPCs were taken from converged low-concentration simulations (a) and arranged in a 5 × 5 array to form an oriented monolayer (b). This monolayer was then stacked on an inverted copy of itself to produce a 14 sterol, 32 POPC bilayer (c). These very small bilayers were simulated for 10 to 15 ns to allow them to relax (d). The relaxed structure was then copied 3 × 3 in the plane of the bilayer to produce a 126 sterol, 288 POPC bilayer (e). 16 POPC and 7 sterols were removed from each monolayer of the resulting structure to produce final structures consisting of 256 POPC and 112 sterols (f), or bilayers of about 30 mole percent of sterols.

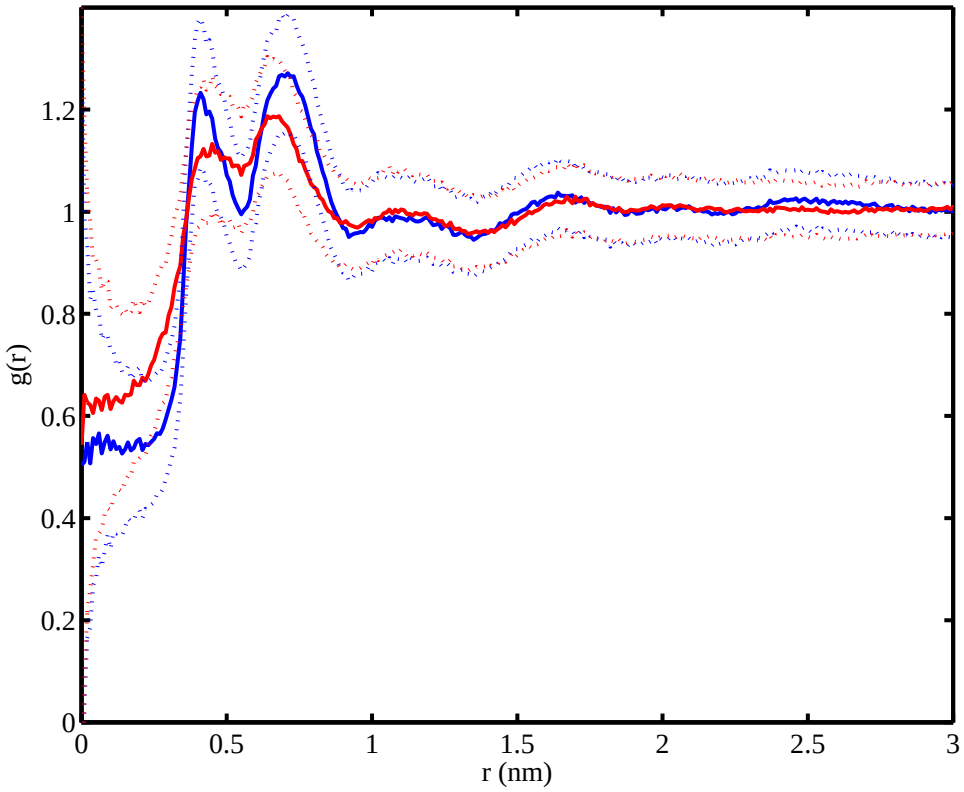

Figure 6.3: 2D radial distribution functions for POPC oleoyl chain packing around cholesterol (blue) and 25-hydroxycholesterol(red) rough faces. Densities are 2-dimensional within the plane of the bilayer and restricted to molecules within the same leaflet of the bilayer. Errors, calculated using a bootstrap sampling method (see main text), are shown as dotted lines.

Table 6.2: United-atom charges used for cholesterol and 25-hydroxycholesterol in our MD simulations.

Atom	Cholesterol charge	25-Hydroxycholesterol charge
Carbon 1	0.00	0.00
Carbon 2	-0.08	-0.10
Carbon 3	0.35	0.35
Carbon 4	-0.12	-0.10
Carbon 5	0.00	-0.05
Carbon 6	0.00	0.00
Carbon 7	0.00	0.00
Carbon 8	0.10	0.10
Carbon 9	-0.10	-0.10
Carbon 10	0.35	0.40
Carbon 11	0.00	0.00
Carbon 12	-0.10	-0.08
Carbon 13	0.15	0.20
Carbon 14	0.10	0.08
Carbon 15	-0.10	-0.10
Carbon 16	-0.05	0.00
Carbon 17	0.15	0.00
Carbon 18	-0.15	-0.10
Carbon 19	-0.15	-0.15
Carbon 20	0.10	0.20
Carbon 21	-0.10	-0.12
Carbon 22	-0.05	-0.13
Carbon 23	0.05	0.05
Carbon 24	-0.10	-0.10
Carbon 25	0.40	0.70
Carbon 26	-0.15	-0.15
Carbon 27	-0.15	-0.15
Oxygen 3	-0.85	-0.85
Hydrogen 3	0.50	0.50
Oxygen 25	N/A	-0.80
Hydrogen 25	N/A	0.50

6.1.7 Sterol Parameters

An initial united atom structure and GROMACS topology for cholesterol modeling were taken from Höltje *et al.* [50], and an additional hydroxyl group was added to both the structure and topology to produce 25-hydroxycholesterol (see figure in main text).

Atomic charges for both cholesterol and 25-hydroxycholesterol molecules were calculated using quantum mechanical/molecular mechanical (QM/MM) methods as described in the text. These charges are shown in Table 6.2, with atomic labels as illustrated in the main text.

Bibliography

[1] N. A. Baker, D. Sept, M. J. Holst, and J. A. McCammon. Electrostatics of nanosystems: application to microtubules and the ribosome. *Proceedings of the National Academy of Sciences*, 98:10037–10041, 2001.

[2] A. D. Becke. Density-functional thermochemistry. III. the role of exact exchange. *Journal of Chemical Physics*, 98:5648–5652, 1993.

[3] H. J. C. Berendsen, J. R. Grigera, and T. P. Straatsma. The missing term in effective pair potentials. *Journal of Physical Chemistry*, 91:6269–6271, 1987.

[4] H.J.C. Berendsen, D. van der Spoel, and R. van Drunen. GROMACS: A message-passing parallel molecular dynamics implementation. *Computer Physics Communications*, 91:43–56, 1995.

[5] O. Berger, O. Edholm, and F. Jahnig. Molecular dynamics simulations of a fluid bilayer of dipalmitoylphosphatidylcholine at full hydration, constant pressure, and constant temperature. *Biophysical Journal*, 72:2002–2013, 1997.

[6] I. Bjorkhem. Oxysterols: Friends, Foes, or Just Fellow Passengers? *Arteriosclerosis, Thrombosis, and Vascular Biology*, 22(5):734–742, February 2002.

[7] I. Björkhem. Are side-chain oxidized oxysterols regulators also in vivo? *Journal of Lipid Research*, 50 Suppl:S213–8, April 2009.

[8] R. A. Bockmann, A. Hac, T. Heimburg, and H. Grubmuller. Effect of sodium chloride on a lipid bilayer. *Biophysical Journal*, 85(3):1647–1655, 2003.

[9] C. M. Breneman and K. B. Wiberg. Determining atom-centered monopoles from molecular electrostatic potentials. The need for high sampling density in formamide conformational analysis. *Journal of Computational Chemistry*, 11(3):361–373, 1990.

[10] A. J. Brown and W. Jessup. Oxysterols: Sources, cellular storage and metabolism, and new insights into their roles in cholesterol homeostasis. *Molecular Aspects of Medicine*, 30(3):111–22, June 2009.

[11] M. S. Brown and J. L. Goldstein. The SREBP Pathway: Regulation of Cholesterol Metabolism by Proteolysis of a Membrane-Bound Transcription Factor. *Cell*, 89(3):331–340, May 1997.

[12] G. Cevc. How membrane chain-melting phase-transition temperature is affected by the lipid chain asymmetry and degree of unsaturation: an effective chain-length model. *Biochemistry*, 30(29):7186–93, July 1991.

[13] T. Chang, C. C. Y. Chang, N. Ohgami, and Y. Yamauchi. Cholesterol sensing, trafficking, and esterification. *Annual Review of Cell and Developmental Biology*, 22:129–57, January 2006.

[14] D. Cheng, Catherine C. Y. Chang, X. Qu, and T. Chang. Activation of Acyl-Coenzyme A:Cholesterol Acyltransferase by Cholesterol or by Oxysterol in a Cell-free System. *Journal of Biological Chemistry*, 270(2):685–695, 1995.

[15] J. Y. L. Chiang. Regulation of bile acid synthesis: pathways, nuclear receptors, and mechanisms. *Journal of Hepatology*, 40:539–551, 2004.

[16] J. E. Chipuk, T. Kuwana, L. Bouchier-Hayes, N. M. Droin, D. D. Newmeyer, M. Schuler, and Douglas R. Green. Direct activation of Bax by p53 mediates mitochondrial membrane permeabilization and apoptosis. *Science*, 303(5660):1010–4, February 2004.

[17] L. E. Chirlian and M. M. Francl. Atomic charges derived from electrostatic potentials: A detailed study. *Journal of Computational Chemistry*, 8(6):894–905, 1987.

[18] S. W. Chiu, E. Jakobsson, R. J. Mashl, and H. L. Scott. Cholesterol-induced modifications in lipid bilayers: A simulation study. *Biophysical Journal*, 83:1842–1853, 2002.

[19] M. P. Czech. PIP2 and PIP3: Complex Roles at the Cell Surface. *Cell*, 100(6):603–606, March 2000.

[20] T. Darden, D. York, and L. G. Pedersen. Particle mesh Ewald: An N log(N) method for Ewald sums in large systems. *Journal of Chemical Physics*, 98:10089–10092, 1993.

[21] O. Edholm. Time and length scales in lipid bilayer simulations. *Current Topics in Membranes*, 60:91–110, 2008.

[22] O. Edholm and J. F. Nagle. Areas of molecules in membranes consisting of mixtures. *Biophysical Journal*, 89:1827–1832, 2005.

[23] M. Edidin. The state of lipid rafts: From model membranes to cells. *Annual Review of Biophysics and Biomolecular Structure*, 32(1):257–283, 2003.

[24] B. Efron and R. J. Tibshirani. *An Introduction to the Bootstrap*. Chapman & Hall/CRC, 1st edition, 1994.

[25] E. Egberts and H. J. C. Berendsen. Molecular dynamics simulation of a smectic liquid crystal with atomic detail. *Journal of Chemical Physics*, 89:3718–3732, 1988.

[26] E. Endress, H. Heller, H. Casalta, M. F. Brown, and T. M. Bayer. Anisotropic motion and molecular dynamics of cholesterol, lanosterol, and ergosterol in lecithin bilayers studied by quasi-elastic neutron scattering. *Biochemistry*, 41:13078–13086, 2002.

[27] R. M. Epand. Cholesterol and the interaction of proteins with membrane domains. *Progress in Lipid Research*, 45:279–294, 2006.

[28] B. Fadeel and D. Xue. The ins and outs of phospholipid asymmetry in the plasma membrane: roles in health and disease. *Critical Reviews in Biochemistry and Molecular Biology*, 44(5):264–277, 2009.

[29] E. Falck, M. Patra, M. Karttunen, M. T. Hyvönen, and I. Vattulainen. Lessons of slicing membranes: Interplay of packing, free area, and lateral diffusion in phospholipid/cholesterol bilayers. *Biophysical Journal*, 87:1076–1091, 2004.

[30] G. W. Feigenson. Phase Boundaries and Biological Membranes. *Annual Review of Biophysics and Biomolecular Structure*, 36(1):63–77, 2007.

[31] S. E. Feller and A. D. MacKerell Jr. An improved empirical potential energy function for molecular simulations of phospholipids. *Journal of Physical Chemistry B*, 104(31):7510–7515, 2000.

[32] S. E. Feller and R. W. Pastor. Constant surface tension simulations of lipid bilayers: The sensitivity of surface areas and compressibilities. *Journal of Chemical Physics*, 111:1281–1287, 1999.

[33] H. Flyvbjerg and H. G. Petersen. Error estimates on averages of correlated data. *Journal of Chemical Physics*, 91(1):461–466, 1989.

[34] R. A. Friesner, R. B. Murphy, M. D. Beachy, M. N. Ringnalda, W. T. Pollard, B. D. Dunietz, and Y. Cao. Correlated ab initio electronic structure calculations for large molecules. *Journal of Physical Chemistry A*, 103(13):1913–1928, 1999.

[35] A. H. Futerman and Y. A. Hannun. The complex life of simple sphingolipids. *EMBO Reports*, 5(8):777–82, August 2004.

[36] S. E. Gale, E. J. Westover, N. Dudley, K. Krishnan, S. Merlin, D. E. Scherrer, X. Han, X. Zhai, H. L. Brockman, R. E. Brown, D. F. Covey, J. E. Schaffer, P. Schlesinger, and D. S. Ory. Side-chain oxygenated cholesterol regulates cellular cholesterol homeostasis through direct sterol-membrane interactions. *Journal of Biological Chemistry*, 284(3):1755–1764, 2009.

[37] G. Gil, J. R. Faust, D. J. Chin, J. L. Goldstein, and M. S. Brown. Membrane-bound domain of HMG CoA reductase is required for sterol-enhanced degradation of the enzyme. *Cell*, 41(1):249–258, May 1985.

[38] S. Gill, R. Chow, and A. J. Brown. Sterol regulators of cholesterol homeostasis and beyond: The oxysterol hypothesis revisited and revised. *Progress in Lipid Research*, 47:391–404, 2008.

[39] J. L. Goldstein and M. S. Brown. Regulation of the mevalonate pathway. *Nature*, 343(6257):425–30, February 1990.

[40] J. L. Goldstein, R. B. Rawson, and M. S. Brown. Mutant mammalian cells as tools to delineate the sterol regulatory element-binding protein pathway for feedback regulation of lipid synthesis. *Archives of Biochemistry and Biophysics*, 397:139–148, 2000.

[41] A. I. Greenwood, S. Tristram-Nagle, and J. F. Nagle. Partial molecular volumes of lipids and cholesterol. *Chemistry and Physics of Lipids*, 143:1–10, 2006.

[42] E. Guardia, J. Marti, L. Garcia-Tarres, and D. Laria. A molecular dynamics simulation study of hydrogen bonding in aqueous ionic solutions. *Journal of Molecular Liquids*, 117:63–67, 2005.

[43] Y. A. Hannun and L. M. Obeid. Principles of bioactive lipid signalling: lessons from sphingolipids. *Nature Reviews Molecular Cell Biology*, 9(2):139–50, February 2008.

[44] J.-P. Hansen and I. R. McDonald. *Theory of Simple Liquids*. Academic Press, San Diego, 2nd edition, 2000.

[45] P. J. Hay and W. R. Wadt. Ab initio effective core potentials for molecular calculations. potentials for k to au including the outermost core orbitals. *Journal of Chemical Physics*, 82:299–310, 1985.

[46] J. Henriksen, A. C. Rowat, E. Brief, Y. W. Hsueh, J. L. Thewalt, M. J. Zuckermann, and J. H. Ipsen. Universal behavior of membranes with sterols. *Biophysical Journal*, 90:1639–1649, 2006.

[47] B. Hess, H. Bekker, H. J. C. Berendsen, and J. G. E. M. Fraaije. LINCS: A linear constraint solver for molecular simulations. *Journal of Computational Chemistry*, 18:1463–1472, 1997.

[48] C. Hofsäß, E. Lindahl, and O. Edholm. Molecular dynamics simulations of phospholipid bilayers with cholesterol. *Biophysical Journal*, 84:2192–2206, 2003.

[49] R. P. Holmes and N. L. Yoss. 25-Hydroxysterols increase the permeability of liposomes to Ca^{2+} and other cations. *Biochimica et Biophysica Acta*, 770:15–21, 1984.

[50] M. Höltje, T. Fórster, B. Brandt, T. Engels, W. von Rybinski, and H. Höltje. Molecular dynamics simulations of stratum corneum lipid models: fatty acids and cholesterol. *Biochimica et Biophysica Acta - Biomembranes*, 1511:156–167, 2001.

[51] W. G. Hoover. Canonical dynamics: Equilibrium phase-space distributions. *Physical Review A*, 31:1695–1697, 1985.

[52] J. D. Horton, J. L. Goldstein, and M. S. Brown. SREBPs: activators of the complete program of cholesterol and fatty acid synthesis in the liver. *Journal of Clinical Investigation*, 109(9):1125–1131, 2002.

[53] M. D. Houslay. Regulation of adenylate cyclase (EC 4.6.1.1) activity by its lipid environment. *Proceedings of the Nutrition Society*, 44:157–165, 1985.

[54] T. Huber, K. Rajamoorthi, V. F. Kurze, K. Beyer, and M. F. Brown. Structure of docosahexaenoic acid-containing phospholipid bilayers as studied by ^{2}H NMR and molecular dynamics simulations. *Journal of the American Chemical Society*, 124(2):298–309, 2002.

[55] G. M. K. Humphries and H. M. McConnell. Potent immunosuppression by oxidized cholesterol. *Journal of Immunology*, 122(1):121–126, 1979.

[56] W. Hung, M. Lee, F. Chen, and H. W. Huang. The condensing effect of cholesterol in lipid bilayers. *Biophysical Journal*, 92(11):3960–3967, 2007.

[57] E. Ikonen. Cellular cholesterol trafficking and compartmentalization. *Nature Reviews Molecular Cell Biology*, 9(2):125–38, February 2008.

[58] Schrödinger Inc. Qsite, 2001.

[59] J. P. Incardona and S. Eaton. Cholesterol in signal transduction. *Current Opinion in Cell Biology*, 12:193–203, 2000.

[60] B. A. Janowski, M. J. Grogan, S. A. Jones, G. B. Wisely, S. A. Kliewer, E. J. Corey, and D. J. Mangelsdorf. Structural requirements of ligands for the oxysterol liver X receptors LXRα and LXRβ. *Proceedings of the National Academy of Sciences*, 96(1):266–271, January 1999.

[61] B. A. Janowski, P. J. Willy, T. R. Devi, J. R. Falck, and D. J. Mangelsdorf. An oxysterol signalling pathway mediated by the nuclear receptor LXRα. *Nature*, 383(6602):728–31, October 1996.

[62] G. Kaminski, R. A. Friesner, J. Tirado-Rives, and W. L. Jorgensen. Evaluation and reparameterization of the OPLS-AA force field for proteins via comparison with accurate quantum chemical calculations on peptides. *Journal of Physical Chemistry B*, 105:6474–6487, 2001.

[63] J. M. Kauffman, P. W. Westerman, and M. C. Carey. Fluorocholesterols, in contrast to hydroxycholesterols, exhibit interfacial properties similar to cholesterol. *Journal of Lipid Research*, 41(6):991–1003, 2000.

[64] N. Kucerka, Y. Liu, N. Chu, H. I. Petrache, S. Tristram-Nagle, and J. F. Nagle. Structure of fully hydrated fluid phase DMPC and DLPC lipid bilayers using X-ray scattering from oriented multilamellar arrays and from unilamellar vesicles. *Biophysical Journal*, 88(4):2626–37, April 2005.

[65] N. Kucerka, J. F. Nagle, J. N. Sachs, S. E. Feller, J. Pencer, A. Jackson, and J. Katsaras. Lipid bilayer structure determined by the simultaneous analysis of neutron and X-ray scattering data. *Biophysical Journal*, 95(5):2356–67, September 2008.

[66] A. Kusumi, W. Subczynski, M. Pasenkiewicz-Gierula, J. Hyde, and H. Merkle. Spin-label studies on phosphatidylcholine-cholesterol membranes: effects of alkyl chain length and unsaturation in the fluid phase. *Biochimica et Biophysica Acta (BBA) - Biomembranes*, 854(2):307–317, January 1986.

[67] N. Kučerka, S. Tristram-Nagle, and J. F. Nagle. Structure of fully hydrated fluid phase lipid bilayers with monounsaturated chains. *Journal of Membrane Biology*, 203(3):193–202, 2006.

[68] P. E. Kuwabara and M. Labouesse. The sterol-sensing domain: multiple families, a unique role? *Trends in Genetics*, 18(4):193–201, 2002.

[69] L. D. Landau and E. M. Lifschitz. *Mechanics*. Pergamon Press, Oxford, England, 3rd edition, 1976.

[70] Y. Lange, D. S. Ory, J. Ye, M. H. Lanier, F. Hsu, and T. L. Steck. Effectors of rapid homeostatic responses of endoplasmic reticulum cholesterol and 3-hydroxy-3-methylglutaryl-CoA reductase. *The Journal of Biological Chemistry*, 283(3):1445–55, January 2008.

[71] Y. Lange and T. L. Steck. Cholesterol homeostasis and the escape tendency (activity) of plasma membrane cholesterol. *Progress in Lipid Research*, 47(5):319–32, 2008.

[72] Y. Lange, J. Ye, M. Duban, and T. L. Steck. Activation of membrane cholesterol by 63 amphipaths. *Biochemistry*, 48(36):8505–15, September 2009.

[73] Y. Lange, J. Ye, and T. L. Steck. How cholesterol homeostasis is regulated by plasma membrane cholesterol in excess of phospholipids. *Proceedings of the National Academy of Sciences of the United States of America*, 101(32):11664–7, August 2004.

[74] A. G. Lee. How lipids affect the activities of integral membrane proteins. *Biochimica et Biophysica Acta*, 1666(1-2):62–87, November 2004.

[75] K. J. B. Lee. Effects of hydrophobic mismatch and spontaneous curvature on ion channel gating with a hinge. *Physical Review E*, 72:031917, 2005.

[76] E. Lindahl and O. Edholm. Mesoscopic undulations and thickness fluctuations in lipid bilayers. *Biophysics Journal*, 79:426–433, 2000.

[77] E. Lindahl, B. Hess, and D. van der Spoel. Gromacs 3.0: A package for molecular simulation and trajectory analysis. *Journal of Molecular Modeling*, 7:306–317, 2001.

[78] L. Liscum and N. J. Munn. Intracellular cholesterol transport. *Biochimica et Biophysica Acta - Molecular and Cellular Biology of Lipids*, 1438:19–37, 1999.

[79] J. A. Lundbaek, O. S. Andersen, T. Werge, and C. Nielsen. Cholesterol-induced protein sorting: An analysis of energetic feasibility. *Biophysical Journal*, 84(3):2080–2089, 2003.

[80] A. Luzar. Resolving the hydrogen bond dynamics conundrum. *The Journal of Chemical Physics*, 113(23):10663–10675, 2000.

[81] E. Lyman and D. M. Zuckerman. The structural de-correlation time: A robust statistical measure of convergence of biomolecular simulations, 2006.

[82] D. Marsh. Thermodynamic Analysis of Chain-Melting Transition Temperatures for Monounsaturated Phospholipid Membranes: Dependence on cis-Monoenoic Double Bond Position. *Biophysical Journal*, 77(2):953–963, 1999.

[83] D. Marsh. Energetics of hydrophobic matching in lipid-protein interactions. *Biophysical Journal*, 94:3996–4013, 2008.

[84] D. Marsh. Protein modulation of lipids, and vice-versa, in membranes. *Biochimica et Biophysica Acta - Biomembranes*, 778:1545–1575, 2008.

[85] G. V. Martinez, E. M. Dykstra, S. Lope-Piedrafita, and M. F. Brown. Lanosterol and cholesterol-induced variations in bilayer elasticity probed by ^{2}H NMR relaxation. *Langmuir*, 20:1043–1046, 2004.

[86] G. V. Martinez, E. M. Dykstra, S. Lope-Piedrafita, C. Job, and M. F. Brown. NMR elastometry of fluid membranes in the mesoscopic regime. *Physical Review E*, 66:050902, 2002.

[87] J. C. Mathai, S. Tristram-Nagle, J. F. Nagle, and M. L. Zeidel. Structural determinants of water permeability through the lipid membrane. *The Journal of General Physiology*, 131(1):69–76, 2007.

[88] T. J. McIntosh. The 2004 Biophysical Society-Avanti Award in Lipids address: roles of bilayer structure and elastic properties in peptide localization in membranes. *Chemistry and Physics of Lipids*, 130:83–98, 2004.

[89] T. J. McIntosh and S. A. Simon. Roles of bilayer material properties in function and distribution of membrane proteins. *Annual review of biophysics and biomolecular structure*, 35:177–98, January 2006.

[90] T. J. McIntosh and S. A. Simon. Roles of bilayer material properties in function and distribution of membrane proteins. *Annual Review of Biophysics and Biomolecular Structure*, 35(1):177–198, 2006.

[91] O. G. Mouritsen and M. Bloom. Mattress model of lipid-protein interactions in membranes. *Biophysical Journal*, 46:141–153, 1984.

[92] R. B. Murphy, D. M. Philipp, and R. A. Friesner. A mixed quantum mechanics/molecular mechanics (QM/MM) method for large-scale modeling of chemistry in protein environments. *Journal of Computational Chemistry*, 21:1442–1457, 2000.

[93] D. Needham and R. S. Nunn. Elastic deformation and failure of lipid bilayer membranes containing cholesterol. *Biophysical Journal*, 58:997–1009, 1990.

[94] F. A. Nezil and M. Bloom. Combined influence of cholesterol and synthetic amphiphillic peptides upon bilayer thickness in model membranes. *Biophysical Journal*, 61(5):1176–1183, 1992.

[95] D. H. Nguyen, T. Dieckmann, M. E. Colvin, and W. H. Fink. Dynamics studies of a malachite green-RNA complex revealing the origin of the red-shift and energetic contributions of stacking interactions. *Journal of Physical Chemistry B*, 108:1279–1286, 2004.

[96] H. Ohvo-Rekila, B. Ramstedt, P. Leppimaki, and J. P. Slotte. Cholesterol interactions with phospholipids in membranes. *Progress in Lipid Research*, 41:66–97, 2002.

[97] B. N. Olsen, P. H. Schlesinger, and N. A. Baker. Perturbations of membrane structure by cholesterol and cholesterol derivatives are determined by sterol orientation. *Journal of the American Chemical Society*, 131:660–670, 2009.

[98] D. S. Ory. Nuclear receptor signaling in the control of cholesterol homeostasis: Have the orphans found a home? *Circulation Research*, 95(7):660–670, 2004.

[99] J. Pan, S. Tristram-Nagle, and J. Nagle. Effect of cholesterol on structural and mechanical properties of membranes depends on lipid chain saturation. *Physical Review E*, 80(2), August 2009.

[100] S. A. Pandit, S. Chiu, E. Jakobsson, A. Grama, and H. L. Scott. Cholesterol surrogates: A comparison of cholesterol and 16:0 ceramide in POPC bilayers. *Biophysical Journal*, 92(3):920–927, 2007.

[101] S. A. Pandit, S. Chiu, E. Jakobsson, A. Grama, and H. L. Scott. Cholesterol packing around lipids with saturated and unsaturated chains: A simulation study. *Langmuir*, 24:6858–6865, 2008.

[102] S. A. Pandit, S. Vasudevan, S. W. Chiu, R. J. Mashl, E. Jakobsson, and H. L. Scott. Sphingomyelin-cholesterol domains in phospholipid lipid membranes: atomistic simulation. *Biophysical Journal*, 87:1092–1100, 2004.

[103] M. Parrinello and A. Rahman. Polymorphic transitions in single crystals: A new molecular dynamics method. *Journal of Applied Physics*, 52:7182–7190, 1981.

[104] M. Patra, E. Salonen, E. Terama, I. Vattulainen, R. Faller, B. W. Lee, J. Holopainen, and M. Karttunen. Under the influence of alcohol: The effect of ethanol and methanol on lipid bilayers. *Biophysical Journal*, 90(4):1121–1135, 2006.

[105] H. I. Petrache, S. W. Dodd, and M. F. Brown. Area per lipid and acyl length distributions in fluid phosphatidylcholines determined by ^{2}H NMR spectroscopy. *Biophysical Journal*, 79(6):3172–3192, 2000.

[106] D. M. Philipp and R. A. Friesner. Mixed ab initio QM/MM modeling using frozen orbitals and tests with alanine dipeptide and tetrapeptide. *Journal of Computational Chemistry*, 20:1468–1494, 1999.

[107] W. H. Press, S. A. Teukolsky, W. T. Vetterling, and B. P. Flannery. *Numerical Recipes in C: The Art of Scientific Computing*. Cambridge University Press, 2nd edition, 1992.

[108] P. H. Purdy, M. H. Fox, and J. K. Graham. The fluidity of chinese hamster ovary cell and bull sperm membranes after cholesterol addition. *Cryobiology*, 51(1):102–112, 2005.

[109] A. Radhakrishnan, Y. Ikeda, H. J. Kwon, M. S. Brown, and J. L. Goldstein. Sterol-regulated transport of srebps from endoplasmic reticulum to golgi: Oxysterols block transport by binding to insig. *Proceedings of the National Academy of Sciences*, 104(16):6511–6518, 2007.

[110] K. Rajamoorthi, H. I. Petrache, T. J. McIntosh, and M. F. Brown. Packing and viscoelasticity of polyunsaturated $\omega - 3$ and $\omega - 6$ lipid bilayers as seen by ^{2}H NMR and X-ray diffraction. *Journal of the American Chemical Society*, 127(5):1576–1588, 2005.

[111] B. Ramstedt. Membrane properties of sphingomyelins. *FEBS Letters*, 531(1):33–37, October 2002.

[112] A. Ridsdale, M. Denis, P. Gougeon, J. K. Ngsee, J. F. Presley, and X. Zha. Cholesterol is required for efficient endoplasmic reticulum-to-Golgi transport of secretory membrane proteins. *Molecular Biology of the Cell*, 17(4):1593–605, April 2006.

[113] T. Róg and M. Pasenkiewicz-Gierula. Cholesterol effects on a mixed-chain phosphatidylcholine bilayer: a molecular dynamics simulation study. *Biochimie*, 88:449–460, 2006.

[114] Tomasz Róg, Marta Pasenkiewicz-Gierula, Ilpo Vattulainen, and Mikko Karttunen. Ordering effects of cholesterol and its analogues. *Biochimica et Biophysica Acta (BBA) - Biomembranes*, 1788(1):97 – 121, 2009. Lipid Interactions, Domain Formation, and Lateral Structure of Membranes.

[115] D. W. Russell. Oxysterol biosynthetic enzymes. *Biochimica et Biophysica Acta - Molecular and Cell Biology of Lipids*, 1529:126–135, 2000.

[116] A. Seelig and J. Seelig. The dynamic structure of fatty acid chains in a phospholipid bilayer measured by deuterium magnetic resonance. *Biochemistry*, 13(23):4839–4485, 1974.

[117] H. Shimano, J. D. Horton, R. E. Hammer, I. Shimomura, M. S. Brown, and J. L. Goldstein. Overproduction of cholesterol and fatty acids causes massive liver enlargement in transgenic mice expressing truncated SREBP-1a. *Journal of Clinical Investigation*, 98(7):1575–1584, 1996.

[118] K. Simons and W. L. C. Vaz. Model systems, lipid rafts, and cell membranes. *Annual review of biophysics and biomolecular structure*, 33:269–95, January 2004.

[119] L. L. Smith. Cholesterol autoxidation. *Chemistry and Physics of Lipids*, 44:87–125, 1987.

[120] Alexander M. Smondyrev and Max L. Berkowitz. Effects of oxygenated sterol on phospholipid bilayer properties: a molecular dynamics simulation. *Chemistry and Physics of Lipids*, 112(1):31 – 39, 2001.

[121] Y. Song, V. Guallar, and N. Baker. Molecular dynamics simulations of salicylate effects on the micro- and mesoscopic properties of a dipalmitoylphosphatidylcholine bilayer. *Biochemistry*, 44(41):13425–13438, 2000.

[122] P. J. Stephens, F. J. Devlin, C. F. Chabalowski, and M. J. Frisch. Ab initio calculation of vibrational absorption and circular dichroism spectra using density functional force fields. *Journal of Physical Chemistry*, 98:11623–11627, 1994.

[123] T. P. Straatsma and H. J. C. Berendsen. Free energy of ionic hydration: analysis of a thermodynamic integration technique to evaluate free energy differences by molecular dynamics simulations. *Journal of Chemical Physics*, 89:5876–5886, 1988.

[124] A. R. Tall. Cholesterol efflux pathways and other potential mechanisms involved in the atheroprotective effect of high density lipoproteins. *Journal of internal medicine*, 263(3):256–73, March 2008.

[125] J. J. H. Theunissen, R. L. Jackson, H. J. M. Kempen, and R. A. Demel. Membrane properties of oxysterols. interfacial orientation, influence on membrane permeability and redistribution between membranes. *Biochimica et Biophysica Acta*, 860:66–74, 1986.

[126] D. P. Tieleman and H. J. C. Berendsen. Molecular dynamics simulations of a fully hydrated dipalmitoylphosphatidycholine bilayer with different macroscopic boundary conditions and parameters. *Journal of Chemical Physics*, 105:4871–4880, 1996.

[127] D. P. Tieleman, L. R. Forrest, M. S. P. Sanson, and H. J. C. Berendsen. Lipid properties and the orientation of aromatic residues in OmpF, influenza M2 and alamethicin systems: molecular dynamics simulations. *Biochemistry*, 37:17554–17561, 1998.

[128] G. van Meer, D. R. Voelker, and G. W. Feigenson. Membrane lipids: where they are and how they behave. *Nature Reviews Molecular Cell Biology*, 9(2):112–24, February 2008.

[129] D. Warschawski and P. Devaux. Order parameters of unsaturated phospholipids in membranes and the effect of cholesterol: a 1H13C solid-state NMR study at natural abundance. *European Biophysics Journal*, 34:987–996, 2005.

[130] R. J. Woods, M. Khalil, W. Pell, S. H. Moffat, and V. H. Smith Jr. Derivation of net atomic charges from molecular electrostatic potentials. *Journal of Computational Chemistry*, 11(3):297–310, 1990.

[131] D. Yabe, M. S. Brown, and J. L. Goldstein. Insig-2, a second endoplasmic reticulum protein that binds SCAP and blocks export of sterol regulatory element-binding proteins. *Proceedings of the National Academy of Sciences of the United States of America*, 99(20):12753–8, October 2002.

[132] Q. Yang, R. Alemany, J. Casas, K. Kitajka, S. M. Lanier, and P. V. Escribá. Influence of the membrane lipid structure on signal processing via G protein-coupled receptors. *Molecular pharmacology*, 68(1):210–7, 2005.

[133] T. Yang, P. J. Espenshade, M. E. Wright, D. Yabe, Y. Gong, R. Aebersold, J. L. Goldstein, and M. S. Brown. Crucial Step in Cholesterol Homeostasis: Sterols Promote Binding of SCAP to INSIG-1, a Membrane Protein that Facilitates Retention of SREBPs in ER. *Cell*, 110(4):489–500, August 2002.

[134] C. Yuan, R. J. O'Connell, R. F. Jacob, R. P. Mason, and S. N. Treistman. Regulation of the gating of BKca channel by lipid bilayer thickness. *Journal of Biological Chemistry*, 282:7276–7286, 2007.